Nanostructured surfaces: challenges and frontiers in nanotechnology

2004 J. Phys.: Condens. Matter 16 S1373

(http://iopscience.iop.org/0953-8984/16/17/001)

INSTITUTE OF PHYSICS PUBLISHING JOURNAL OF PHYSICS: CONDENSED MATTER

J. Phys.: Condens. Matter **16** (2004) S1373–S1436 PII: S0953-8984(04)59022-7

Nanostructured surfaces: challenges and frontiers in nanotechnology

Federico Rosei

Institut National de la Recherche Scientifique—Énergie, Matériaux et Télécommunications, Université du Québec, 1650 Boulevard Lionel-Boulet, J3X 1S2 Varennes (QC), Canada

Received 23 October 2003
Published 16 April 2004
Online at stacks.iop.org/JPhysCM/16/S1373
DOI: 10.1088/0953-8984/16/17/001

Abstract

Nanostructured surfaces can be broadly defined as substrates in which the typical features have dimensions in the range 1–100 nm (although the upper limit of 100 nm may be relaxed to greater sizes in some cases, depending on the material and the specific property being investigated). The recent surge of interest in these systems stems from the remarkable effects that may arise from the critical size reduction. Interesting novel properties (catalytic, magnetic, ferroelectric, mechanical, optical and electronic) occur as we reduce the dimensions from a practically infinite (and periodic) solid crystal to a system composed of a relatively small number of atoms. So far, nanostructured materials or *nanomaterials* are perhaps the only sub-field of nanoscience that has made the transition from fundamental science to real world applications, thus becoming a technology (a good example of this are nanostructured surface coatings). This paper describes some selected examples of recent progress in the study of nanostructured surfaces. Surface reconstructions, which occur either naturally or as a consequence of the interaction with adsorbates, are discussed because of their importance in model chemical reactions and for their potential use as templates for the ordered growth of nanostructures. Supramolecular assemblies and molecular nanostructures, resulting from the balance between molecule–molecule and molecule–surface interactions, are described because of their fundamental interest and their potential use in nanoelectronic devices. Recent progress in the growth of semiconductor nanostructures, in particular Ge–Si and InAs–GaAs, is briefly reviewed. A few selected examples of nanostructured functional materials, such as ferroelectric and magnetic nanostructures, are discussed in view of their potential for applications in future data storage devices. Nanostructured materials used in catalysis and gas sensor applications are briefly described. Finally, perspectives and future challenges in this emerging field of research are also discussed.

(Some figures in this article are in colour only in the electronic version)

Contents

Nomenclature

AES	Auger electron spectroscopy
AFM	Atomic force microscopy/microscope
C_{60}	Buckminsterfullerene
DC	Decacyclene
EELS	Electron energy loss spectroscopy
ESQC	Elastic scattering quantum chemistry
FIM	Field ion microscopy
HAS	Helium atom scattering
HDS	Hydrodesulfurization
HtBDC	Hexa-di-*tert*-butyl decacyclene
HOPG	Highly oriented pyrolytic graphite
HREELS	High resolution electron energy loss spectroscopy
LEED	Low energy electron diffraction

LEEM	Low energy electron microscopy
MFM	Magnetic force microscopy
OMBD	Organic molecular beam deposition
PEEM	Photo-emission electron microscopy
PFM	Piezoresponse force microscopy
RAIRS	Reflection–absorption infra-red spectroscopy
RHEED	Reflection high energy electron diffraction
SAM	Self-assembled monolayer
SEM	Scanning electron microscopy/microscope
SFM	Scanning force microscopy/microscope
SNOM	Scanning near-field optical microscopy/microscope
SPM	Scanning probe microscopy
STM	Scanning tunnelling microscopy/microscope
STS	Scanning tunnelling spectroscopy
TBPP	*tert*-butylphenyl
TDS	Thermal desorption spectroscopy
TEM	Transmission electron microscope/microscopy
UHV	Ultra-high vacuum
UPS	Ultra-violet photoelectron spectroscopy
XPD	X-ray photoelectron diffraction
XRD	X-ray diffraction
XPS	X-ray photoelectron spectroscopy

1. Introduction

In the past decade, research efforts in nanoscience and nanotechnology have grown explosively worldwide. While we are just beginning to understand the functionalities that can be accessed through the use of nanostructured materials and surfaces, the tremendous potential of '*nano*' approaches[1] to revolutionize the ways in which matter is fabricated, synthesized and processed is already apparent. Presently atoms (Eigler and Schweizer 1990), molecules (Heinrich *et al* 2002), clusters and nanoparticles (Brust *et al* 1994, 1995, Kiely *et al* 1998) can be used as functional building blocks for fabricating advanced and totally new phases of condensed matter on the nanometre length scale. The optimal size of these unit components depends on the particular property to be engineered: by altering the dimensions of the building blocks, controlling their surface geometry, chemistry and assembly, it will be possible to tailor functionalities in unprecedented ways. Some 30–40 years later, the vision proposed by Richard Feynman in the famous speech 'There is plenty of room at the bottom' (Feynman 1960) has now become reality. Already at that time, Feynman noted that nanoscale science and engineering would require the development of new experimental techniques and of specific instrumentation that could visualize the nanoworld, and possibly even intervene directly to modify it.

At the start of the new millennium we are thus confronted with the need and desire to learn more about the atomic scale structure of matter. Besides our intrinsic interest in fundamental science, in fact today the ultimate goal in this context is to develop tomorrow's functional devices so that they can operate on the nanoscale. This obsessive trend towards miniaturization is driven partly by an analogous trend in the semiconductor industry, with the

[1] By *nano* here I mean that at least one of the three dimensions is smaller than 100 nm, with a consequent, strong size effect resulting from the reduction of dimension.

aim of developing ever smaller and faster computers, all the way to the quantum computer[2] (Schulz 1999, Reed and Tour 2000, Kane 1998) and partly by the desire to develop novel devices of other types, for example microelectromechanical systems (MEMS) and nanoelectromechanical systems (NEMS), gas and chemical sensors or even biomedical equipment. Examples include nanostructured biomaterials for tissue engineering (Tambasco de Oliveira and Nanci 2004) and mechanical devices that operate at sub-micron length scales that may perform surgical or similar operations in blood vessels or other vital organs of the human body. For all these reasons, it is expected that nanotechnology will have a much greater impact on our modern society than the Si integrated circuit (which led to the 'electronic revolution' of the 20th century), since it will be applicable to many different fields of human activity, including medicine, security and telecommunications[3].

Clearly, proper tools must be used to study the properties of materials and surfaces on the nanometre length scale. Whenever we push the limits of instrumentation and develop new probes, novel and unexpected phenomena may suddenly appear[4]. In fact, the development of this multidisciplinary field was undoubtedly accelerated by the advent of relatively recent technologies that allow the visualization, design, characterization and manipulation of nanoscale systems. It is generally accepted that the advent of scanning probe microscopy (SPM) techniques, such as scanning tunnelling microscopy (STM) (Binnig *et al* 1982a, Binnig and Röhrer 1999, Röhrer 1994), atomic force microscopy (AFM) (Binnig *et al* 1986), scanning near-field optical microscopy (SNOM), magnetic force microscopy (MFM) (see, for example, Grütter *et al* 1992) and piezoresponse force microscopy (PFM), is largely responsible for the emergence of nanoscience as a novel field of research. Although it does not have a strong chemical sensitivity and, in most cases, it also lacks time resolution, the STM has proved to be a powerful tool in the study of adsorbate–surface interactions and of elementary surface processes in general (Besenbacher 1996, Neddermeyer 1996, Rosei and Rosei 2002, 2003, Rosei 2003).[5] Very recently STM was used to investigate the single-electron states and the corresponding squared wavefunctions of single and free-standing strain-induced InAs quantum dots grown on GaAs(001) (Maltezopoulos *et al* 2003). The implication is that this tool may now be used to perform wavefunction mapping of surfaces. Similarly, the AFM can now be used to image highly oriented pyrolytic graphite (HOPG) with atomic resolution (Hembacher *et al* 2003, Hersam and Chung 2003), a surprising feat.

Recent advances in theoretical calculations (e.g. Hofer *et al* 2001, Hofer and Fischer 2003) has also proved to be extremely important for the development of nanoscience. For example, the investigation of organic molecules on surfaces by SPM has required the development of sophisticated theoretical and simulation tools for the interpretation of SPM images. Atomic and molecular adsorbates typically induce a modification of the local density of states (LDOS) on a surface, thereby causing new features (depressions or protrusions) to appear in STM images (Besenbacher 1996). The perturbation induced by complex molecules is usually much stronger. In this case, the STM measures the molecule's local *transparency* to tunnelling electrons, giving a *characteristic local tunnelling footprint*, from which important information may be deduced. STM images of conjugated molecules are often dominated by quantum interference effects, which may hinder the overall resolution of the actual molecular shape

[2] Recent progress towards the fabrication of a *quantum computer* using P atoms implanted in Si(001) surfaces as 'qubits' (following Kane 1998) was reported at the University of New South Wales (Oberbeck *et al* 2002, Schofield *et al* 2003).

[3] Paraphrased from Neal Lane, science and technology advisor to President Clinton (2000).

[4] The first scientist to witness this was probably Galileo Galilei. By increasing by a factor of ten the resolving power of the human eye, in the seventeenth century Galilei discovered Jupiter's satellites.

[5] Before the advent of the STM, atomic scale imaging of materials had been demonstrated using transmission electron microscopy (TEM).

(Sautet 1997). The most advanced theoretical technique in this context is undoubtedly the elastic scattering quantum chemistry (ESQC) routine, which allows simulating STM images from first principles (Sautet and Joachim 1991, 1992).

The idea of manipulating atoms and molecules on the nanoscale appeared to be just a fascinating dream only a couple of decades ago, before the invention of SPM-related instrumentation. The underlying fascination for these experiments may have been motivated simply by scientific and technological opportunities, or by the curiosity about the implications of being able to *play* with atoms, placing them in particular locations on a surface, using them as 'building blocks' to assemble new structures on a substrate of our choice. The first demonstration of controlled STM manipulations was published less than a decade after the invention of the STM itself (Eigler and Schweizer 1990): Xe atoms were deposited on Ni(110) at 4 K and were displaced to form the 'IBM' logo. Although the practical value of these experiments is perhaps limited (they are simply too slow for industrial applications), this initial scientific breakthrough has led to a series of outstanding manipulation experiments, which have provided new insight into surface quantum phenomena and molecule–surface interactions, among others (Eigler *et al* 1991, Manoharan *et al* 2000, Braun and Rider 2002, Moresco *et al* 2001a, 2001b, Rosei *et al* 2002a, 2003, Schunack *et al* 2002a).

More recently, the STM has been employed to induce atomic scale chemical transformations on surfaces (Ho 1998, Hla and Rieder 2003). Remarkable results have come from Wilson Ho's group. Firstly the STM was successfully used to break a C–H bond in a single acetylene molecule adsorbed on Cu(001) (Lauhon and Ho 2000); then, they proceeded to dehydrogenate the ethynyl species to form dicarbon (CC).

It has also been demonstrated that, besides the breaking of selected molecular bonds, the STM tip can be used to *induce* the formation of a single chemical bond. For example, Lee and co-workers (Lee and Ho 1999) were able to form Fe(CO) and $Fe(CO)_2$ molecules starting from individual Fe atoms and CO molecules adsorbed on a Ag(110) substrate. Subsequently Hla *et al* (2000) have demonstrated the feasibility of inducing all the steps of a surface chemical reaction by using a STM tip. In particular, Hla and co-workers succeeded in the synthesis of biphenyl molecules starting from iodobenzene adsorbed on Cu(111). This series of impressive experiments proves the concrete possibility of controlling chemistry at the spatial limit of individual atoms and molecules. In turn, it has provided new insights into the nature of chemical bonds and surface reactivity.

The ability to manipulate matter with atomic scale precision has opened new frontiers in physics, chemistry and materials science. At the same time, it has demonstrated that single-molecule synthesis is possible with the STM. The motivations for such syntheses are manifold and may have practical value besides their fundamental character. It is now possible to study how the environment of the reactants affects surface reactions or how the conformation of reactants affects reaction barriers. For example, if it were possible to perform such studies by AFM, it would allow us to measure the forces acting between the reactants as a function of molecular conformation. In this context, the main problem from a practical point of view is perhaps the serial nature of the manipulations versus the parallel processes commonly used in industry like optical lithography, which are much faster and therefore economically advantageous.

The development of such new tools and thus of nanoscience and nanotechnology research at large requires high levels of funding. With few exceptions, each industrialized country today has developed a special research programme devoted to nanotechnology. The most striking example is undoubtedly the National Nanotechnology Initiative, championed by President Clinton in 2000, with a total investment that reaches several hundred million US$ per year. Similarly, the European Union's Sixth Framework Program focuses on various aspects of

nanoscience. At the same time, individual countries within the Union (e.g. Denmark and the UK) have their own nanotechnology programmes. Major efforts are underway in Asia, particularly in Japan, Korea, Taiwan and Singapore. '*Nano*' research in Canada today is funded in various ways, for example through the National Institute for Nanotechnology (NINT) which is presently being built in Edmonton[6], the Nano Innovation Platform of the Natural Science and Engineering Research Council, and indirectly through various other sources (e.g. NanoQuébec, which is a Research Network on Nanotechnology sponsored by the Province of Québec).

If this high level of funding is to persist, scientists working in this field will have to make a sustained effort to describe their work to the general public, to avoid erroneous perceptions that may build up as a consequence of science fiction stories[7] and pressure from special groups. At present the mass media are systematically airing divergent views on the potential benefits and risks associated with nanotechnology and the ethical, economic, societal and political implications related to it[8]. Recently the hopes and promises surrounding this field of research are being undermined by several pressure groups. For example, environmental campaigners have voiced concerns on the potential hazards of nanomaterials (e.g. nanoparticles and carbon nanotubes). One of the challenges that lie ahead is to prove that nanomaterials pose no threat to our health and to the environment, or to show that any potential risk can be reasonably contained.

In this paper I will begin by providing a general description of the science of surfaces and interfaces and its objectives, with particular emphasis on '*surface effects*' which typically arise when a material's surface-to-volume ratio becomes high. I will attempt to describe such surface effects at large, with various examples drawn from the recent literature. These include studies of active sites in catalytic reactions, the observation of unexpected reaction pathways and anomalous surface reconstructions and deconstructions. All these remarkable phenomena are somehow mediated by nanoscale properties and structures at the substrate of choice. Unless specified otherwise, the experimental investigations described hereafter were carried out in ultra-high vacuum (UHV) ambient conditions ($p < 10^{-10}$ mbar).

Section 3 is devoted to nanostructured magnetic materials. Similar to most nanostructured surfaces, nanomagnetic materials can be produced either by direct growth or by microfabrication techniques, such as lithographic patterning. These systems have potential applications in the development of novel data storage devices.

In section 4 I outline briefly the properties of nanostructured ferroelectric materials. These are found to exhibit some analogies (e.g. hysteretic behaviour), besides many differences, with respect to magnetic structures. For example, they can be used as nanoscale capacitors and as switching cells for memory devices.

Section 5 describes surface diffusion processes in general, but with particular emphasis on the diffusion properties of large organic molecules, which have recently been shown to exhibit a rich and surprising phenomenology.

Section 6 contains a description of the adsorption properties of complex molecules on metal substrates. Unexpected phenomena include the dependence of molecular conformations on surface symmetry and chemistry, molecule-induced reconstructions and the ability of molecules to self-assemble into ordered structures using either directional or non-directional chemical interactions (e.g. hydrogen bonding and van der Waals forces).

[6] This is a joint venture between the University of Alberta and the National Research Council of Canada, for a total investment of 120 M$ (CAD) over the next five years.

[7] See Crichton's recent novel, *Prey*.

[8] Emmanuelle Schuler, paper presented at the Second 'Nanomaterials Crossroads' Workshop, Montreal, Quebec, October 2003.

In section 7, I describe several morphological properties of semiconductor nanostructures, including morphological instabilities and interdiffusion processes that occur in the growth of InAs on GaAs surfaces and the growth of Ge on Si substrates.

The section 8 illustrates a few general perspectives on *nano* research and important challenges that remain to be faced in the decades to come. In this context, a few selected examples of the nanoscale properties of insulating materials are provided. Indeed, the study of insulators, which has proved to be extremely difficult so far from an experimental point of view, represents one of the new, challenging frontiers that need to be addressed in future nanotechnology research.

This paper, which has no pretense of being complete or exhaustive, somewhat extends and complements a previous excellent review (Moriarty 2001).

2. Surface effects: relevant examples in catalysis and gas-sensing applications

Today it is widely accepted that the uppermost few atomic layers of a solid (i.e. the solid's *surface*) represent its interface with the surrounding environment; on this interface a variety of ongoing atomic and molecular processes take place in a virtually two-dimensional (2D) world. Surface phenomena are actually responsible for some of the most important technologies on which our society depends for its economic development and prosperity. For simplicity, I will restrict the present description of nanostructured surfaces to crystalline systems, since our present ability to explore in detail amorphous structures is still severely limited.

The concept of surface has been a topic of study and an argument of debate for scientists and philosophers since ancient Greek times (Paparazzo 2003). In the very first philosophical descriptions of the world, surfaces were in fact considered conceptual abstractions; at the time, philosophers could not accept the notion that a '*surface*' had any material substance. Today, *surface science* deals with the physical and chemical properties of surfaces and interfaces (Lüth 1997), including technologically important processes such as catalysis, crystal growth, corrosion and friction. Most of these phenomena are completely determined by the interaction of surface atoms with atoms and molecules impinging on the substrate of choice.

Clearly the study of solid surfaces represents a great challenge when compared, for example, to the investigation of the bulk properties of crystals (Ashcroft and Mermin 1976). In fact, out of the 10^{24} atoms that are found in a macroscopic crystal, only about one in 10^8 are located in the proximity of the surface. The detection, identification and characterization of elementary surface and interface processes are undoubtedly arduous tasks. Indeed, it was not until the 1960s that new techniques, such as x-ray photoelectron spectroscopy (XPS) and Auger electron spectroscopy (AES), permitted us to investigate the electronic and chemical properties of crystal surfaces, only probing a few atomic layers below the substrate, instead of the whole bulk material. Ideally, to fully describe surface processes (e.g. the diffusion and reaction of atoms and molecules), we need insight at atomic length scales and at the characteristic timescales of elementary step evolution (i.e. at least sub-picosecond time resolution in most cases). However, the experimental techniques available today are still a long way from this performance. To address these challenging tasks, in the last 30 years or so surface scientists have developed an arsenal of different experimental techniques (Weaver and Poirier 1994, Woodruff and Delchar 1994).

The recent interest in nanoscale properties of condensed matter is directly correlated to the appearance of surface effects when one or more dimensions are reduced below a critical length scale. A very good, and quite surprising, example of this is gold (Au). This precious element has long been known as being essentially chemically inert (and therefore catalytically inactive) in its bulk form (Hammer and Norskov 1995). Quite recently, however, it was found that, when dispersed in the form of nanoscale clusters and supported on transition metal oxide

surfaces such as TiO_2 (Valden *et al* 1998, Wahlström *et al* 2003), Au exhibits a very high (low-temperature, LT) catalytic activity for the partial oxidation of hydrocarbons, hydrogenation of unsaturated hydrocarbons and reduction of nitrogen oxides (Haruta 1997). It was shown that the catalytic properties of Au nanoparticles depend specifically on the support, the preparation method and, critically, on the size of the Au clusters, which are active when their diameter is smaller than 3.5 nm (Bamwenda *et al* 1997, Valden *et al* 1998). A further decrease in cluster diameter below ∼3 nm causes a decrease in reactivity. Remarkably, despite the extensive recent efforts addressing this extraordinary catalytic behaviour, no atomic-level understanding currently exists. This type of insight could prove to be extremely useful, for example to design novel catalyst materials from first principles.

2.1. Direct observation of the active sites in a catalytic surface reaction

The concept of '*active site*' is fundamental in heterogeneous catalysis. This notion reflects experimental evidence that, in general, catalytic surfaces are not uniformly active. Rather, only sites distinguished by a special arrangement of surface atoms (including defects) or by a particular chemical composition are actually reactive. To address this issue, Zambelli *et al* (1996a) studied the dissociative chemisorption of NO[Note 9] on the (0001) surface of ruthenium, which is known to be the most selective catalyst. The surface was exposed to a small dose of NO (0.3 Langmuir, 1 L $= 10^{-6}$ Torr s) at room temperature (RT) and subsequently STM images were recorded (about 0.5 h after exposure). From the distribution of product atoms observed in STM micrographs, it is inferred that NO molecules, once adsorbed, diffuse rapidly across surface terraces until they meet a step, where they are observed to dissociate with high probability. After dissociation, O atoms move rapidly away from the steps. Nitrogen atoms also move away but more slowly, so that sequences of STM images show a diffusion profile of N atoms, with the origin at the step. Both terraces were observed to host a comparable number of N atoms. Since N atoms do not cross the step upon dissociation, it is concluded that NO molecules approaching the step, either from the lower or from the upper adjoining terrace, dissociate with approximately the same probability. This observation led to the conclusion that the reaction takes place at the frontmost metal atoms at the step (Zambelli *et al* 1996a, Hammer 1999).

This experiment clearly demonstrated that Ru(0001) is not uniformly active for the process of dissociation of NO but, rather, that monatomic steps (always present on real surfaces) are highly preferential sites for this reaction. Despite the importance of active sites, their exact nature and hence the atomistic mechanisms by which they act had remained elusive for a long time, mainly because of the lack of a local and sensitive probe like the STM.

Besides validating directly the concept of '*active site*' in catalysis, this experiment showed that kinetic processes are influenced by surface structure at the sub-nanometre and atomic level and confirmed that 'macroscopic' experiments can only measure an overall reactivity which results from weighted contributions from various surface structure elements at the microscopic level, and are therefore not reliable in general (Wintterlin *et al* 1997).

2.2. Surface reconstructions

In general, a surface is not to be simply considered as a static checkerboard (Woodruff 2002, Rosei and Rosei 2002, Rosei *et al* 2003). Upon adsorption of a foreign atom or molecule, the uppermost atomic planes typically undergo a local deformation. The first-layer atoms of the host surface, while forming new chemical bonds with guest species, must also modify the structure and strength of the bonds they form with the underlying bulk layers. For stronger

[9] This is an important elementary step in the catalytic reduction of noxious gases such as nitric oxides.

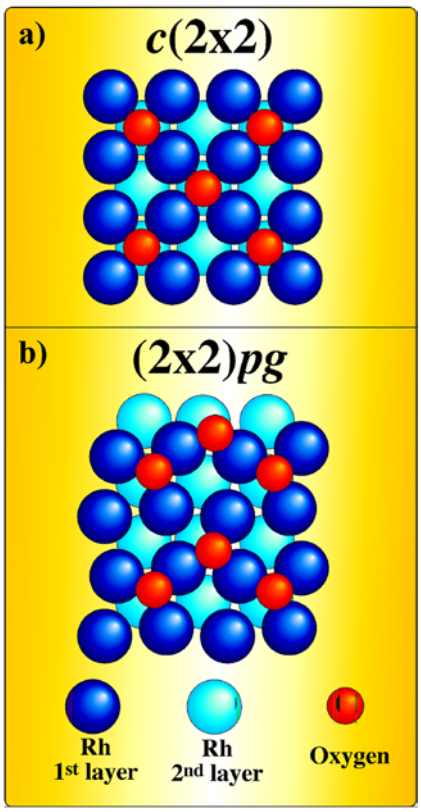

Figure 1. Adsorbate over layers on a (100) fcc metal surface (Rh in this case) at a coverage of 0.5 ML. (a) Regular c(2 × 2) structure; (b) (2 × 2)pg structure formed by oxygen on Rh(100) (Rosei and Rosei 2002).

interactions the adsorbate may even cause a so-called *reconstruction* of the underlying surface. In this case, surface atoms are rearranged into a new, ordered geometrical structure. This can range from a simple distortion of the elementary cell, up to a complete, large-scale repositioning of surface atoms. Reconstructions can also occur without interaction with adsorbates, to optimize the arrangement of unsaturated bonds that is caused by the abrupt two-dimensional termination.

An example of the first type of reconstruction is reported in figure 1(b), where the distortion induced by the adsorption of oxygen atoms on the (100) surface of rhodium is sketched. When the coverage approaches half a monolayer (ML), the elementary cell elongates from the original square to a rhombus in which oxygen atoms sit in one of the corners, thus forming a new surface symmetry (Baraldi *et al* 1999, Alfè *et al* 1998). For comparison, figure 2(a) shows a c(2 × 2) (centred two by two) structure which is the most common one formed by an adsorbate on a (100) surface of a face centred cubic crystal, at a coverage of 0.5 ML.

Figures 2(a) and (b) display the structure of a Rh(110) surface and the same surface after 0.5 ML adsorption of oxygen, respectively. In this case a considerable mass transport of rhodium atoms takes place during adsorption, giving rise to a (2 × 1) 'missing row' reconstruction[10], characterized by depressions that are three atomic layers deep. Surface

[10] A (2 × 1) reconstruction means that the periodicity in one direction is twice the original cell size, while the other remains the same.

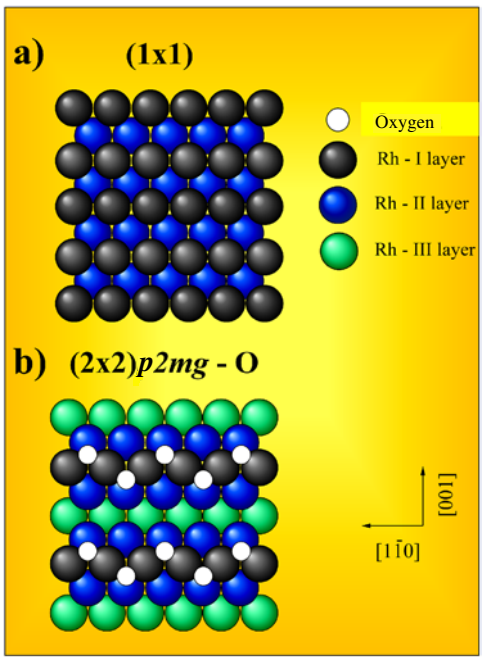

Figure 2. Ideal structure of a clean Rh(110) surface. (a) Structural change upon adsorption of 0.5 ML of oxygen, (b) the reconstructed (2 × 2)p2mg implies a major process of mass transport during its formation (Rosei and Rosei 2002).

reconstructions, whether spontaneously occurring or induced by an adsorbate, are important phenomena since they imply, besides a geometrical change, a strong long-range modification of electronic structure and chemical reactivity of the surface.

With respect to such surface reconstructions, one of the most spectacular experiments in the history of surface science has been the real-space visualization of the geometric structure of the (7 × 7) reconstruction of the Si(111) surface (Binnig *et al* 1982a) by STM. A thorough understanding of this peculiar reconstruction, first observed in K space by low energy electron diffraction (LEED), had previously proved to be particularly elusive. This complex surface structure was then solved by Takayanagi *et al* (1985), who proposed the dimer–adatom stacking fault (DAS) model. A STM image of this surface with atomic resolution is shown in figure 3.

Besides their importance in fundamental surface studies, processes such as reconstruction and faceting are directly relevant to several technological problems, such as the heteroepitaxial growth of nanostructures and the stability of catalysts (Besenbacher 1996, Rosei and Rosei 2002, 2003). The restructuring of an initially flat, pristine substrate into a reorganized surface with different periodicity or into an assembly of facets with new surface orientations is generally driven by a tendency to lower the total energy of the system. The presence of adsorbates may enhance the directional anisotropy of the surface free energy so that substrate reconstruction leads to a net decrease in energy, in spite of the increase in surface area. Extensive work has been reported on faceting and reconstructions induced by adsorbed gases, sulfur, metal growth and organic molecules on metal surfaces (Africh *et al* 2001, Vesselli *et al* 2001, Comelli *et al* 1998, Besenbacher 1996, Rosei and Rosei 2002, 2003, Schmid *et al* 2000a, Schunack *et al* 2001, 2002a, Rosei *et al* 2002a, 2003). I will provide some specific examples in the section on the adsorption properties of complex molecules.

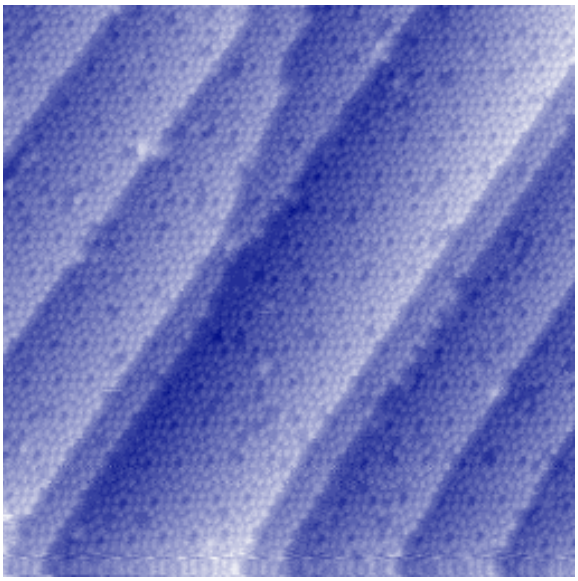

Figure 3. Atomic scale structure of the Si(111) surface, imaged by STM at room temperature. The 7×7 reconstruction with atomically resolved Si atoms, as well as monatomic steps with sharp edges, are clearly visible (Rosei 2001).

2.3. Elementary reaction steps

The precise determination of the basic mechanisms that occur in catalytic reactions is a long-standing yet elusive goal of research in applied physical chemistry. The determination of a complete set of rate equations which accurately describes the sequence of elementary steps leading to the formation of a chemical product is generally hampered by the lack of information of one or more intermediate steps and species. The possible existence of parallel branches of a reaction, which may proceed through different mechanisms in different regimes, represents an additional complication. The identification and characterization of different reaction pathways are therefore of great importance in surface science.

By combining experimental measurements of scanning tunnelling microscopy (STM) and density functional theory (DFT) it was recently possible to detect two different reaction mechanisms in the catalytic oxidation of carbon monoxide on the (110) surface of rhodium (Castellarin-Cudia *et al* 2001). The reaction was carried out through a titration experiment. The Rh(110) surface was first exposed to oxygen until a reconstructed c(2×8) structure was obtained. It was then exposed to CO at a selected temperature for a specific time and finally STM images were acquired. The reaction process was found to be strikingly different at 160 and 300 K, suggesting parallel reaction branches and mechanisms in the two cases displayed in figures 4(a) and (b).

Sequences of LT STM images showed that the reaction starts from centres that nucleate uniformly across the surface. At RT instead, the reaction runs in a quasi-one-dimensional fashion along narrow terraces that are formed in the aftermath of the surface reconstruction. With the help of DFT calculations it was possible to elucidate both reaction pathways and the complex influence of temperature on the overall mechanism.

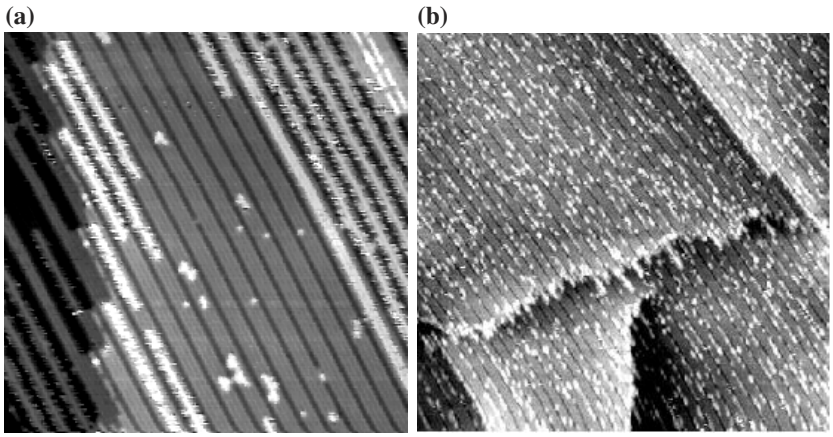

Figure 4. (a) 34×34 nm^2 STM image of the c(2×8) O/Rh(110) after dosing 2 Langmuir (L) of CO at 300 K. Bright *Christmas garland* lines are reacted stripes occupied by CO. (b) 70×70 nm^2 STM image of the c(2×8) O/Rh(110) after dosing 0.2 L of CO at 160 K. The straight features at the top right and lower left are monatomic steps (Castellarin-Cudia *et al* 2001).

2.4. Examples of adsorbate-induced reconstructions

Adsorbate–surface interaction has been a very important branch of surface science ever since the first surface-sensitive techniques were developed (Woodruff 2002, Rosei and Rosei 2002). The earlier studies were carried out by means of instrumentation that is still in use today, such as LEED, reflection–absorption infra-red spectroscopy (RAIRS), electron energy loss spectroscopy (EELS), high resolution EELS (HREELS) and x-ray photoelectron spectroscopy (XPS). For example, Ertl (1967) was the first to report the partial (2×1) reconstruction induced by oxygen on Cu(110), using LEED.

Towards the end of the 1980s and the beginning of the 1990s, work on adsorbate–surface interactions was enormously revived by the use of the STM (Coulman *et al* 1990, Jensen *et al* 1990, Kern *et al* 1991) and by progress in theoretical calculations. These studies were reviewed thoroughly at an early stage (Besenbacher and Norskov 1993, Besenbacher 1996).

High coverage oxygen layers on transition metal substrates are of great current interest because their formation and reactivity are important in understanding the catalytic activity of oxide surfaces, which are widely used in real catalysts.

As I outlined previously, at temperatures above ∼400 K, the adsorption of oxygen on Rh(110) induces a variety of surface reconstructions (Rosei and Rosei 2002, 2003, Comelli *et al* 1998, Vesselli *et al* 2001, Africh *et al* 2001, 2002). In all cases, oxygen atoms adsorb in fcc-threefold sites, forming *zig-zag* chains along the close-packed $[1\bar{1}0]$ direction. In particular, by dosing 0.5 ML the surface reconstructs with (1×2) periodicity, where one $[1\bar{1}0]$ rhodium row out of every two is missing. The symmetry of the oxygen overlayer is (2×2)p2mg, as shown in figure 5(a). Upon heating, or by adsorbing further oxygen at temperatures (below 500 K) where Rh adatom mobility is too low to lead to surface reconstructions, this causes a *strained* reconstruction with (10×2) symmetry and high local oxygen coverage (figure 5(b)). STM images reveal that, in the (10×2) layer, the oxygen adsorbed in the rhodium close-packed rows is strongly compressed. In this strained structure, Rh rows appear to be 'segmented' along the $[1\bar{1}0]$ direction.

Africh and co-workers have also followed substrate dynamics during oxygen removal. By taking STM movies[11], they have investigated the titration of a (2×2)p2mg–O/Rh(110)

[11] That is, sequences of hundreds of STM images from the same area of the surface.

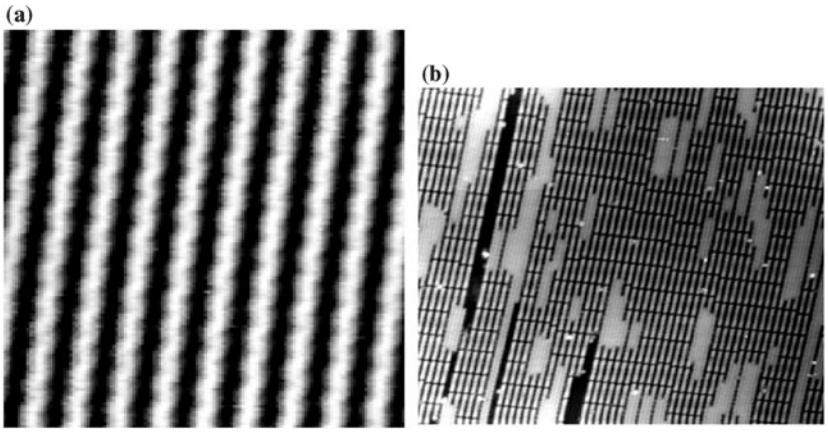

Figure 5. (a) STM image of the (2 × 2)p2mg–O reconstructed surface obtained by exposure to oxygen (Africh *et al* 2002). (b) STM images of the (10 × 2) recorded at room temperature. Dimensions: 400 × 300 Å^2 (Vesselli *et al* 2001).

surface by hydrogen and the subsequent *deconstruction* of the non-equilibrium (1 × 2) reconstructed substrate. At temperatures above 380 K, the Rh(110) surface evolves from the reconstructed state (figure 6(a)) towards the more stable (1 × 1) *ground state* or *deconstructed* state (figure 6(b)). The deconstruction dynamics has also been studied by helium atom scattering (HAS). Cvetko *et al* (1994) observed that the evolution takes place by forming (1 × 1) islands, elongated along the [1$\bar{1}$0] direction. The transformation rate is extremely slow at 400 K, whereas it becomes very rapid at $T = 500$ K.

STM analysis revealed that the deconstruction process occurs via two distinct mechanisms. Since the (1 × 2) state is only metastable, the first mechanism sets in immediately after the oxygen is removed from the surface. Rhodium rows appear to be paired, forming regions with a local (1 × 4) symmetry. The second deconstruction mechanism is of local nature and does not lead to any particular symmetry and is therefore not detectable by means of non-local techniques. It is related to the formation of vacancies and to the mobility of single rhodium atoms. Once vacancies are created, the ejected Rh atoms diffuse freely over distances of ∼10 nm along the close-packed direction, then condense into small (1 × 1) islands. Both mechanisms are observed to start predominantly at defect sites and (1 × 2) surfaces with a lower density of defects are observed to deconstruct much slower, suggesting that a perfect (1 × 2) structure is not likely to deconstruct, and thus that this state is *metastable*. These deconstruction pathways are similar to those observed for the thermally induced deconstruction of Au(110) and Pt(110) (Koch *et al* 2000), which also occurs by forming pairs of correlated steps and is influenced by defect density.

The work by Africh and co-workers has provided new insight into the elementary steps and the dynamics of surface reactions occurring on rhodium substrates. This type of atomic-scale understanding is important for developing future generations of environmental catalysts.

2.5. Chemical reactivity of transition-metal clusters

Transition-metal oxides and sulfides are two widely used classes of catalytically active materials. In particular, transition-metal sulfide nanoclusters are of interest as lubricants, as models of the active part of some enzymes and as hydrodesulfurization (HDS) catalysts. These are particularly important because of the current worldwide demand for cleaner transport fuels.

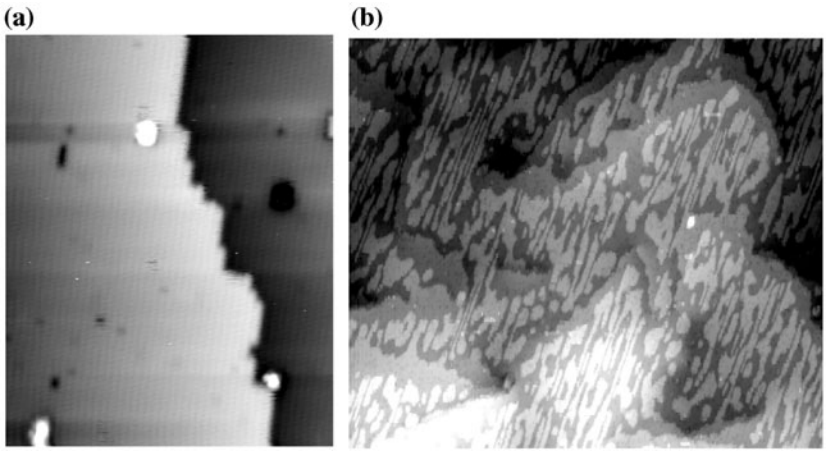

Figure 6. (a) STM images of oxygen uptake (0.01 L) on Rh(110) showing the step edges becoming squared due to kink atom removal and the added/missing row reconstruction starting from steps and defects. Image size: 162 Å × 205 Å (Africh *et al* 2001). (b) STM image of the final state of the surface after deconstruction at $T = 405$ K. The islands have coalesced into large structures. Image size: 2070 Å × 1800 Å (Africh *et al* 2002).

At the same time, Cu, Pd, Pt and Au clusters supported on metal oxide surfaces, such as TiO_2, Al_2O_3, and MgO, are used for applications in catalysis and in gas sensors. In general, their chemical activity is typically described in terms of the geometric coordination of surface atoms.

In model catalysis studies, a transition metal is deposited in sub-monolayer quantities on a substrate and the morphology and reactivity are then studied using surface-sensitive techniques such as STM, TDS and XPS. In general, the substrate should mimic the properties of the support material used in a real catalyst and thus TiO_2 and MgO single crystals are widely used. However, some of these materials are insulating and therefore difficult to study experimentally. To overcome this difficulty in the case of Al_2O_3, for example, a NiAl(110) surface can be oxidized, forming a thin film of alumina on which the clusters are then grown[12].

The alternative is to use a relatively inert substrate material, such as gold or graphite, so that the properties of the clusters can be isolated from those of the underlying surface. In this context, Besenbacher's group in Aarhus has reported outstanding results on the properties of single-layer MoS_2 nanostructures. These structures can be grown, for example, on Au(111), which is used as a template. This particular surface is a model substrate, since gold is noble and chemically inert on the one hand, and since its characteristic long-range herringbone reconstruction provides convenient nucleation sites for epitaxial growth of highly dispersed metal islands on the other hand. When depositing molybdenum on Au(111), Helveg *et al* (2000) observed the formation of a self-assembled, regular array of one or two layer high Mo islands that nucleate in the elbows of the herringbone reconstruction. The array actually extends over a mesoscopic length scale. After the growth of Mo the surface is then exposed to H_2S and this leads to the formation of nanometre size MoS_2 clusters. These nanostructures are triangular in shape, consistent with the threefold symmetry of the underlying surface (figure 7(a)).

In a subsequent investigation, Lauritsen *et al* (2001) have obtained the first atomic-scale images of Co–Mo–S clusters, which are widely used in HDS catalysis. Following the same procedure as described above, submonolayer quantities of Mo and Co were deposited on a reconstructed Au(111) surface, then exposed to H_2S. It was reported that the presence of the Co promoter atoms causes the shape of the MoS_2 nanoclusters to change from triangular to

[12] If the film is relatively thin, the substrate is conductive enough to allow investigation by STM.

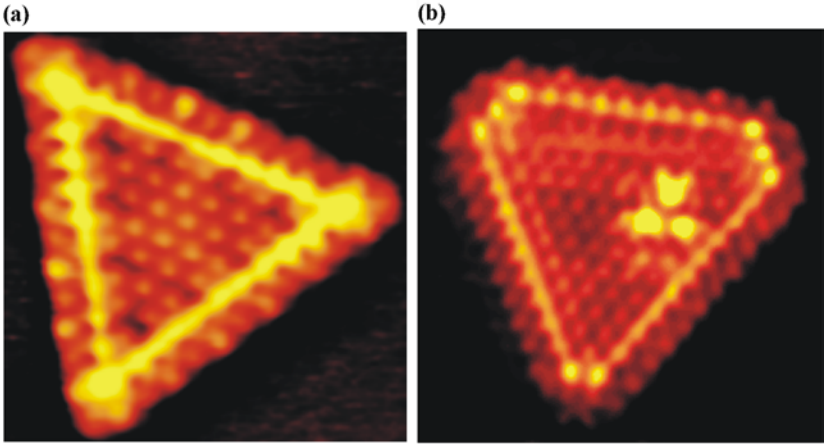

Figure 7. (a) An atom-resolved STM image (41 Å × 42 Å, $I_t = 1.28$ nA and $V_t = 5.2$ mV) of a MoS_2 nanocluster grown on Au(111) by depositing Mo in an H_2S atmosphere (Helveg *et al* 2000). (b) STM image (dimensions: 48 Å × 53 Å) of a single-layer Co–Mo–S nanocluster grown on Au(111) (tunnelling parameters: $I_t = 1.95$ nA, $V_t = 430$ mV) (Lauritsen *et al* 2001).

hexagonal (figure 7(b)). The morphological change appears to be driven by a preference for Co to be located at the S-edge of MoS_2 clusters. This work also clearly showed that the presence of the Co atoms perturbs the local electronic environment of the neighbouring S atoms, providing further insight into the effect of the promoter atoms on the cluster's reactivity.

More recently, Lauritsen *et al* (2003) found a new kind of chemical activity associated with fully sulfur-saturated active sites on two-dimensional MoS_2 nanoclusters. This reactivity appears to be related to highly localized metallic electron states present at the perimeter of the triangle-shaped nanoclusters. This is another surprising *size* effect: the reduction to nanoscale clusters drastically changes the electronic structure of MoS_2, which is an insulator in its bulk form. It was also suggested that such electronic states, which are dominant in nanosized clusters, may constitute a new class of active centres in heterogeneous catalysis.

When imaged by STM, these clusters exhibit a characteristic bright feature that extends all around the edges. This *brim* was associated with a one-dimensional metallic electronic state at the edge of the otherwise insulating MoS_2 nanoclusters, in which electrons are strongly localized perpendicularly to the edge, but delocalized along the direction of the cluster edges. Comparison with DFT calculations showed that the activity in the HDS process is associated with the edges terminating the clusters (whereas the basal plane of MoS_2 is known to be catalytically inactive). It is speculated that the metallic states associated with S atoms at the edges have the ability to donate and accept electrons and thus act as catalytic sites, as if they behaved like ordinary transition-metal surfaces.

This is yet another example of the direct observation of the *active sites* in a catalytic material. The chemical activity associated with active centres on the metallic edge states of MoS_2 and Co–Mo–S clusters is undoubtedly of general importance. For example, it may provide a new route for the hydrogenation of aromatic molecules, which is an integral part of hydro-treating catalysis.

2.6. Applications of nanostructured surfaces in gas sensors

Nanostructured thin films typically exhibit a larger surface-to-volume ratio, which is a characteristic geometric property that arises when dimensions are drastically reduced. This

feature, among other things, considerably improves their performance as gas sensors (Gopel and Schierbaum 1995, Madou and Morrison 1989).

Tin oxide (SnO_2) is an n-type semiconductor that is widely used as a solid-state gas sensor (Dolbec *et al* 2002). Nanostructured tin oxide films can be grown by a variety of deposition techniques including chemical vapour deposition (CVD), sol–gel processing, reactive sputtering and pulsed laser deposition (PLD) (El Khakani *et al* 2001).

In a recent study, Dolbec *et al* (2002) have investigated the influence of the substrate deposition temperature under two different background gas conditions (vacuum and oxygen background pressure) on the nanostructure and the properties (resistivity and optical transmittance) of SnO_2 thin films grown by PLD. Film morphology and properties were shown to be correlated to a size variation in SnO_2 grains and to the concentration of oxygen vacancies in the films.

Figure 8 displays three sets of SEM micrographs (top and cross-sectional views) of tin oxide films deposited under a partial pressure of oxygen of 150 mTorr at three selected substrate temperatures (300, 450 and 600 °C). A close inspection shows that the morphology of the SnO_2 films changes significantly by varying the deposition temperature. For example, the films deposited at 300 °C exhibit a *cauliflower-like* (Dolbec *et al* 2002) porous fine-grained structure (figure 8(a)). Layer porosity is observed to be deep, suggesting a tendency of the nanostructures to stack into columns. As the temperature is raised to 450 °C, the films become columnar (figure 8(b)). The tin oxide columns (average diameter of ∼25 nm) are densely packed with other larger fine-grained columns (∼50 nm average diameter). Finally, when growing at 600 °C, the films exhibit a completely columnar nanostructure, composed of well defined SnO_2 columns (20–30 nm in diameter, as shown in figure 8(c)). The nanograins were also characterized in detail by means of high resolution TEM. It was found that the average grain size of the films gradually increases from about 4 nm at 20 °C to about 12 nm at $\geqslant$450 °C.

The room-temperature electrical resistivity of the tin oxide films was studied as a function of the substrate growth temperature. The films deposited under vacuum (regardless of T) or under oxygen at the lowest temperature (20 °C) were observed to be highly insulating. The significant increase of grain size (from 4–5 to 10 nm) coincides with an abrupt decrease of film resistivity observed in the 150–300 °C interval and this indicates a probable correlation between growth temperature and morphology, which also affects the resistivity. Above 300 °C, the mean grain size is practically constant and is related to slight variations in resistivity. This suggests that the conductivity of the tin oxide films is most likely influenced by free-carrier scattering at grain boundaries. At the same time, the slight resistivity changes measured in the 300–600 °C range are correlated with the corresponding nanostructured morphologies. In fact, the apparent inter-columnar porosity exhibited at 600 °C (cf figure 8(c)) accounts, at least partially, for the slight increase in resistivity.

These studies confirm that substrate temperature is a key kinetic parameter that can be used to control the morphological properties of heteroepitaxial films grown by laser ablation. I will show in the section on semiconductor nanostructures that this is true for growth processes in general: changes in growth temperature (as well as changes in growth rate, for example) lead to drastic changes in the size and shape of the as-grown nanostructured material and may even lead to changes in composition (caused by intermixing, or interdiffusion processes that are thermally activated).

3. Nanostructured magnetic surfaces

It is well known that crystal solids in which individual magnetic ions have net average vector moments below a critical temperature T_c (called the Curie temperature) are called

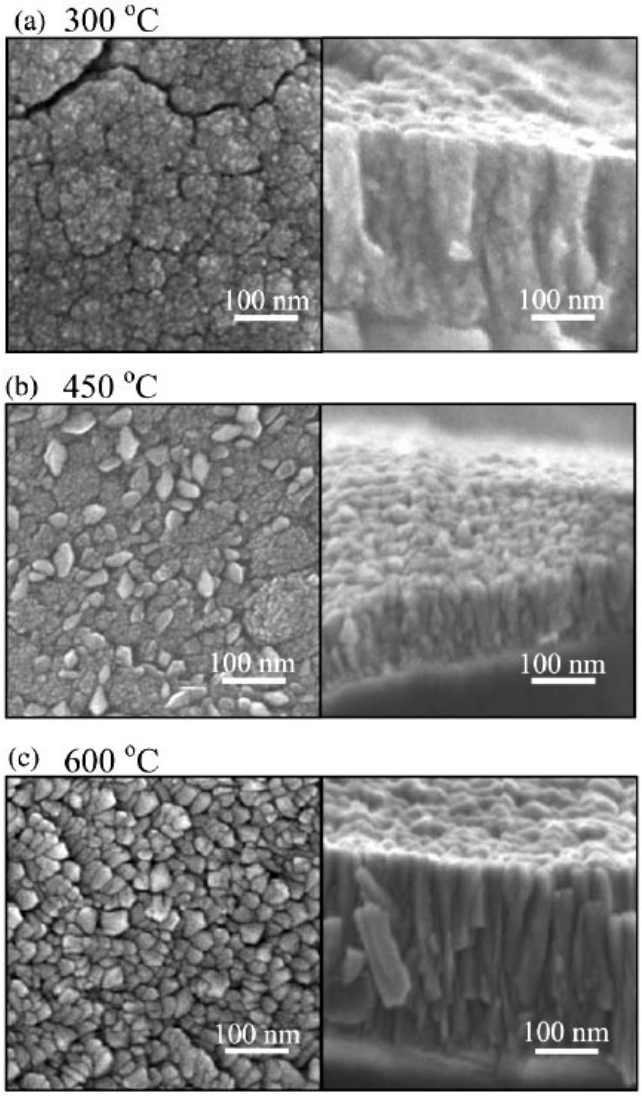

Figure 8. SEM micrographs (top (left-hand column) and cross-sectional (right-hand column) views) of SnO_2 films grown by laser ablation on poly-Al_2O_3 substrates under 150 mTorr partial pressure of oxygen at increasing T values: (a) 300 °C; (b) 450 °C and (c) 600 °C. Nanostructured grains and domains are clearly visible (Dolbec *et al* 2002).

magnetically ordered. If the magnetic moments in such a magnetically ordered crystal sum up to a net magnetization density, they exhibit a macroscopic bulk magnetization and are called *ferromagnetic*. This section will focus on magnetic nanostructures such as thin films, nanoparticle arrays and patterned films. I will discuss some aspects of these systems, including growth, fabrication and characterization. Examples include low-dimensional magnetism, magnetic anisotropy, effects of structural disorder and hysteresis.

The magnetic structure and magnetization reversal of small magnets have been studied intensively due to fundamental research interest and for potential applications in high density storage media (e.g. magnetoresistive random access memory (MRAM) devices (Wiesendanger

1994)). As the particle size becomes smaller, the formation of domain structures (which are present in bulk magnetic crystals) is not energetically favourable (Kleiber *et al* 1998, Shen *et al* 1997). Indeed, below a certain critical size (typically in the 10–100 nm range), a magnetic particle cannot support more than one domain. Elliptical particles or elongated particles with a high aspect ratio can form single domain structures, while particles with a circular shape tend to form a *vortex* state (Schneider *et al* 2000, Cowburn *et al* 1999).

Just as I have discussed at length in the section on surface effects, the magnetic properties of nanometre-scale structures can differ significantly from bulk properties, giving rise to interesting and technologically important behaviour. Indeed, ultrathin magnetic films are widely studied because of their surprising phenomenology: as the film thickness is reduced, the influence of the surfaces increases and, in some cases, there may be an unexpected change in anisotropy, from in-plane to out-of-plane easy axis.

In this context, major advances were made possible by the development of new instrumentation, such as scanning electron microscopy with polarization analysis (SEMPA), spin-polarized STM, Lorentz force microscopy, magneto-optical Kerr effect (MOKE) and MFM (Grütter *et al* 1992). Indeed, MFM has led to the investigation of magnetic configurations in nanostructured surfaces with unprecedented resolution and sensitivity, opening new perspectives in this field of research. Magnetic domains as small as 50 nm across have been imaged with high contrast (Hehn *et al* 1996, Gehanno *et al* 1997) and down to extremely low thicknesses of the magnetic layer (Bochi *et al* 1995).

3.1. Arrays of magnetic nanoparticles and patterned magnetic films

Standard micro/nanofabrication methods (e.g. focused ion beam (FIB), photolithography, electron-beam lithography (EBL) and lift-off techniques) may be used to obtain nanopatterned magnetic films. In a recent series of studies (Zhu *et al* 2002a, 2002b, 2002c, 2003a, 2003b) these techniques were used to fabricate magnetic disks with different aspect ratios and widths. Magnetic force microscopy with *in situ* magnetic fields was then used to study vortex structures and magnetization reversals. The configurational anisotropy originating from inter-dot coupling was measured directly from hysteresis curves obtained by MFM and imaging.

In this context, it is important to be aware that the MFM tip can cause a severe distortion of the observed magnetic structures (Grütter *et al* 1992). In particular, when the particle size is of submicron dimensions, the tip's stray field may cause strong effects, especially when imaging magnetically soft clusters or while scanning in the presence of an external magnetic field.

A typical example of this type of distortion is reported in figure 9. The MFM image on the left reveals that the nanoparticle forms single domains. The middle scan shows that the particle has a *double* domain structure. By closely inspecting the raw data, Zhu *et al* (2002b) noticed that the contrast changed abruptly in a single scan line. This implies that the stray field induced by the tip is responsible for reversing the particle's moment. Finally, the image on the right pinpoints the same particle again forming a single domain state, but with reversed orientation compared to that in the first image. This kind of reversal is very common in large area scans, to the point that *multiple* reversals of the same particle are often observed. Clearly, the occurrence of tip-induced magnetic reversal may depend on the tip's stray field, the local switching field of the individual particles and on the separation between tip and sample. Therefore, because of the unavoidable perpendicular and in-plane tip stray fields, it can be very challenging to image the undistorted magnetic structure of soft, small particles by MFM. The tip's magnetic moment may be minimized, thereby reducing the tip's influence: however, this occurs at the

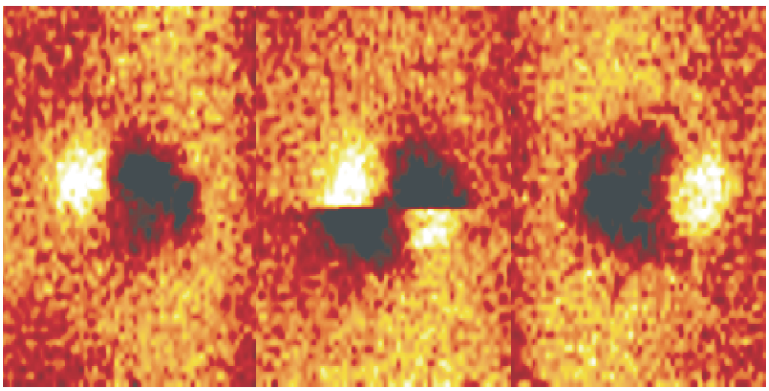

Figure 9. Three consecutive MFM images of the same 200 nm × 500 nm particle. The tip is a 60 nm permalloy coated probe. The images were acquired in air using tapping/lift mode with a lift height of 80 nm on a digital instruments multimode nanoscope (Zhu *et al* 2002b).

expense of the signal that can be measured. Zhu *et al* (2002b) observe that the signal-to-noise ratio can be somewhat improved by operating the MFM in vacuum, and/or by working at LT. Interestingly, they also show that, at small tip–sample separations, the tip can change the particle's moment (i.e. write information), while at large tip–sample distances the tip can read (digital) information stored in the particle. This technique may be used to control the inputs and outputs of submicron-sized magnetic cellular automata (Cowburn and Welland 2000).

In a related series of experiments, Zhu *et al* (2002a, 2002c) examined the vortex structure of microfabricated *permalloy* disks (realized by means of EBL and lift-off techniques) and its magnetization reversal. Again, these experiments were performed in constant height mode to reduce MFM tip–sample interactions, which can be destructive. High-resolution MFM images show that a vortex state may form inside the disk, as shown in figures 10(a) and (b). In the micrograph, the disk shows weak contrast with a bright spot in the centre. This spot represents a flux core, i.e. a singularity of the vortex state in the permalloy dot, which was directly observed only recently (Schneider *et al* 2000, Shinjo *et al* 2000). Figures 10(c) and (d), on the other hand, display images obtained with an external field applied diagonally along the image area. Not surprisingly, the flux core moves closer to the edge and perpendicular to the field direction.

A distinct characteristic of magnetic disks, recently confirmed by measuring the hysteresis loop of arrays of dots or by studying individual disks, is that the magnetization reversal has two transitions: the nucleation and annihilation of the magnetic vortex. By developing a local hysteresis loop technique, and with a careful analysis of tip stray fields, Zhu *et al* (2002a) characterized the two transitions of a single dot. In particular, there were obtained accurate measurements of the disk's switching fields, without artefacts caused by tip stray fields. By characterizing ensembles of disks, Zhu and co-workers reported hysteresis curves (corresponding to switching probabilities) along two different surface directions. These curves clearly show a two-step transition. The work by Zhu *et al* (2002a, 2002b, 2002c) has provided new and important insights into the nanoscale properties of microfabricated magnetic surfaces.

3.2. Direct growth of magnetic thin films

An alternative to the use of lithography and other surface patterning techniques is to use self-assembly, or the direct growth of thin films, for example by molecular beam epitaxy (MBE). Such deposition processes are typically carried out at substrate temperatures that are well below the Curie temperature of the material and this leads to the nucleation of magnetic

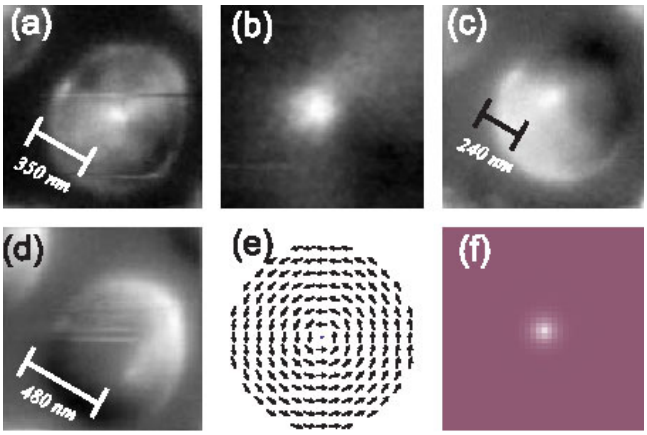

Figure 10. Series of MFM images showing: (a) vortex structure of permalloy disk; (b) zoom-in of a vortex core with 140 nm scan size; (c) image at a field of 23 Oe; (d) image at a field of −55 Oe; (e) simulated moment distribution of a permalloy disk with the same size as the experiment; and (f) grey scale shows the moments of the out-of-plane component in a 140 nm area of (e) (Zhu *et al* 2002a).

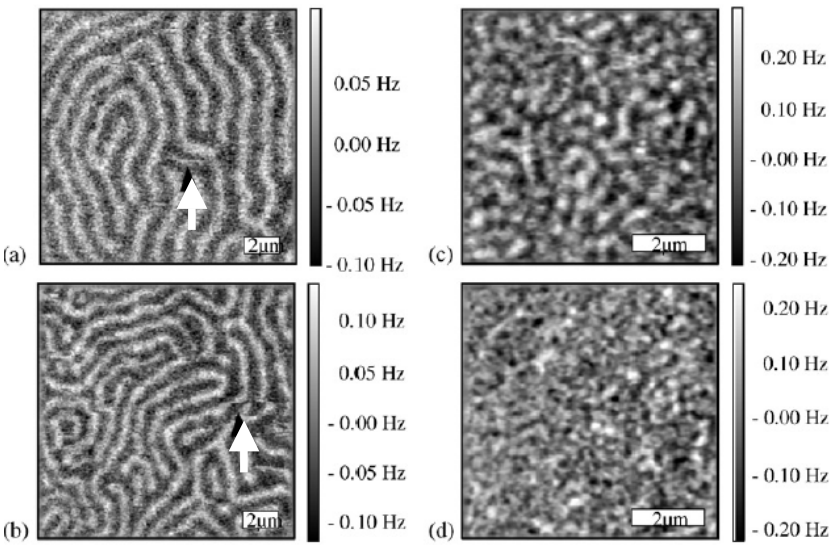

Figure 11. Four MFM images of magnetic domains for different Fe thicknesses: (a) 3.43, (b) 3.51, (c) 3.69 and (d) 3.77 atomic layers of iron. All images have been filtered. The arrows indicate movement of the domain walls under the influence of the tip. (Note that the scan size in (a) and (b) is larger in images (c) and (d).) (Hoffmann *et al* 2002).

domains during growth. If the growth is heteroepitaxial, i.e. the deposited material is different from the host substrate, the equilibrium size of the magnetic domains may decrease as the deposited thickness increases (the heteroepitaxial growth of thin films will be discussed more thoroughly in a separate section). In this case, the domains that nucleate at the early stages of growth are subject to a very large strain as the layer thickness increases. This is what happens, for example, during the growth of FePd films on MgO(001) (Hoffmann *et al* 1999).

In this case, MFM images show that the equilibrium domain size decreases exponentially when increasing the layer thickness. This is ascribed to the competition between the domain wall energy and the magnetostatic energy. As a result, the pre-existing magnetic pattern that results from direct growth is subject to very high strain fields. This study offered a more complete understanding of the pathway followed by an out-of-equilibrium magnetic configuration to shift towards equilibrium in an ultra-thin magnetic layer.

Another interesting phenomenon that may occur during the growth of thin magnetic films is the change of anisotropy from in-plane to out-of-plane easy axis, caused by surface anisotropy. This is what happens, for example, during the growth of Ag/Fe/Ag multilayers, or 'sandwiches'. These films show a magnetic reorientation transition as a function of film thickness and temperature. In particular, if the film thickness is thinner than 3–5 monolayers (ML), the Fe layer is magnetized *out of plane*, whereas film magnetization lies *in the plane* above this critical thickness. The anomaly of thin iron films embedded in silver layers is that this reorientation transition takes place at low thicknesses, so that the film essentially still behaves like a 2D structure.

In a recent study (Hoffmann *et al* 2002), Fe films (thicknesses between 0 and 7 MLs) sandwiched between two Ag thin layers were investigated by MFM. Magnetic domains with the axis perpendicular to the surface were imaged for film thicknesses ranging from 3.34 to 3.77 iron atomic layers, as shown in figure 11. In the simplest description, black contrast in MFM images (attractive force) corresponds to domains that point into the sample plane, while white contrast (repulsive interaction) is related to domains pointing out of the sample plane. At small thicknesses, the domains are observed to be somewhat larger and stripe-shaped, whereas in thicker films the domain size decreases and the domains become more isotropic. When the magnetic contrast is very small, MFM images may be severely influenced by sample topography (i.e. film roughness). However, by comparing their MFM images to STM images acquired on similar samples, Hoffmann *et al* (2002) pointed out that the observed structural morphologies are completely different. Thus the contrast observed in MFM micrographs must originate from the magnetic domain structure of the film.

To advance our understanding of nanostructured magnetic surfaces, it will be beneficial to work on the atomic scale. Recently a bottom-up approach was used to investigate the development of the magnetization in transition-metal particles (Co) deposited on a nonmagnetic (Pt(111)) substrate (Gambardella *et al* 2003; see also Rusponi *et al* 2003). Isolated magnetic atoms were deposited on an atomically ordered metal surface. Subsequently the particle size was increased in a quasi-atom-by-atom fashion. The measurement of the orbital magnetic moment and the magnetic anisotropy energy in single-surface adatoms and small particles in this critical size range was reported and compared with *ab initio* calculations. The work reported by Gambardella and co-workers is highly innovative, because it provides a fundamental understanding of the magnetic properties of nanoscale clusters and enables us to test state-of-the-art theoretical models at the atomic scale.

4. Nanostructured ferroelectric surfaces

A solid crystal whose primitive cell has a permanent dipole moment $\mathbf{p}_0$ is called *pyroelectric* (Ashcroft and Mermin 1976). A crystal, whose structure is non-pyroelectric above a certain temperature T_c (known as the Curie temperature, in analogy with ferromagnetic crystals) and pyroelectric below it, is known as *ferroelectric*.

Generally speaking, ferroelectricity is a collective phenomenon that is directly related to crystal composition and symmetry. In the context of nanoscale phenomena, the critical size of atomic domains needed to induce ferroelectricity is a crucial issue (Damjanovic 1998).

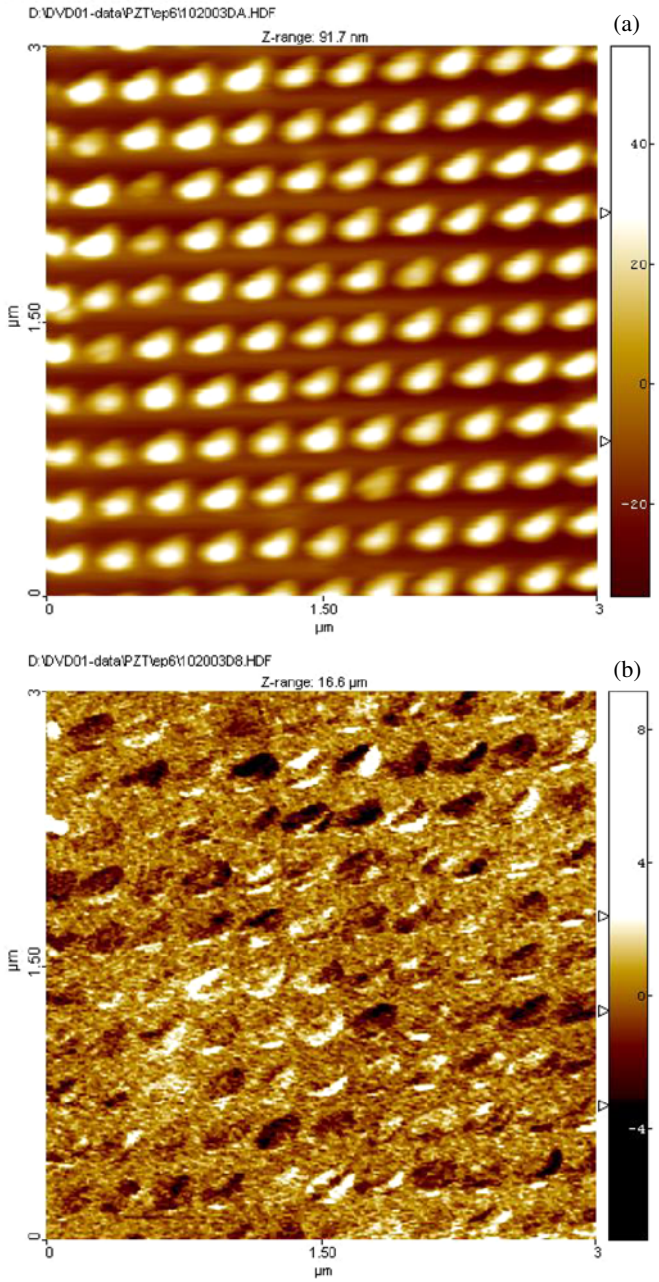

Figure 12. (a) AFM image of an array of PZT (lead zirconium titanate) ferroelectric nanostructures. The nanostructures were fabricated using e-beam lithography. (b) Piezoresponse image presenting the ferroelectric domains of the nanostructures shown in (a). Scan size is $3 \times 3\ \mu m^2$ (Harnagea 2001).

In the effort to increase the capacitance of microelectronic devices, ferroelectric materials may soon come to replace silicon oxide microcapacitors. A ferroelectric capacitor has a 100 times larger dielectric constant and therefore can provide the same capacitance in an area 100 times smaller. The pyroelectric properties of these materials are exploited in infrared sensors

and fire detectors, while their piezoelectric properties are used in integrated actuators and sensors and MEMS devices. At the same time, the study of the photoelectric properties of ferroelectric oxide thin films and heterostructures has shown that these materials have good detection properties in the UV region of the electromagnetic spectrum. A prominent advantage with respect to III–V semiconductors and other detecting materials is that ferroelectric thin films can be deposited using inexpensive methods (e.g. chemical solution deposition (CSD)) with a quality sufficient to use them as photoconductive or photovoltaic detectors.

The issue of a critical thickness for ferroelectricity has recently been revived by industrial interest in integrating ferroelectric oxide films into microelectronic devices, compatible with the constraints in size reduction imposed by today's technology (Satyalakshmi *et al* 1999, Alexe *et al* 2000, Pignolet *et al* 2000, Harnagea *et al* 2003). Recent experiments showed that ferroelectric phenomena may occur in perovskite films as thin as 4 nm (equivalent to ten unit cells). On the other hand, several theoretical predictions state that there should be a polarization reduction in the vicinity of surfaces and interfaces, caused by depolarizing fields. This implies a loss of stability of the polar state, below a certain domain size. In this case, effects that are already present but negligible at larger sizes may become dominant in nanoscale structures. Moreover, if ferroelectricity is still present in domains composed of only a few unit cells (with dimensions of the order of the nanometre), quantum effects are likely to intervene or even become predominant.

Several methods may now be exploited to fabricate sub-micron ferroelectric structures, with a lateral resolution smaller than what can usually be obtained by means of photolithography[13]. Examples include: patterning by FIB, EBL, nanoimprint lithography (NIL) (Harnagea *et al* 2003), nanostencil techniques (deposition through a shadow mask) and self-assembly of nanostructures by direct growth, for example by MBE, PLD or reactive ion sputtering. Figure 12(a) displays an AFM image of an array of ferroelectric nanostructures obtained by EBL. The smallest features have a lateral dimension of $\sim$100 nm.

The most widely used technique for probing the ferroelectric properties of structures at the nanometric scale is called piezoresponse force microscopy (PFM) (Harnagea *et al* 2000, Alexe *et al* 1999a). This is an indirect method, since it only measures the piezoelectric properties that are always present in a ferroelectric material. In brief, the ferroelectric structure is immersed in a modulated electric field by applying a potential difference between the conducting tip of an AFM and a bottom electrode located underneath the material. Subsequently the amplitude of the synchronous surface vibration produced by the converse piezoelectric effect is detected by the SPM (using the normal detection mode, with the aid of a lock-in amplifier). The SPM tip can also be used to apply a much larger switching electric field to the nanostructures. This allows us to image the existent ferroelectric domain structure and to modify it in a controlled way at the same time. A PFM image of an array of ferroelectric nanostructures (the same as imaged by AFM in figure 12(a)) is displayed in 12(b).

A complete analysis of the piezoresponse of ferroelectric domains in nanocrystallites allows, in principle, the study of ferroelectric properties at nanometre length scales. For example, ferroelectricity was observed for PZT nanocrystallites about 100 nm in lateral size, with different orientations (i.e. the film is *polycrystalline*). A study of the ferroelectric properties of nanostructures with even smaller sizes has yet to be performed and is one of the most important challenges to be addressed in the near future. These investigations may soon lead to practical ferroelectric random access memory (FRAM) cells, to be used as data storage devices.

[13] This is the 'traditional' microfabrication technique that has been used by the semiconductor industry for the past three decades.

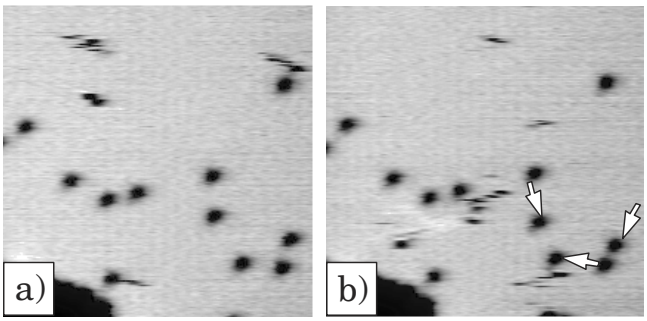

Figure 13. STM images of Ru(0001) recorded after the adsorption (dissociative chemisorption) of 0.1 L NO at 300 K. (a) and (b) were recorded successively on the same area. The arrows mark N atoms that have moved between images (a) and (b). Image size: 70 Å × 70 Å; tunnelling parameters: $V_t = 20.6$ V, $I_t = 1$ nA (Zambelli *et al* 1996a).

5. Surface diffusion phenomena studied by STM

In the last decade, progress in instrumentation, such as the development of fast-scanning STM prototypes (typically home built), has significantly advanced the investigation of surface diffusion processes on the nanometre length scale. The diffusion of adparticles, previously studied by field ion microscopy for metals on metals (Kellogg 1994), has been directly observed on the atomic scale in a large number of cases by STM for various adsorbates (Oh *et al* 2002, Zambelli *et al* 1996a, Renish *et al* 1999, Linderoth *et al* 1999, Swartzentruber 1996, Barth 2000) on a wide range of surfaces. A thorough understanding of surface diffusion processes is important, because diffusivity induces adatoms and molecules to interact on a substrate and eventually form heterostructures, molecular nanostructures and self-assembled monolayers.

Previous macroscopic experiments for determining adsorbate diffusion constants had encountered severe difficulties, as reviewed by Barth (2000). Even a well prepared single crystal surface in fact exhibits defects, mostly in the form of atomic steps, kinks and impurities. Hopping energies at sites with different local structures may differ significantly, to the point that macroscopic experiments can only probe 'effective' diffusion parameters averaged over many different elementary hopping processes. Thus, the information resulting from integrated techniques is often difficult to interpret, if not meaningless altogether.

By using newly developed fast STMs, capable of acquiring up to 20 images (typically 50×50 Å^2 wide) per second while still maintaining atomic resolution, it is now possible to follow the dynamic behaviour of individual guest atoms, vacancies and molecules on several host metal surfaces (Pedersen *et al* 2000, Wintterlin *et al* 1996, Zambelli *et al* 1996a, Renish *et al* 1999, Schaub *et al* 2003, Linderoth *et al* 1999, 1997, Schunack *et al* 2002a). This method consists in taking a long sequence of images of the same region of the surface and recording those atoms which have moved (normally by one lattice parameter) between consecutive frames, as shown in figure 13.

A surface diffusion process can be generally described as a two-dimensional *random walk* performed by an adsorbate species that hops with a rate h between adjacent adsorption sites on a given substrate. Even while being bound to the surface in fact, the adsorbate may jump around on the surface, provided that it has enough energy. This excess energy is, in general, a fraction of the adsorbate's binding energy to the substrate and it may be supplied by surface phonons, if the temperature is high enough.

The three parameters that are generally used to describe diffusion processes are the following:

(i) to hop between nearest-neighbour sites, an adsorbate has to overcome a barrier on the potential energy surface. This barrier is called the activation energy for diffusion, E_d;
(ii) the frequency with which an adsorbate tries to overcome the energy barrier is called the attempt frequency, h_0;
(iii) finally, the root-mean-square jump length λ contains information on the average number of sites spanned in a single jump.

The diffusion constant $D = \langle(\Delta x)^2\rangle/2dt$ is defined as the molecular mean-square displacement, $\langle(\Delta x)^2\rangle$, during the image acquisition time t (here d is the dimension of the random walk: hence, in general, it is 2 in the case of a surface, but it may be 1 if the substrate is anisotropic). Both the hopping rate h and the diffusion constant D have a temperature dependence that is generally described by the Arrhenius law (see, e.g. Barth 2000):

$$h = h_0 \exp(-E_d/kT) \qquad \text{and} \qquad D = D_0 \exp(-E_d/kT). \tag{1}$$

Here h_0 and D_0 are the prefactors for the hopping rate and the diffusion constant, respectively, k is Boltzmann's constant and T is the temperature. The activation energy of diffusion E_d as well as the prefactors can then be extracted from equation (1) by means of a so-called Arrhenius analysis or *plot*, in which $\ln h$ or $\ln D$ is plotted versus $1/kT$.

From an experimental point of view, the probability P that atoms are still found on their original site at time t (i.e. the probability of moving zero steps) is obtained by counting the proportion of atoms or molecules that have not moved between consecutive images. If we assume that the jumps are statistically independent (which is usually the case if coverage is low enough), then as a first approximation this probability is given by the Poisson statistics:

$$P(t) = \exp(-t/\tau). \tag{2}$$

Here τ is the mean time an adatom spends on its adsorption site. The hopping rate h is just the inverse of τ. By performing the experiment at several different temperatures, it is generally found (as expected) that the elementary jump rate follows the law of a thermally activated process (Arrhenius behaviour).

To carry out a quantitative analysis in terms of the diffusion constant D, on the other hand, it is necessary to evaluate atomic or molecular displacements Δx between consecutive images. The atomic or molecular mean-squared displacement, $\langle(\Delta x)^2\rangle$, can be calculated directly from the displacement distribution (Linderoth 1998).

The values of the pre-exponential h_0 and of the energy barrier have now been determined for several systems (Pedersen *et al* 2000, Wintterlin *et al* 1996, Zambelli *et al* 1996a, Renish *et al* 1999, Schaub *et al* 2003, Linderoth *et al* 1999, 1997, Schunack *et al* 2002a). These results are to be viewed as real breakthroughs: having isolated a single elementary step of a surface process, this can now yield a detailed comparison between theory and experiment.

However, there are very few detailed studies so far on the surface mobility of complex molecules (Weckesser *et al* 1999, 2001a, Barth *et al* 2000). To exploit organic molecules as building blocks in nanoscale devices it is *essential* to acquire quantitative information on their mobility on a substrate of choice. This knowledge, for example, may lead to the design from first principles of molecules which will *not* diffuse on the surface at RT. On the other hand, quantitative information on energy barriers and diffusion constants is important to predict the growth properties of organic thin films. In turn, this is necessary to fine-tune the morphology and physical properties of such films.

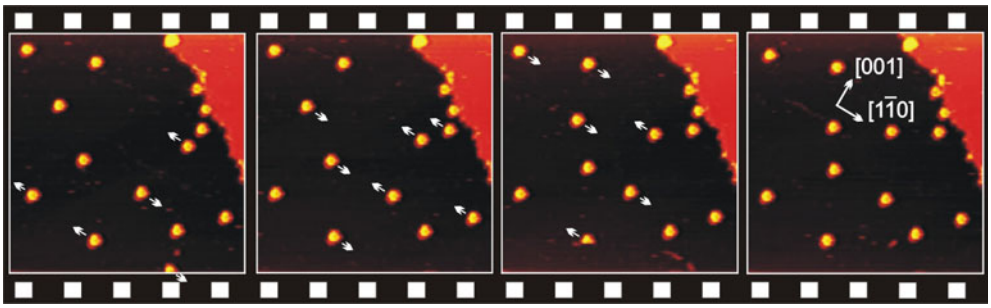

Figure 14. Four stills extracted from a STM movie of HtBDC molecules diffusing on Cu(110) at $T = 194$ K. The molecules are imaged as bright spots. Image size is 50×50 nm^2. Each movie is composed of 400–2500 image-to-image observations of individual, diffusing molecules (a complete movie can be downloaded at http://www.phys.au.dk/camp/movies/ht79.mpg). Molecular displacements are clearly visible: arrows indicate the direction in which the molecules will have moved in the successive image (Schunack *et al* 2002a).

An elaborate quantitative analysis of surface diffusion shows that it is possible, to some extent, to tailor molecular diffusion properties by designing molecules with the appropriate chemical structure. This was recently demonstrated by Schunack *et al* (2002a), who compared the diffusion of two related organic molecules, decacyclene (DC) and hexa-di-*tert*-butyl decacyclene (HtBDC), on the same anisotropic metal substrate, Cu(110). It was inferred that, by raising the aromatic plane common to DC/HtBDC away from the surface using appropriate spacer groups in the case of HtBDC, this molecule has a diffusion constant which is approximately four orders of magnitude higher compared to that of its related DC molecule on the same surface (Schunack *et al* 2002a, 2003, Schunack 2002). This work also showed that, at very low coverage, molecular surface diffusion depends critically on molecule–surface interactions. Direct observations indicated that at higher coverages molecule–molecule interactions become important, although quantitative results are still missing. Although an atomistic description of the origin of long jumps is still lacking, clearly the higher diffusivity for HtBDC is both due to larger root-mean-squared jump lengths and to a lower activation barrier for diffusion. This, in turn, implies that the adsorption energy of HtBDC on Cu(110) is comparatively smaller than that of DC.

The surface diffusion of large organic molecules was studied by acquiring time-resolved STM movies, using a fast-scanning, home-built STM (Schunack *et al* 2002a, Laegsgaard *et al* 2001). Both DC and HtBDC were observed to diffuse along the close-packed [1$\bar{1}$0] direction of the Cu(110) substrate, as indicated in figure 14 (Schunack *et al* 2002a). They are therefore constrained to move in only one dimension because of the anisotropy of Cu(110).

From the Arrhenius plots of h and D for DC and HtBDC, the activation energies and prefactors were determined to be 0.60 eV (HtBDC) and 0.72 eV (DC), respectively. The lower activation barrier for diffusion of HtBDC (compared to DC) is attributed to its six *tert*-butyl spacer groups. The effect of these groups is to effectively increase the distance between the aromatic π system and the surface, which are generally believed to have a strong attractive interaction.

Another important parameter for diffusion is the average jump length of molecules between different adsorption sites. In the simplest picture, adsorbate migration occurs by random jumps between nearest-neighbour sites (Linderoth *et al* 1997). Long jumps (spanning more than one lattice site) are also believed to contribute to the diffusion process in the case of weak adsorbate–substrate interaction (Boal *et al* 2000), but experimental evidence for such events is still very limited and restricted to the mobility of metal adatoms and clusters (Linderoth *et al* 1999).

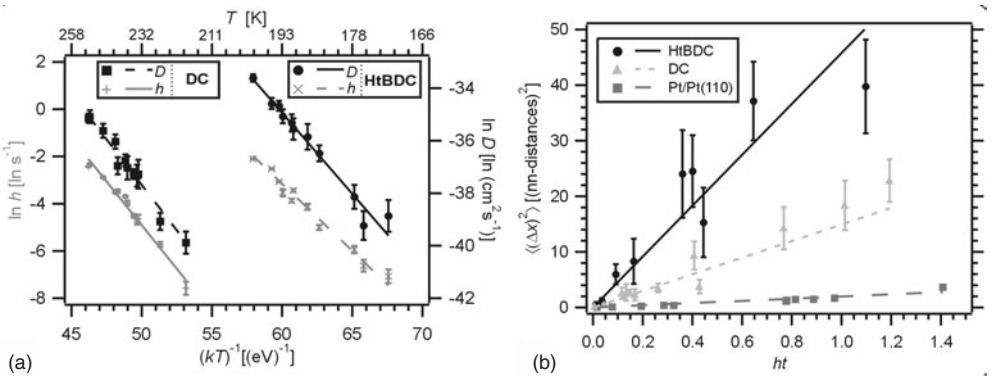

Figure 15. (a) Arrhenius plots of hopping rates h (grey) and tracer diffusion constants D (black) for DC (left) and HtBDC (right). Straight lines are best fits to the Arrhenius expression for h and D (see equation (1)). (b) Plot of mean-squared displacement $\langle(\Delta x)^2\rangle$ versus ht for HtBDC and DC. The data for diffusion of Pt on Pt(110) are also reported. Straight lines are best fits to equation (2). yielding root-mean-squared jump lengths (Schunack *et al* 2002a).

A new, simple approach to determine root-mean-square jump lengths λ in surface diffusion was recently proposed. It is based on the fundamental relation (Schunack *et al* 2002a)

$$\langle(\Delta x)^2\rangle = \lambda^2 ht. \tag{3}$$

This equation can be used to determine the root-mean-squared jump length, if $\langle(\Delta x)^2\rangle$ and h are measured independently from sequences of consecutive STM images. Surprisingly, it was found that long jumps play a dominant role in the diffusion of DC and HtBDC on Cu(110) (Schunack *et al* 2002a). The root-mean-squared jump lengths are determined (see figure 15(b)) to be as large as $\lambda = 3.9 \pm 0.2$ and 6.8 ± 0.3 Cu nearest-neighbour distances for DC and HtBDC, respectively (Schunack *et al* 2002a).

This result is in strong contrast to what is observed in metal-on-metal diffusion, for which typical root-mean-squared jump lengths are close to one lattice spacing. Figure 15(b) also displays data for the diffusion of Pt on Pt(110), in which $\lambda = 1.1$ Pt nearest-neighbour distances. This shows that Pt adatoms preferentially jump between nearest-neighbour sites and the contribution of long jumps is only of the order of 10%, in excellent agreement with previous work (Linderoth *et al* 1997).

In conclusion, these results show the possibility of tailoring molecular diffusion properties: by raising the aromatic plane common to DC/HtBDC away from the surface by spacer groups in the case of HtBDC, this molecule has a diffusion constant which is approximately four orders of magnitude higher compared to that of its related molecule (DC) on the same surface. The higher diffusivity is due to a combination of larger RMS jump lengths and a lower activation barrier for diffusion.

5.1. Correlated diffusion processes

As I mentioned above, surface diffusion processes become significantly more complex when coverage is higher (Trost *et al* 1996, Renish *et al* 1999), because molecule–molecule interactions may become significant, if not even predominant. If the coverage is sufficiently high, molecular dimerization or chain formation may occur.

A striking example of this was reported by Briner *et al* (1997), who studied the diffusion of carbon monoxide on the (110) surface of copper in the temperature range 42–53 K. They report an attractive interaction between CO molecules, which leads to the formation of CO

dimers and even longer molecular chains. Surprisingly, CO chains and dimers were observed to diffuse much faster than isolated molecules, indicating that they are less bound to the surface than single molecules.

In a more recent, very elegant study, Renish *et al* (1999) observed the diffusion of O atoms on a Ru(0001) surface. By means of a special fast-scanning STM system, they were able to study atoms with ultra-short residence times (down to 10 ms) at RT and to record large data sets within reasonable periods of time. From a statistical analysis of the changes of atom configurations in sequences of more than 1000 images, mean residence times of oxygen atoms in the neighbourhood of other oxygen atoms were extracted. The jump distribution was observed to be completely isotropic, meaning that it did not show any correlation with the scanning direction. Careful checks for a possible STM tip effect (see the next subsection) revealed that it remained negligible as long as the tunnelling resistance is not too low (<1 MΩ).

5.2. Influence of the STM tip in studying diffusion processes

As I have outlined in the introductory section, it is now well known that, besides the normal imaging mode, the STM tip can also be used to manipulate atoms and molecules bound to a surface in a controlled manner (Eigler *et al* 1991, Stroscio and Eigler 1991, Hofer *et al* 2001, Rosei *et al* 2002a). Clearly, when studying adsorbate surface diffusion any influence from the tip must be carefully avoided. This phenomenon was treated theoretically, revealing that, besides a direct attractive/repulsive interaction between tip and adsorbate, the tip can actually modulate the potential energy hypersurface, thereby indirectly influencing the diffusion process through the activation energy of the process itself (Sørensen *et al* 1996, Kürpick and Rahman 1999, Hofer *et al* 2001).

I will now draw again from a recent experiment to show that, by choosing appropriate tunnelling parameters, it is possible to avoid any tip influence (Linderoth 1998, Schunack 2002). In particular, I will show that the mean square displacement and the hopping rate of DC and HtBDC molecules chosen for the comparative diffusion study described previously (Schunack *et al* 2002a) can be made independent of the scanning process. (The tip's influence was minimized by scanning with a tunnelling resistance above 5 GΩ (Schunack 2002).) To clarify whether or not the tip influences the diffusion process, displacement distributions were inspected at several different temperatures[14]. These distributions were always found to be symmetric around a mean value of $\langle \Delta x \rangle = 0.0 \pm 0.8$ Å, indicating that there is no appreciable tip influence. Possible tip-induced artefacts were further investigated by varying the interaction time between tip and molecule[15]. This was done by either changing the image size and/or acquisition time, resulting in a variation of the interaction time (Schunack 2002) between 30% and 300% (as compared to regular 500×500 Å^2 images, which were acquired in $\sim$14 s). No deviation beyond the usual spread around the linear Arrhenius plots was observed. This confirms that there is no influence of the scanning process on the hopping rate or the hopping displacements (Schunack 2002). Finally, the influence of the tip was investigated directly by performing controlled STM manipulation experiments. It was found that it is not possible to manipulate DC and HtBDC if tunnelling resistances above 100 MΩ and 1 GΩ are used, respectively. These values are well below the ones used for imaging during the study of surface diffusion. All the results support the conclusion that, under the specified experimental conditions, the obtained diffusion parameters are not influenced by the scanning process (Schunack 2002).

[14] From high resolution, small-scale images it is known that DC and HtBDC have specific adsorption sites which are spaced in integral multiples of the nearest-neighbour lattice distance.

[15] The interaction time is defined as the time necessary for the tip to scan directly over a molecule.

6. Organic molecules at metal surfaces: a few selected examples

Complex organic molecules have recently attracted interest (Rosei *et al* 2003) both from a fundamental point of view and for prospective applications in nanotechnology, since they may be used as basic building blocks for molecular nanodevices (Nilius *et al* 2002, Meyer zu Heringdorf *et al* 2001, Gross *et al* 2003, Forrest 1997, Böhringer *et al* 1999, Barth *et al* 2003, Yokoyama *et al* 2001, Weiss 2001, Hamers 2001). To develop molecular devices that operate on the nanoscale it is important to gain an insight into the fundamental processes that occur when a largish molecule adsorbs on a substrate. Complex molecule–surface interactions (Lippel *et al* 1989, Boland 1990, 1992) are responsible for a variety of phenomena, such as molecular diffusion and self-assembly of molecules into ordered structures (Okawa and Aono 2001, Qiu *et al* 2003, Ruiz *et al* 2003, Casalis *et al* 2003, Theobald *et al* 2003). Furthermore, upon molecular adsorption surfaces often do not generally behave as static templates, but may rearrange dramatically to accommodate different molecular conformations. In turn, the strong interaction with the substrate can lead to conformational changes within the adsorbed molecules.

Developing nanomolecular devices involves investigating several different aspects such as changes of the molecular conformation upon adsorption, diffusion, molecule-induced restructuring of the topmost metal layers and finally molecular self-assembly, with the ultimate aim of designing bottom-up nanomachines (Aviram and Ratner 1974, Avouris 1995, Andres *et al* 1996, Barth *et al* 2000).

A subtle balance between competing molecule–molecule and molecule–substrate interactions in general controls the bonding and ordering of molecules on surfaces. Non-covalent intermolecular interactions are believed to dominate over molecule–substrate interactions and metal substrates are sometimes considered a static checkerboard that simply provides bonds and specific adsorption sites to the molecules (Boal *et al* 2000, Kühnle *et al* 2002, Marchenko and Cousty 2000). However, when adsorbing organic molecules, the complexity of molecule–surface interaction may increase dramatically, sometimes leading to surface restructuring processes (Gimzewski *et al* 1994, Murray *et al* 1997). Similarly, changes in molecular conformations on the surface compared to gas phase conformations can occur (Jung *et al* 1996, Zambelli *et al* 2001), indicating that it is not possible to transfer *a priori* certain molecular functionalities, designed for molecules in the gas phase, to situations where molecules are adsorbed on a substrate. For example, the exact adsorption conformation may play an important role when measuring the conductance through a single molecule (Kuntze *et al* 2002).

In this section I will mainly address how high resolution STM can be used to investigate the basic adsorption properties of fairly complex (a few hundred atoms at most) organic molecules at metal surfaces (Zambelli *et al* 2002, Schunack *et al* 2003). In general, these studies are made possible by combining the unique imaging and manipulation capabilities of variable temperature STM (Rosei *et al* 2003). Most of the molecules described in the following are to be considered prototypes of molecular electronic devices (designed to act, for example, as molecular wires: see, for example, Joachim *et al* 2000, Rosei *et al* 2002a). In all these experiments, the molecules were transferred onto metal substrates by organic molecular beam deposition (OMBD). Other groups (Lopinski *et al* 1998, 2000a, Kruse *et al* 2002, Lu *et al* 1999, 2000, Petsalakis *et al* 2003, Jiang *et al* 2003, Naumkin *et al* 2003a, 2003b) are investigating the adsorption of organic molecules on semiconductor surfaces[16]. I will illustrate different aspects of molecule–surface interaction as a function of sample

[16] This type of work is outside the scope of the present section, and of this paper at large, and it will be the subject of a forthcoming article (Lopinski and Rosei 2004).

temperature. At LT these systems are essentially static, allowing us to observe conformational changes of the adsorbed molecules. With increasing temperature molecular diffusion sets in and, at RT, molecular self-assembly phenomena take place. These may be accompanied by a restructuring of the underlying metal surface, depending on substrate material and symmetry.

A typical molecule of this type generally consists of a central aromatic board (π system), which is lifted from the surface by so-called spacer groups (see figures 16(a) and (c) and 17(a)). The function of these spacer groups is to act as support legs, thereby electrically isolating the aromatic plane from the metal substrate (Joachim *et al* 2000).

6.1. Molecular adsorption geometries

The structure of a molecule and its many possible conformations when adsorbed on a substrate mostly determine its chemical and physical properties. When organic molecules adsorb on the surface of a metal single crystal, where they typically extend over a considerable number of sites, they must adapt to surface chemistry, geometry and corrugation. It is therefore reasonable to expect that their internal configurations will vary as a result of the interaction.

Molecular conformations at interfaces are very important in organic thin films, particularly in organic optoelectronic devices, since they affect device properties and performance. As a result of the adsorption process, strong molecule–surface interactions may set in, inducing intra-molecular conformational changes, sometimes causing severe distortions, which in turn may affect its overall characteristics. In fact, such conformational changes can be induced not only by the chemical properties of the substrate of choice, but also by its geometrical structure. It is therefore necessary to gain detailed information on the binding geometry of the molecules on the substrate of choice. Until now, molecular conformations have not been studied extensively (Rosei and Rosei 2002, Rosei *et al* 2002a, Schunack *et al* 2002a, Moresco *et al* 2003a). In the following, I will describe some recent experimental and theoretical results that have led to significant insight into conformational changes of complex molecules on metallic substrates. The focus is on molecules from the '*Lander*' family (model systems that are designed to act as 'molecular wires', so named because of their resemblance to a molecular-scale interplanetary spacecraft, similar to the Mars Lander), all of which have a conducting backbone made of an aromatic π system. We will show that, in general, the leading molecule–substrate interaction is determined by the attraction between the π system and the underlying surface, which often causes distorted configurations in the observed molecular shapes. This information is important because it points to the necessity and possibility of custom-designing molecules to confer upon them predefined properties upon adsorption.

When molecules are deposited on a surface at LT, their individual adsorption geometries can be identified in STM micrographs and their conformations can be extracted. These details are accessible by comparing high-resolution STM images with state-of-the-art theoretical calculations. Figures 16(a) and (c) display the chemical structure of two related complex molecules: DC and HtBDC[17]. The two molecules consist of the same aromatic π system, which adsorbs parallel to the Cu substrate. Additionally to DC, HtBDC has six *tert*-butyl groups surrounding its aromatic core (Schunack *et al* 2001, Schunack 2002).

At temperatures below 150 K, the molecules are essentially still and individual molecules can be imaged by STM. The HtBDC molecules are found in two symmetry-equivalent adsorption conformations where each molecule is imaged as six lobes (see figure 16(d)) (Schunack *et al* 2002a) that are arranged in a distorted hexagon with threefold rotational symmetry. From molecular dimensions and elastic scattering quantum chemistry (ESQC)

[17] The diffusivity of these two molecules on Cu(110) was previously compared in the subsection on surface diffusion.

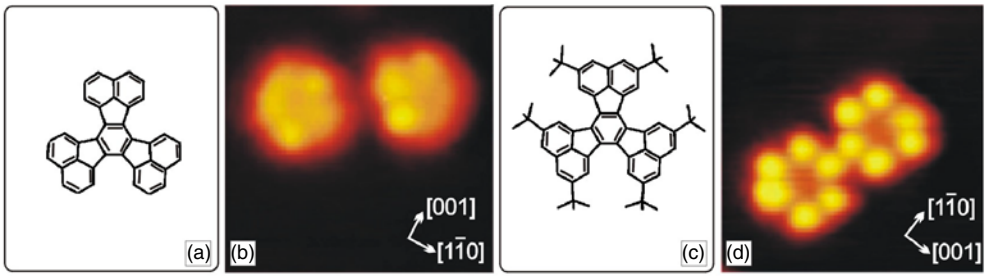

Figure 16. (a) Chemical structure of DC. (b) STM image of DC (5×5 nm^2, $V_t = -1215$ mV, $I_t = -0.11$ nA). (c) Chemical structure of HtBDC. (d) STM image of HtBDC (5×5 nm^2, $V_t = 1250$ mV, $I_t = 0.34$ nA) (Schunack *et al* 2002a).

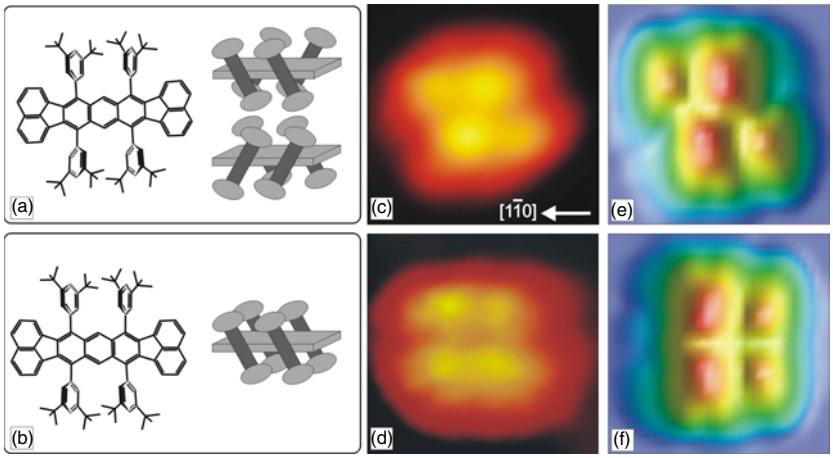

Figure 17. Chemical structure and space-filling model of the Lander molecule in (a) rhomboidal and (b) rectangular shape. STM image of a Lander molecule on Cu(110) at 100 K (2×2 nm^2, $V_t = -1000$ mV, $I_t = -0.21$ nA) with (c) rhomboidal shape and (d) rectangular shape. (e), (f) ESQC-calculated images of rhomboidal (chiral) and rectangular (achiral) Lander molecules, respectively, using the same tunnelling parameters as in experiments. The aromatic board of the Lander molecules is parallel to the close-packed Cu direction indicated in the image (Rosei *et al* 2002a). Copyright American Association for the Advancement of Science ©2002.

calculations (Sautet 1997) it is inferred that the lobes correspond to tunnelling through single *tert*-butyl groups. Accordingly, HtBDC adsorbs, as expected, with the aromatic plane parallel to the substrate.

DC molecules are also found in two symmetry-equivalent adsorption conformations (cf figure 16(b)). However, this molecule does not show a pronounced internal structure as in the case of HtBDC, since the *tert*-butyl groups are missing in this case. STM images again reveal that DC molecules prefer the adsorption geometry with the aromatic plane parallel to the surface, which is caused by the strong interaction between the substrate and the aromatic π system.

Similarly, the Lander[18] molecule ($C_{90}H_{98}$) consists of an aromatic π system (frequently referred to as the '*board*') and four spacer legs that elevate the board from the substrate (figures 17(a) and (b)) (Rosei *et al* 2002a, Schunack *et al* 2002a). Figures 17(c) and (d)

[18] This molecule was originally designed to act as a segment of a molecular wire.

displays a LT (100 K), high-resolution STM image of a single Lander molecule deposited on the Cu(110) surface and the corresponding calculated images (figures 17(e) and (f)) (Schunack *et al* 2002a). The STM images the Lander molecule as four lobes arranged in either a rhomboidal or rectangular geometry.

Based on ESQC calculations (Sautet and Joachim 1991), the two different observed molecular shapes in turn correspond to the two possible geometrical conformations of adsorption of the molecule on this surface: one with the four legs arranged parallel and the other with its legs arranged anti-parallel to each other (figures 17(a) and (b)). The four lobes in the images again correspond to tunnelling through spacer groups of the molecule.

6.2. Manipulation processes

The controlled assembly of molecular arrays (supramolecular chemistry) requires atomic-scale positioning and interlocking of intact molecules, carefully preventing a disruption of their internal structure. This possibility can be explored by using SPM, which combines high-resolution imaging for determining structure and orientation, and the ability to manipulate individual atoms and molecules, virtually at will. At present, scanning probes allow us to perform engineering operations on the nanoscale, manipulating single atoms, molecules and bonds, and have thus become a tool that operates at the very limits of nanofabrication. Manipulations of individual entities on the nanoscale allow the building of pre-designed supramolecular structures, the exploration of the influence of the chemical and geometrical environment on a particular molecule or the development and testing of concepts for new nanodevices. Even though this is, at present, a serial approach and therefore, as such, unsuitable for direct practical applications, it has greatly enhanced our understanding of molecule–substrate and molecule–molecule interactions, opening new perspectives in this field (Heinrich *et al* 2002).

Generally speaking, manipulation experiments can involve the selective disruption of atomic bonds by means of voltage pulses, electric fields or mechanical contact between the probe's tip and the adsorbed entity. Controlled positioning of atoms and simple individual molecules (like CO) without rupture of intramolecular bonds was first achieved only at low temperatures (Eigler and Schweizer 1990, Stroscio and Eigler 1991). Later it was extended to RT for single atoms (Fishlock *et al* 2000).

A variation of the distance between the STM tip and the sample may be employed to exert a force on an atom or molecule adsorbed on a surface. A controlled manipulation experiment can be performed by lowering the tip towards the target adsorbate, thereby increasing the interaction between tip and atom or molecule. By adjusting the tip position and reducing tunnelling voltage, or increasing the tunnelling current (or both), it is possible to adjust the magnitude and direction of the force, so that the tip can push or drag an atom or molecule across a surface, with the adsorbate still remaining bound to the surface (Eigler and Schweizer 1990, Stroscio and Eigler 1991, Bartels *et al* 1997, Schunack *et al* 2001, Rosei *et al* 2002a, Moresco *et al* 2001a). After such an operation, the tip is withdrawn by resetting the tunnelling voltage/current to the imaging values and this effectively terminates the attractive interaction between molecule and tip. The lateral translation of atoms, clusters and molecules is normally defined in terms of pulling, sliding or pushing, depending on the type of interaction that is used between the tip apex and adsorbate (attractive for pulling and sliding, repulsive for pushing). While increasing the strength of the interaction by reducing the tip height, the manipulation mode changes from pulling to sliding. This occurs because the adsorbate is mainly following substrate minima in the case of weak tip–adsorbate interactions, exhibiting the discontinuities of adsorbate jumps. Normally lateral and vertical manipulation processes are employed for the manipulation of large molecules and clusters, so as to avoid their fragmentation.

During the manipulation process, changes in tunnelling current indicate the distances between the adsorption sites adopted by the adsorbate. In general, the direction of motion of the atom or molecule on the substrate will depend, on the one hand, on the shape of the molecule's and the tip's orbitals involved in the electrostatic (repulsive) interaction and, on the other hand, on the molecule–substrate interaction at various surface sites. This latter interaction in turn depends on the chemistry and geometry of the chosen substrate.

6.3. Molecule-induced surface restructuring

In the following subsection, I present a few selected studies in which molecular overlayers or single molecules were shown to induce an unexpected local restructuring process on the metal substrate on which they were adsorbed. Similar phenomena were observed for fullerene molecules on various metallic surfaces.

More specifically, I will describe STM results that directly prove that anchoring of complex molecules and the subsequent self-assembly of molecular nanostructures on a metal surface can be associated with a local disruption of the uppermost surface layer, just underneath the molecules. I will hereby illustrate how a surface can undergo a restructuring process in order to accommodate specific molecular geometries (Rosei *et al* 2002a, Weckesser *et al* 2001a, Schunack *et al* 2001, Rosei *et al* 2003), also leading to conformational changes within individual molecules (Schunack *et al* 2002a). Furthermore we will describe how a single fairly large molecule can act as a template on the nanometre scale, reshaping portions of a metallic step edge into characteristic nanostructures that are adapted to the dimensions of the molecule (Rosei *et al* 2002a). The restructured surface or step edge provides a preferential adsorption site to which the molecules are effectively anchored (Schunack *et al* 2001, Rosei *et al* 2002a).

When depositing large organic molecules onto surfaces at the technologically relevant temperature range around RT they are often observed to diffuse very rapidly, and it is generally not possible to resolve individual molecules in a STM micrograph. However, it has been observed that, when molecules are adsorbed at RT, they may anchor to the surface by inducing a restructuring of the topmost metal layer, thereby significantly reducing the diffusivity of the molecules.

This phenomenon was demonstrated for HtBDC, for which molecular adsorption at RT results in the formation of characteristic double rows (Schunack *et al* 2001). Within these double rows HtBDC molecules are imaged as six lobes, just as for the individual HtBDC molecules that were deposited at low temperatures. However, compared to the latter the intensity of molecular lobes within the double rows in STM images points to significant differences in their apparent heights. To unravel this difference the STM tip may be used as a tool to manipulate the molecules within the double row structure.

The manipulation is performed by lowering the tip towards the surface in a controlled manner and by decreasing/increasing the tunnelling voltage/current, respectively. This exerts a force on the surface adsorbates and, by tuning the magnitude and direction of this force, the tip can push or pull molecules across the surface (Eigler and Schweizer 1990, Bartels *et al* 1997, Hla *et al* 2000, Moresco *et al* 2001a). Finally, withdrawing the tip by resetting the tunnelling voltage/current to imaging values terminates the attraction between molecules and tip. By controlling precisely the tip's position, it is possible to manipulate individual molecules one at a time along a predefined path, leaving the rest of the scan area unperturbed.

Scanning over the double row structure with reduced tunnelling resistance effectively displaces all adsorbed HtBDC molecules from a certain portion of the surface, in a collective fashion. A 'clean' Cu surface area is revealed by the STM manipulation process (Schunack *et al* 2001). A local restructuring of the topmost Cu surface layer is directly revealed: 14 Cu vacancies are rearranged in two adjacent $[1\bar{1}0]$ rows, forming a trench-like base to which the molecules are anchored. From atomically resolved images where the molecular double

rows and the Cu(110) lattice are resolved simultaneously, the registry of the molecules can be determined. The three more dimly imaged *tert*-butyl lobes of each molecule are located on top of the missing Cu atoms.

If HtBDC molecules are deposited on the sample at temperatures below 250 K, molecular double row structures do not form. Apparently at these temperatures there is not enough thermal energy available to promote adatom–vacancy formation and diffusion on Cu(110) (Schunack *et al* 2001). The spontaneous surface disruption formed underneath the largish molecules during the adsorption process at RT is a generic way to reduce the mobility of the molecules and bind them to the surface, even at low coverages.

I described previously the conformational changes of Lander molecules upon deposition on a surface at low temperatures. Upon deposition of the Lander at RT, these molecules adsorb on the surface and diffuse readily towards step edges, as shown in figure 18(a).

Surprisingly, it was found that, when molecules are moved away from the anchoring positions at step edges, STM manipulation experiments reveal a restructuring of monatomic Cu steps induced by individual 'docked' molecules (Rosei *et al* 2002a). A manipulation sequence is shown in figures 18(a)–(d), in which two neighbouring molecules are removed from the step edge (neighbours in figures 18(a) and (c)). A characteristic metal nanostructure appears at the site where molecules were previously attached (attachment sites can be visualized in figures 18(b) and (d)): a zoom-in with atomic resolution is displayed in figure 18(e).

The overall process for anchoring a Lander molecule to the Cu nanostructure can be described as follows. When the molecule diffuses towards step edges at RT, it reshapes fluctuating Cu step adatoms into a nanostructure, which remains trapped underneath the molecule. It is favourable for the Lander to anchor to this nanostructure at the step edge, because the gain in energy by adsorbing the molecule on the nanostructure relative to the flat terrace is higher than the energy required for creating the structure itself. The dimensions of the board and leg fit such that two atomic rows can be accommodated between the legs under the board. This leads to a favourable interaction between the π system and the Cu atoms underneath. The dimensions and shape of the molecule form a perfect template for the double row of Cu atoms to be stabilized when the temperature is lowered.

Height profiles were measured across Lander molecules just before and after manipulation sequences, showing that the molecules undergo a conformational change during manipulation. Remarkably, the distances between the four lobes across the nanostructure decrease from 0.85 ± 0.25 nm (on the step edge) to 0.60 ± 0.25 (on a flat Cu(110) terrace). In the same way, the apparent height of the molecules in STM images decreases from 0.58 ± 0.02 to 0.45 ± 0.02 nm (Rosei *et al* 2002a).

ESQC calculations provided further insight into the conformational changes of the molecules on the terrace and the nanostructure (figures 18(f) and (g)). The molecule's central board is strongly attracted to the surface because of the large π system facing the metal substrate (Hahn and Ho 2001, Boal *et al* 2000). This introduces a severe constraint on the legs on a flat terrace, which leads to an out-of-plane distortion of each leg-board σ bond. This σ bond almost restores its planarity relative to the board because, when the Lander is anchored to the structure, its central board is lifted up by more than 0.1 nm relative to the surface (figure 18(f) and (g)). This reduces the steric constraint existing on the leg-board σ bond, leading to an increased width (0.83 versus 0.63 nm) and height (0.50 versus 0.45 nm) of the Lander in the STM image, in good agreement with experimental findings (Rosei *et al* 2002a).

As in the case of HtBDC, adsorption of Lander molecules at LT (150 K) does not lead to a restructuring of the Cu step edges and the molecules simply anchor to a step edge. At these temperatures, the mobility of Cu kink atoms at the step edge is not high enough for the template to be effective. It is therefore concluded that this process is thermally activated.

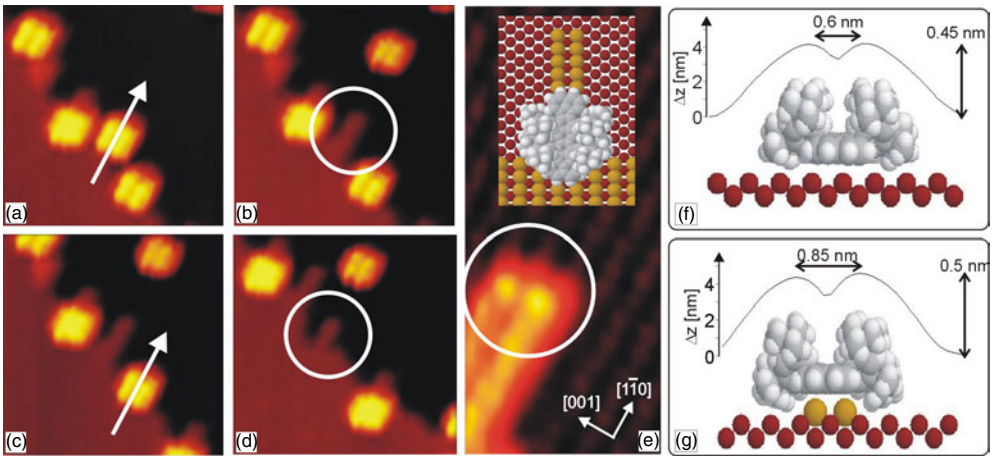

Figure 18. (a)–(d) Manipulation sequence of Lander molecules adsorbed on a step edge on Cu(110). The arrows show which molecule is being pushed aside, whereas the circles mark nanostructures that are visible on the step where the molecule was docked. $13 \times 13\,\mathrm{nm}^2$. $I_t = 20.47\,\mathrm{nA}$; $V_t = 21.77\,\mathrm{V}$; tunnelling parameters used for manipulating individual molecules: $I_t = 21.05\,\mathrm{nA}$; $V_t = 255\,\mathrm{mV}$. (e) Zoom-in smooth-filtered STM image showing characteristic two-row width of the nanostructure (right corner) after removal of a single Lander molecule from the step edge. Cu rows are also visible. The inset shows the molecular structure, extracted from a comparison between experimental and calculated STM scans, demonstrating that the board is parallel to the nanostructure. Arrows show the directions on the surface (image size: $5.5 \times 2.5\,\mathrm{nm}^2$. $I_t = 20.75\,\mathrm{nA}$; $V_t = 21.77\,\mathrm{V}$). (f), (g) Cross section of the nanostructure on a (flat) terrace and on a step nanostructure, respectively, together with ESQC calculated height profiles (Rosei *et al* 2002a). Copyright American Association for the Advancement of Science ©2002.

More recently it has been shown that this process can be conveniently extended. Otero and co-workers (Otero *et al* 2003) have designed from first principles a molecule similar to the Lander, called the violet lander (VL, $C_{104}H_{108}$). When adsorbed on Cu(110) the VL, which is slightly larger and longer than the Lander, operates a similar step edge restructuring. However, the structures that appear after displacing the molecule are systematically longer and often wider than those formed by the Lander. This work shows that the reconstruction induced by complex molecules can be fine-tuned by means of a rational design of molecular size and shape. This possibility points to new opportunities to imprint predefined patterns on a metal surface at the atomic scale.

I have thus shown that the ability to image surfaces with atomic resolution and to displace individual atoms and molecules in controlled processes makes the STM a unique tool for studying the interaction between complex molecules and metal surfaces. I have also illustrated how the bonding and ordering of molecules on surfaces are indeed governed by molecule–substrate interactions (Schunack *et al* 2001, Rosei *et al* 2003). More specifically, I have discussed STM results, which prove directly that anchoring of complex molecules, and the subsequent self-assembly of molecular nanostructures on a metal surface, may be associated with a local disruption of the uppermost surface layer, directly underneath the molecules. Finally, I have shown that a surface can undergo a restructuring process to accommodate a specific molecular geometry (Rosei *et al* 2002a, 2003) and conformational changes may occur within individual molecules (Rosei *et al* 2002a, Schunack *et al* 2002a). The restructuring processes that occur on surface terraces or step edges provide preferential adsorption sites to which the molecules are anchored (Schunack *et al* 2001, Rosei *et al* 2002a). These results

effectively demonstrate that, in many cases, molecule–surface interactions may be the driving force for the self-assembly of molecules on surfaces. Tuning these interactions should offer the opportunity to obtain ordered arrays of molecular nanostructures, which may be used for various applications.

Spontaneous surface restructuring processes observed under complex molecules during adsorption is a route to reduce molecular mobility and optimize the binding energy to the surface, even at low coverages. A more thorough understanding of the forces and mechanisms underlying the observed adsorption processes holds the promise of exploiting these phenomena in a controlled manner, for example by using specially designed molecules (Rosei *et al* 2003). This may ultimately lead to new routes for nanostructuring surfaces with atomic precision.

7. Direct growth of nanostructures: the bottom-up approach

At present, the great majority of semiconductor devices are fabricated using the *top-down* approach: circuits are patterned and written on suitable substrates using parallel techniques such as, for example, optical lithography. An alternative, appealing possibility to top-down micro-fabrication methods is to explore the so-called *bottom-up* approach. By this is generally meant the formation of functional devices from the bottom up, by direct growth or self-assembly. Candidates for components of these future systems include quantum wires (QWs) and quantum dots (QDs), or artificial atoms. In particular, a semiconductor QD is the ultimate quantum confined structure. Its unique electronic properties rely on the delta-function-like energy dependence of its density of states due to the quantum confinement of carriers (both electrons and holes) in atomic-like potentials in all three spatial dimensions. To exploit these electronic properties in novel quantum effect devices the lateral dimensions of these QD structures have to be smaller than the de Broglie (i.e. quantum) wavelength of the electrons inside the material (typically 10–50 nm). For applications in semiconductor devices, millions of these quantum structures, arranged in densely packed assemblies with a uniform size, shape and composition are necessary to achieve the desired active volume. This achievement will require more precise fabrication methods to provide better control of the size and shape of large ensembles of nanostructures. If this could be done successfully, it would allow the realization of novel high-speed, quantum interference, optoelectronic and single-electron devices.

The word *epitaxy* (from the ancient Greek words $\varepsilon\pi\iota$ (on top) and $\tau\alpha\xi\iota\sigma$ (to order)) indicates a growth process in which the impinging atoms attach to an existing crystalline surface by forming layers that have the same order as the original matrix (Brune 1998, Finnie and Homma 2002). Heteroepitaxy is therefore defined as an epitaxial growth realized by depositing an atomic species on a substrate with a different composition.

Epitaxial growth is strictly a non-equilibrium kinetic phenomenon. As implied by the principle of detailed balance, at thermodynamic equilibrium atomic processes compete with equal rates. Thus in equilibrium conditions, adsorption and desorption from the gas phase occur at the same rate, the same holds for cluster nucleation and decay and there is no net growth. In essence, this means that macroscopic variables, like surface roughness or coverage, must remain constant. In these conditions, statistical mechanics may be used to describe in detail the fluctuations around equilibrium quantities, which are caused by microscopic surface processes.

Depending on the forces that act between the substrate and the material that is being deposited, that give rise to different thermodynamic conditions, three epitaxial growth modes have been studied and classified so far:

(1) Layer by layer growth in lattice matched systems (Frank–Van der Merwe). This is typically observed in homoepitaxy, for example in the growth of Si on Si.

(2) The island growth mode (Volmer–Weber). This growth mode, in which islands nucleate on a bare substrate, is typical of systems with a large lattice mismatch, for example Ag on GaAs.
(3) The layer by layer, then island growth mode (Stranski–Krastanov, SK) in lattice mismatched systems. The SK mode occurs frequently in systems with a small lattice mismatch, for example Ge on Si (4.2%) or InAs on GaAs (7%).

In modes 2 (VW) and 3 (SK), the formation of three-dimensional islands is driven by the tendency of the system to relax the strain that results from the difference in lattice parameter.

The desired growth morphology—for example, the direct formation of islands—can be achieved only in particularly favourable cases within the stringent limits imposed by thermodynamics. A typical problem is the challenge of growing ultraflat layers, even when the film material cannot '*wet*' the substrate because the thermodynamics does not allow it to. Other effects (sometimes undesired), such as interdiffusion and alloy formation, may occur during growth. For example, the heteroepitaxial growth of Ge on Si may be regarded in principle as a model SK system, because both species belong to the IVth group, their bond being purely covalent, without any ionic character. However, the mixing of the two species is greatly favoured, particularly at high temperatures. Intermixing processes are also a serious limitation to the growth of small-sized QDs, because they lower the effective lattice mismatch, thus favouring the formation of large islands. I will discuss all these points in the following subsections.

In general the growth morphology is essentially determined by kinetic parameters, such as substrate temperature and deposition rate, and the particular microscopic pathway followed by the system under study becomes decisive once the kinetics is fixed. For example, if the temperature is too low, the resulting film may be amorphous. Under kinetic conditions therefore, microscopic events like atomic diffusion must be studied and understood in great detail. Most of these events are thermally activated and their rates generally follow an Arrhenius behaviour. Activation barriers and prefactors must be measured so as to predict, and possibly influence, film morphologies during growth. (These concepts were already discussed in the section on the surface diffusion of large organic molecules.)

7.1. III–V semiconductor nanostructures

One of the most studied examples of self-assembled QDs is the growth of InAs on GaAs. This system has been investigated in great detail with the aim of obtaining greater control over the positioning, shape, size and composition of quantum dots. In turn, this could greatly improve the performance of QD-based optoelectronic devices (Schukin and Bimberg 1999, Schukin *et al* 1995).

In this case the lattice mismatch is 7.2% and the formation of 3D islands begins beyond a critical coverage of ∼1.7 ML. Joyce *et al* (1998) have shown that this system does not follow a pure SK mode. Indeed, it was observed that the same InAs depositions on substrates kept at increasing temperatures led to larger fractions of WL and substrate participation to QD formation. Other studies have demonstrated that the composition of the growing surface at about 500 °C is an InGaAs alloy. It has also been speculated that alloying in these systems is favoured by partial surface melting, caused by heteroepitaxial stress (Bottomley 1998, Rosei and Raiteri 2002).

7.1.1. Migration-enhanced growth versus continuous growth. An interesting snapshot on this system comes from Balzarotti and co-workers at the University of Rome 'Tor Vergata'. In

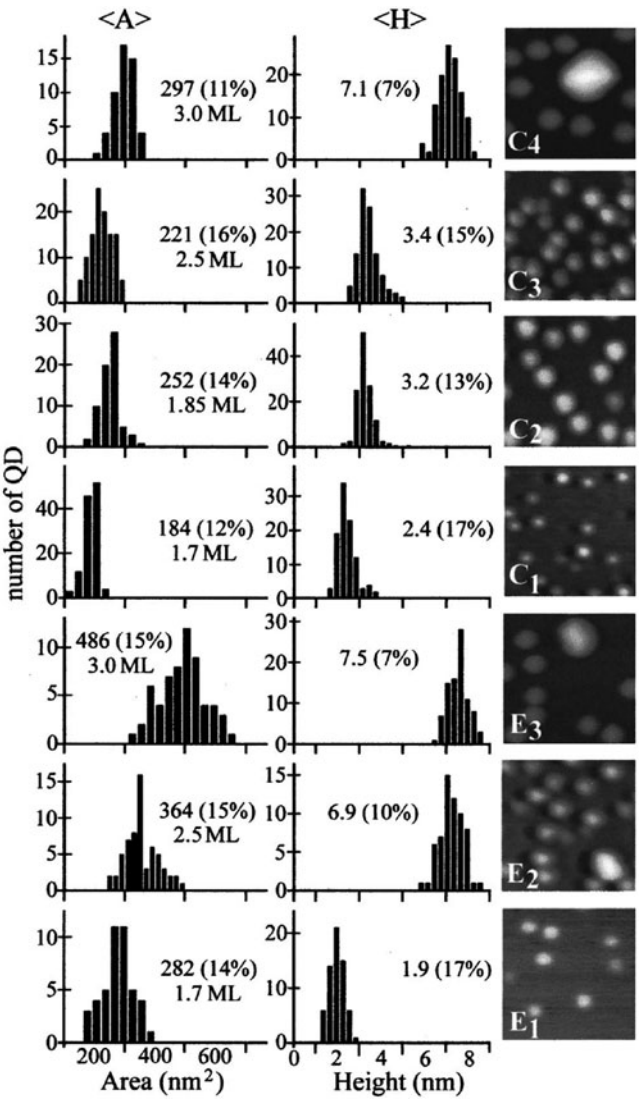

Figure 19. Histograms of height and basal area of the dots are shown for MEG samples (E1–E3) and CG samples (C1–C4) (ripened islands were discarded from the statistics). The average values of the single-dot area $\langle A \rangle$ and height $\langle H \rangle$ with the standard deviation of each distribution are indicated for each sample. On the right-hand side, a 450×450 nm^2 AFM image is shown for each sample (Patella *et al* 2001).

a preliminary study, Patella *et al* (2001) showed that different growth procedures that modify relevant kinetic factors, such as the migration length of the element III, may strongly affect the morphology and final composition of the film—even though the overall growth parameters remain unchanged. Different InAs thicknesses (1.7, 1.85, 2.5 and 3.0 ML) were deposited by MBE at low evaporation rates (about 0.028 ML s^{-1}, with an In/As flux ratio of $\sim 1/15$). The InAs deposition was carried out in two ways: continuous growth (CG) and migration-enhanced growth (MEG). While keeping the As beam incident on the sample, in the first case the In flux was delivered continuously until the given InAs thickness was reached (CG). In the

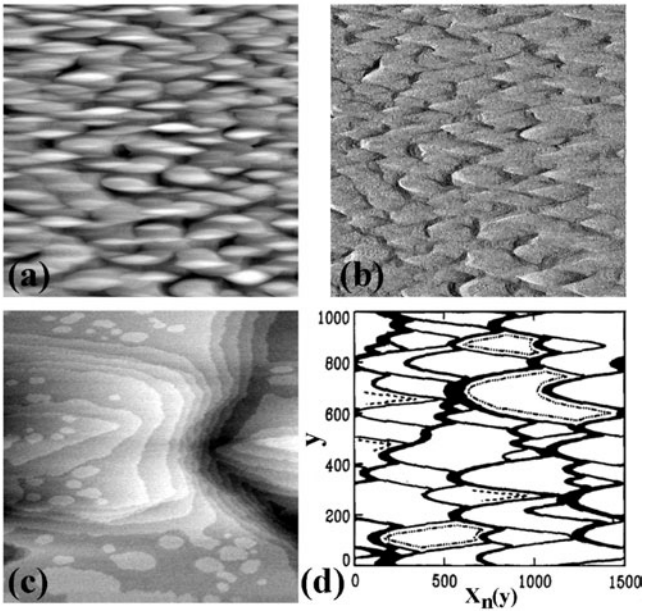

Figure 20. (a) AFM topography, $10 \times 10\ \mu m^2$, of about 1.3 ML of InAs deposited on the GaAs(001) substrate. Mounds, $1.2\ \mu m \times 0.3\ \mu m$, about 3 nm high, are elongated in the $[1\bar{1}0]$ direction; (b) AFM 2D phase image, $10 \times 10\ \mu m^2$, corresponding to topography $\sim a!$ showing the sharp variations of the profile; (c) $1.5 \times 1.5\ \mu m^2$ image showing bunching of steps and nucleation of 2D islands on terraces; (d) figure adapted from Kandel and Weeks (1994) displaying the numerical simulation of a step-train instability. Steps, moving from left to right, are marked by full curves. Thick full curves correspond to step bunches (Patella *et al* 2002).

second case the In evaporation time was sub-divided into 5 s of growth followed by 25 s of growth interruption (MEG). During the interruption of the In flux in MEG, surface In atoms, which are freed by the As detachment, diffuse toward more stable sites and reach monatomic steps. Meanwhile, the incident As_4 beam inhibits the formation of defect sites. The overall effect is an increased migration length of In atoms, which flattens the surface and produces higher-quality layers than those obtained by CG.

Figure 19 displays the statistical distributions of height and area of self-assembled InAs/GaAs islands. The sampling was obtained from a large number (>100) of (AFM) images. Remarkably, samples grown by MEG are characterized by a lower island density and larger island size than the corresponding CG samples. Assuming that the number of islands is inversely proportional to the diffusion coefficient and to the average monomer lifetime, this observation confirms that the monomer diffusion length is enhanced in the MEG mode (Venables *et al* 1984).

In this system, the island height does not increase continuously. Rather, it jumps from 3.0–3.5 nm in dots with areas lower than $\sim 300\ nm^2$ to 7.0–7.5 nm in islands of larger bases. The latter's distributions have the smallest standard deviation, which suggests a more efficient size-regulation mechanism. According to a recent model (Barabasi 1997), two strain-induced mechanisms account for this observation:

(i) the progressive decrease in strain energy upon moving away from island edges, which causes a net adatom diffusion current from island borders and
(ii) the competition between strain energy and binding energy at island edges, which favours atom detachment.

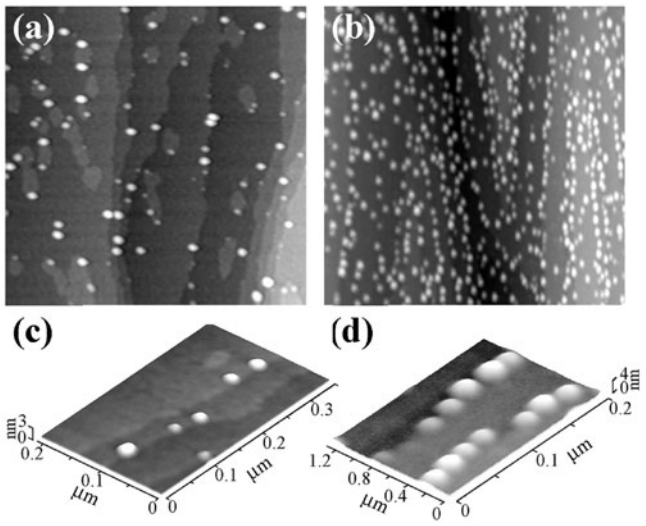

Figure 21. Nucleation of InAs nanostructures on GaAs(001). (a) and (b) AFM images for InAs depositions of 1.5 and 1.7 ML, respectively (image size: $0.8 \times 0.8\ \mu m^2$); (c) and (d) 3D plots of top sections from (a) and (b) (Patella *et al* 2002).

For CG samples, the size of the single island is fairly constant up to a coverage of ∼2.5 ML (figure 19); hence, the depositing material forms islands with equal sizes, the density of which increases linearly. Conversely, at the same thicknesses, MEG favours large-size structures that increase their volume at constant density. These results demonstrate that a mismatched heterostructure may follow a very different strain relaxation pathway, simply by varying a single kinetic factor (in this case the migration length), while the other growth parameters are kept constant (Patella *et al* 2001).

7.1.2. Effects of morphological instabilities on island self-assembly. During the growth of thin films, morphological instabilities may play an important role in the composition, structure and lateral ordering of the self-assembled nanostructures (Elder *et al* 2002, Gray *et al* 2002). In this context, recently Patella *et al* (2002) have shown that the substrate texture and the dependence of cation diffusion on the elastic strain field fully control lateral island ordering in the growth of InAs/GaAs(001) thin films and determine the final morphology of InAs structures stacked into multiple arrays. It was shown that diffusion in the presence of strain is the main mechanism of MBE growth. In these systems, very different morphologies for the same InAs deposition were observed, depending on the thickness of the GaAs layer used to space alternating InAs island layers.

Figure 20(a) displays a large-scale AFM micrograph of the strained, *intermixed* wetting layer (WL) that forms on GaAs(001) for ∼1.3–1.4 ML InAs thicknesses. The rippled morphology is made of mounds aligned along the $[1\bar{1}0]$ direction with average lateral dimensions $1.2 \times 0.3\ \mu m^2$ and ∼3 nm height. On the other hand, the smaller-scale AFM image displayed in figure 20(c) reveals at least three competing morphologies that intervene during growth: step bunching, step-edge meandering and nucleation of 2D islands on surface terraces. The measured distance between the steps forming the bunch is observed to decrease progressively from ∼120 nm down to a minimum of 40 nm, regardless of the original substrate miscut. Phenomena such as step bunching and meandering are indicative of anisotropic

diffusion currents (Kandel and Weeks 1994) and interlayer energy barriers. In turn, these are at the basis of kinetic instability models.

The occurrence of kinetic instabilities can also be inferred by the roughened morphology of figure 20(a), and is further confirmed by the step bunches observed in figure 21(b), which displays the corresponding AFM phase-mode image. In fact, figure 21(b) is strikingly similar to figure 21(d), which was taken from Kandel and Weeks (1994), who simulated the instability of a 2D step train.

However, other mechanisms could be responsible for kinetic instabilities (Burton *et al* 1951, Bales and Zangwill 1990, Schwöbel and Shipsey 1966). The SK process of self-assembly into islands beyond 1.5 ML of InAs is heavily influenced by the morphology of the strained WL. Figure 21 displays AFM micrographs corresponding to coverages of 1.5 and 1.7 ML. Step edge decoration in figure 21(b) (1.7 ML) reveals that the lateral ordering of the islands is constrained by substrate morphology. The transition between 2D and 3D growth initially occurs at the step upper edges and at large 2D islands (platelets): small nuclei rapidly convert into 3D islands (figure 21(a)). This interpretation is consistent with the existence of a minimum of the energy potential near the step edge, on the one hand, and with a diffusion barrier (the Schwöbel barrier) that prevents In adatoms from stepping down onto the lower terrace, on the other.

In conclusion, the results reported by Patella *et al* (2002) clearly point to instabilities that occur during the growth of InAs on GaAs(001). The observation of step bunching and step-edge meandering are direct confirmations of the validity of kinetic instability models. The step pattern completely determines lateral island ordering, since the 2D–3D transition initially occurs at the upper edge of steps and at platelets on the intermixed InGaAs wetting layer. This observation relates to a minimum in the binding energy of In adatoms at upper step edges of a terrace and of a Schwöbel energy barrier for interlayer mass transport. The elastic strain field of the substrate strongly affects cation diffusion, leading to very different morphologies in dots stacked into multiple arrays for different interlayer thicknesses. This observation points to the possibility of controlling island nucleation (shape, size and ordering) by appropriately manipulating the strain field caused by the lattice mismatch.

7.2. Ge–Si nanostructures

The Si devices now used in microelectronics (98% of sales in the global semiconductor market) are both very suitable and reasonably cheap. However, despite its dominance on the microelectronics sector, Si is hardly used at all in optoelectronics. In that sector III–V semiconductors are largely preferred, because of their direct bandgap and consequent much higher luminescence efficiency. Both optically and electrically pumped semiconductor lasers are widely used in fields ranging from telecommunications and information storage and processing to medical diagnostics and therapeutics (Weisbuch and Vinter 1991).

By adding another semiconductor material to silicon, it may be possible to engineer the band structure, leading to *tailor-made* materials that would allow solving specific problems and the investigation of new avenues in physics, chemistry and materials science. Indeed, the idea that semiconductor band structures could be engineered by the direct growth of heteroepitaxial thin films was first proposed by Tsu *et al* (1969). Si-based optoelectronic devices (lasers in particular) are an area that would profit enormously from these flexible design capabilities. This is where Ge enters the picture. By replacing some of the Si atoms near and on surface patches with Ge atoms, it should be possible to engineer the bandgap of the material and change charge carrier mobilities and many other properties. These circuits can be fabricated by using the same techniques that are used to manufacture conventional Si chips. Ge/Si-based materials

therefore could combine, in principle, the cost benefits of Si with the technological advantages of more expensive technologies (currently based on GaAs or other III–V compounds).

As a consequence, the growth of Ge layers on Si surfaces has recently been a subject of great interest, both from a fundamental point of view and for possible applications in optoelectronics. Research on this particular system has grown exponentially in the last decade (Eaglesham and Cerullo 1990, Mo *et al* 1990, Voigtländer and Zinner 1993, Ross *et al* 1999, Vescan *et al* 2000, Sutter and Lagally 2000, Ross *et al* 1998, Rastelli and von Känel 2002, Rosei and Fontana 2001, Voigtländer 2001, Brunner 2002, Medeiros-Ribeiro *et al* 1998, 1999, De Crescenzi *et al* 1995, Motta *et al* 1998, Rosei *et al* 2000, Rastelli *et al* 2001, 2002, 2003, Masuda and Shigeta 2001, Castrucci *et al* 2002, Rastelli and von Känel 2003, Tersoff *et al* 2003, Raiteri *et al* 2003, Kawamura *et al* 2003, Horn-von Hoegen 2003, Ratto and Rosei 2003, Zhong *et al* 2003). The ultimate goal in this context is to create useful electronic and optical nanomaterials that have been quantum mechanically engineered by tailoring QD shape, size, composition and position. Similar to the growth of InAs on GaAs, Ge on Si is a model Stranski–Krastanov (SK) system (Zinke-Allmang *et al* 1992, Zinke-Allmang 1999): by increasing the coverage, a strain-driven transition is observed, from smooth 2D WLs to coherent 3D islands (Eaglesham and Cerullo 1990, Mo *et al* 1990). These 3D islands are good candidates to act as QDs, similar to the case of III/V nanostructures. The controlled growth of such QDs would represent a major breakthrough in the optoelectronics sector, allowing the integration of microelectronic and optoelectronic circuits on the same Si wafer. While for some potential applications (e.g. photosensors or emitters), the QDs should have a uniform size, they could be randomly distributed on the substrate at some average density. In other applications, however, the islands should form an ordered, 2D array on the plane. Still other applications may require that the islands also be aligned to lithographically formed features (e.g. to interface with conventionally fabricated input/output circuitry).

7.2.1. Growth of the wetting layer in Ge/Si(111). Because of its lesser importance for applications, the Si(111) surface has been rarely used for Ge growth. Thus, although the literature on the growth of Ge on Si(001) is more extensive (since the (001) surface of Si is widely used in industrial devices), I will describe here in some detail the growth of Ge on Si(111), which exhibits a rich and surprising phenomenology.

When a few ML (0.5–2) of Ge are deposited on the surface, 2D Ge islands start to grow on the Si substrate. These islands have a triangular shape, with a lateral size which increases progressively with deposition (Motta *et al* 1998, Rosei *et al* 2000). The triangular shape is consistent with the threefold symmetry of the underlying surface. By analysing a large number of images taken at several different coverages (while keeping growth rate and temperature fixed), it is possible to derive a dynamic growth law for the WL. Assuming that all deposited Ge contributes to the formation of the WL, it is expected that $S \propto \theta$ (here S is the fraction of surface covered with Ge, while θ is the total Ge deposited, or coverage). However, a log–log plot of N versus θ yields a linear behaviour, meaning that the average number of islands per unit surface, N, scales as a power of the total coverage:

$$N(\theta) \propto \theta^{\alpha}. \tag{4}$$

In this case, a value of $\alpha = 1.80 \pm 0.80$ was found (Rosei *et al* 2000). The average number of islands per unit surface must be proportional to the ratio of the fraction of covered surface to the average dimensions of the islands:

$$N(\theta) \propto S/\langle r \rangle^2 \tag{5}$$

leading to a growth law of the type (Siegert and Plischke 1994, Thurmer *et al* 1995)

$$\langle r(\theta) \rangle \propto \theta^{1/z} \tag{6}$$

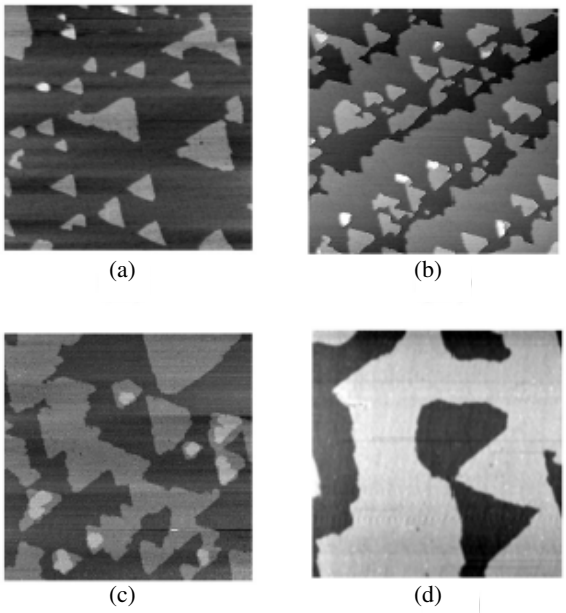

Figure 22. STM micrographs of a partial Ge/Si(111) WL grown at $T = 500\,^{\circ}$C. (a) 0.65 ML Ge, $(270\times270\times0.3)$ nm^3; (b) 1 ML Ge, $(400\times400\times0.5)$ nm^3; (c) 1.35 ML Ge, $(200\times200\times0.6)$ nm^3; (d) 2 ML Ge, $(200 \times 200 \times 0.36)$ nm^3 (Rosei *et al* 2000).

with a critical index $z = 0.70 \pm 0.20$ (Rosei *et al* 2000). Here, r denotes the average island dimension (as a function of deposited thickness).

This result could seem rather puzzling at first thought: however, in some cases (as illustrated in figure 22(b)) the presence of steps due to lattice strain severely affects the completion of the wetting layer (Rosei *et al* 2000). At this stage it becomes difficult to count precisely the average number of islands. As coverage increases (2–4 ML) the islands start impinging on each other (figure 22(c)), forming larger islands each made of several smaller triangular islands. When about 70% ($S/S_0 = (0.69 \pm 0.05)$) of the surface is covered with Ge, a percolated structure appears (figure 22(d)). This experimental value is consistent with the results reported by Isichenko (1992) for calculated values of percolation on the continuum.

7.2.2. Change of the reconstruction from 7×7 *to* 5×5 *in Ge/Si(111).* Because of the 4.2% lattice mismatch, even during the formation of the initial 2D layer, the surface reconstruction may change to accommodate the increasing strain energy. For example, in the case of Ge epitaxy on Si(001), a $(2 \times N)$ reconstruction is observed on the 2D strained WL. This reconstruction consists of a periodic array of *missing* dimers of the (2×1) dimer reconstruction: every Nth dimer of the (2×1) missing row reconstruction is absent. The reconstruction periodicity (N) is dependent on the stoichiometry of the WL, i.e. the amount of Si/Ge intermixing Moison *et al* (1994).

In the case of Ge deposited on Si(111), the reconstruction gradually changes from the typical 7×7 reconstruction of the Si(111) surface to the 5×5 of the Ge–Si WL. This process occurs in several distinct steps:

(1) Up to a deposition of 0.45 ML of Ge only the 7×7 reconstruction is visible. This has been observed by STM and was confirmed by the reflection high energy electron

diffraction (RHEED) pattern (Motta *et al* 1998), which can probe a larger and deeper region of the surface (Woodruff and Delchar 1994). The absence of islands on the terraces and of reconstructed ($2 \times N$) areas of Ge at this coverage indicate that Ge atoms diffuse into the Si substrate. As proposed in the case of sub-monolayer deposition of Ge on Si(001) surfaces, Ge exchange places with Si and mobile Si adatoms diffuse towards step edges (displasive adsorption). This interpretation is indirectly confirmed by the fact that the 7×7 reconstruction observed by RHEED becomes *brighter* (i.e. more intense) after the deposition of a small amount of Ge. Although the formation of a random alloy is strongly suspected even for such small coverages, the incoming Ge atoms are likely to fill the vacancies of the surface, represented for example by atomic defects.

(2) As the amount of Ge deposited is increased, the RHEED signal shows two distinct superimposed patterns, i.e. a mixture of 7×7 and 5×5 phases (Motta *et al* 1998). The appearance of this mixed reconstruction with 7×7 and 5×5 domains is also observed by high resolution STM.

(3) At a critical thickness of about 3–5 ML (depending on the substrate temperature and the deposition rate), the 5×5 reconstruction covers the whole surface. This is confirmed by extensive STM measurements (Motta *et al* 1998).

In excess of this critical coverage, the energy of the system can be optimized by forming 3D islands. Similar to the case of III/V semiconductors, the growth temperature strongly influences the WL thickness and morphology, partly because it affects the mobility of impinging adatoms and partly because it alters the composition of the epilayer by Ge–Si interdiffusion. In turn, the properties of the WL determine the characteristics of 3D islands.

An interesting issue about the surface composition of the 5×5 phase is the possibility of distinguishing Ge from Si adatoms by using STM. Unfortunately, the covalent bonding of Ge and Si and their similar atomic radii do not allow for a simple distinction[19]. A first attempt was made by Becker *et al* (1985) on the basis of the observed height modulation of the adatoms along selected lines of the topographic images. Later, Fukuda (1996) performed a statistical analysis of the height differences between neighbouring adatoms in the same half-unit and compared it with spectroscopic characterization. Within the limitations posed by the different sample preparations, the two conclusions are opposite: Becker *et al* (1985) find an ordered distribution of adatoms, while Fukuda (1996) suggests a random substitution of Ge atoms by Si. Very recently, Qin *et al* (2000) and Sutter and Lagally (2000) identified with STM the atomic sites of Ge which occur randomly on the Si(100) surface at sub-monolayer coverages.

An estimate of the average level of intermixing of the WL (i.e. of its composition) was obtained by x-ray absorption fine structure (XAFS) measurements (Boscherini *et al* 2000a, 2000b, Rosei *et al* 2000). The XAFS technique is a powerful tool for the study of the local chemical composition of solids and surfaces. Its usefulness rests on the fact that it is a local spectroscopy and therefore it does not require a sample exhibiting long range order.

For Ge–Si bonds the coordination number is found to be $N_{Ge/Si} = 2.0 \pm 0.3$. Since Ge and Si are group IV elements, this implies 50% alloying in the WL, as discussed below.

The value obtained is simply a measure of the average coordination of Ge atoms in the alloy. Several reports in the literature claim that both amorphous (Boscherini 1992) and crystalline (De Gironcoli *et al* 1991, Kajiyama *et al* 1992) Ge–Si alloys are random alloys, which means that there is no preference for or against heteroatomic bonding. This is also consistent with the very similar electronegativities and the small difference in covalent radius of the constituent atoms. It is therefore reasonable to use the coordination numbers as a measurement of the average composition. Thus, the average composition measured by XAFS

[19] Notably this experiment is quite difficult, since the STM intrinsically lacks chemical sensitivity.

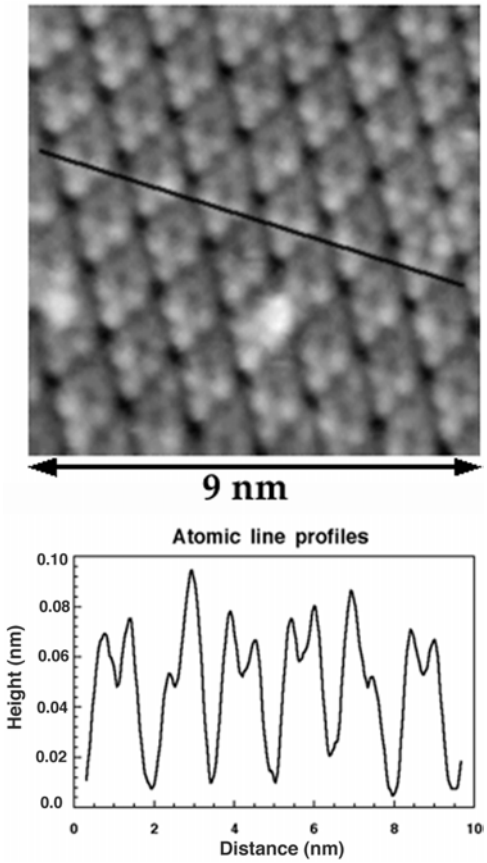

Figure 23. Upper panel: STM image of 3 ML of Ge grown on Si(111) at $T = 500\,^{\circ}\mathrm{C}$. The 5×5 reconstruction typical of the Ge–Si wetting layer is clearly visible. Lower panel: line profile along the direction indicated by the black line in the upper panel (Rosei *et al* 2000).

for the WL is $Ge_{0.5}Si_{0.5}$ (Boscherini *et al* 2000a, Rosei *et al* 2000). Clearly these are average values, which therefore neglect any gradients that might exist, but to which the XAFS technique is not sensitive.

To clarify the issue of surface composition, Rosei *et al* (2000) have acquired several topographic STM images of the 5×5 Ge/Si(111) surface with atomic resolution (figure 23, upper panel). A close inspection reveals that, in some of the faulted units, one adatom appears darker than the other two (in the 5×5 reconstruction, each unit cell contains 3 atoms).

In several line profiles (figure 23, lower panel) taken from images with atomic resolution, differences in the adatoms' heights of each subunit of about 0.2 Å were measured. This value is comparable to the difference in the covalent radii of Si (1.1 Å) and Ge (1.2 Å). This suggests either a random replacement of some Ge adatoms by Si or a bond-length relaxation, possibly caused by the presence of Si in the underlying layers. On the other hand, the Si atoms mixed in the subsurface layers could also contribute to modifying the local electronic density of states of the adatoms[20].

Current image tunnelling spectroscopy (CITS) measurements reported by Motta *et al* (1998) showed similar features. The combined information drawn from the comparison of

[20] Indeed, the STM measures a contour plot of the local density of states (LDOS) at the Fermi level.

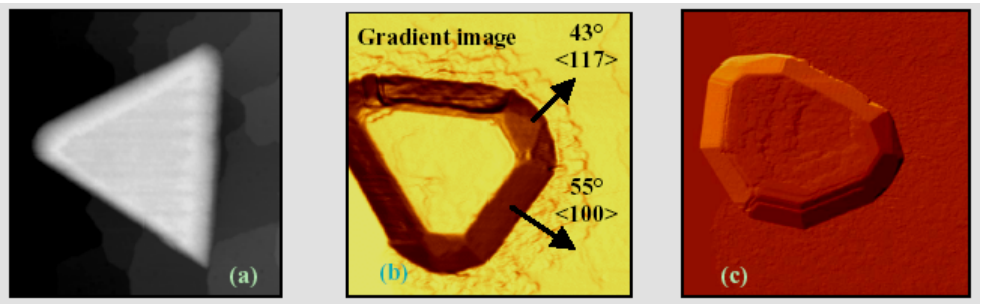

Figure 24. (a) STM topography of Ge islands on Si(111); growth conditions: $T = 550\,^{\circ}$C, $\theta = 2$ nm; image size, $236 \times 236 \times 8.5$ nm^3. (b) Gradient mode image. Island height, 40 nm; image size: 230×230 nm^2. Growth conditions: $T = 450\,^{\circ}$C, $\theta = 2.5$ nm Ge. (c) 3D view of Ge island on Si(111). Image size: 300×300 nm^2; island height, 40 nm. Growth conditions: $T = 450\,^{\circ}$C, $\theta = 4.5$ nm (Rosei 2001).

topographic and spectroscopic images does not allow us to rule out the mixing of Ge and Si in the top-layer adatoms, although it does not confirm it, either.

Due to the high diffusion of Si in Ge (as determined directly by XAFS) a model description was proposed, in which the Si concentration in the wetting layer is nearly constant and the topmost layer is randomly occupied Rosei *et al* (2000).

7.2.3. Ge–Si 3D islands on Si(111). As soon as Ge coverage exceeds 3–5 ML (depending on substrate temperature and growth rate; see Motta *et al* 1998, Rosei *et al* 2002a, Rosei 2003), 3D islands appear at random locations on the surface. After the WL is completed, platelets (2D or flat islands) are never observed. This may be due to the fact that growth is mostly carried out at near-to-equilibrium conditions, since typical evaporation rates are very low. These deposition conditions imply that:

(i) platelets may form, with ample time to rearrange (either attaching to steps or immediately forming 3D islands);
(ii) the formation of platelets may simply not be favoured, since Ge–Si intermixing favours instead the occurrence of undulations in the WL.

In a recent experiment, Jesson *et al* (2000) showed by AFM imaging that an initially planar 2 nm epitaxial layer of Ge/Si(001) deposited at 400 °C can give rise to 3D islands when annealed for 5 min at 600 °C. This means that, if the necessary energy is available (thermal in this case), the system can be stabilized by the formation of islands.

In the early stages of growth on Si(111) the island shape is triangular (truncated triangular pyramids, or tetrahedra, figure 24(a)), with average lateral dimensions of 50–100 nm and a height of ∼10 nm. This morphological transition is believed to occur when the free energy of the islands is lower than that of the strained layer.

At 9 ML coverage two kinds of islands are visible (Motta *et al* 1998): small, tall islands (typically 180 nm wide and 10 nm high) or large and ripened flat islands (average dimensions 350 nm wide and 2.5 nm high). After nucleation, the islands grow vertically up to a critical value, at which the strain energy introduces a morphological transition with the possible formation of dislocations. Subsequently islands grow laterally, apparently drawing material from the top or from the substrate or merging with other islands. This process is called *ripening* and leads to the formation of flat, round islands. Some ripened islands are characterized by a

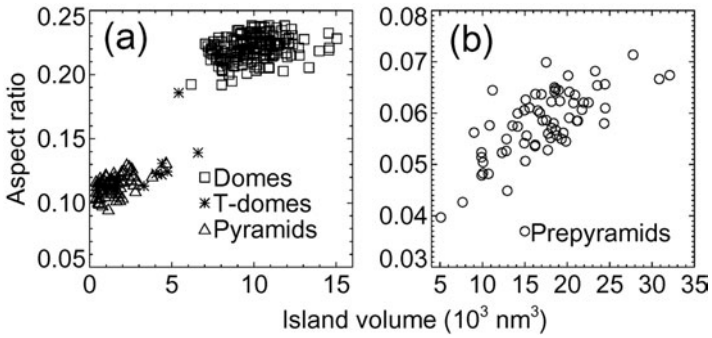

Figure 25. Measured aspect ratio versus island volume prior to Si capping (a) and at a Si coverage of 16 monolayers (b). The island shape was defined in relation to the facets surrounding its surface. The Si capping induces a strong flattening (Rastelli *et al* 2001).

hole at their centre, whereas other ones display a depletion surrounding them. These features are related to strain and intermixing (Motta *et al* 1996, 1998, Rosei *et al* 2000, Boscherini *et al* 2000a, 2000b, Motta *et al* 2002a, Motta 2002, Rosei and Raiteri 2002, Motta *et al* 2003, Rosei 2003). Enlarged images of the top of the islands (both for strained and ripened islands) and of the substrate display the 7×7 structure of the former and the 5×5 reconstruction of the latter.

7.2.4. Effects of Si capping on Ge islands grown on Si(001). As I mentioned previously, the literature on the growth of Ge on Si(001) is very extensive and has been recently reviewed in depth by other authors (Voigtländer 2001, Brunner 2002). In this subsection, I will rather describe recent studies that focus on the Si capping of Ge islands grown on Si(001).

To integrate self-assembled QDs in optoelectronic devices (Schmidt and Eberl 2001), these nanostructures have to be embedded, or *capped*, in a semiconductor matrix. However, the capping process is likely to modify island shape and composition. In turn, this will change the electronic properties of the buried structures (Schmid *et al* 2000a). Thus, an in-depth knowledge of island evolution is an essential step to develop new applications.

During Ge deposition, coherent islands typically undergo several shape transitions (Daruka *et al* 1999). Starting from *prepyramids* that are up to ∼1 nm tall (Vailionis *et al* 2000), they transform into *pyramids* (Vailionis *et al* 2000, Medeiros-Ribeiro *et al* 1998) bound by (105) facets and eventually into multifaceted nanocrystals (*domes* Medeiros-Ribeiro *et al* 1998) with a typical height of ∼10 nm. All the islands are found to have a square base, consistent with the fourfold symmetry of the underlying Si(001) surface.

The same evolution has been reported for the growth of Si_xGe_x alloys on Si(001) (Ross *et al* 1999, Chen *et al* 1997, Floro *et al* 1999). In this case, the lattice mismatch is supposedly reduced by a factor x with respect to the growth of nominally pure Ge on Si, leading to an increase of the typical island size[21]. Despite the rich literature on this subject, critical issues, such as island stability and the kinetic pathways of the shape transitions, are still not well understood (Daruka *et al* 1999).

Figure 25 displays the measured aspect ratio[22] versus volume of individual islands grown on Si(001) before (a) and after (b) capping with 16 ML of Si. Most of the shape changes that take place during Si capping are observed to occur after the deposition of a few ML of Si.

[21] In reality the mismatch is probably not reduced by much, because of the significant Ge–Si intermixing that occurs during the growth of pure Ge on Si in the temperature range (400–600 °C) that is typically used for deposition.
[22] The aspect ratio is defined as the ratio of the height to the square root of the base area.

Rastelli *et al* (2001, 2002) observed several island shapes during the growth of Ge on Si(001). These shapes correspond to different transition stages and accordingly were called *T domes*. Therefore, the occurrence of a single intermediate step in the pyramid-to-dome transition, proposed by Liu *et al* 2000, was excluded. Rather, it was proposed that the morphological changes occur gradually, confirming earlier work by Ross *et al* (1999) and Vailionis *et al* (2000).

In their investigation, Rastelli *et al* concentrated on the shape evolution of Ge domes during exposure to a Si flux, extending previous work on pyramids by Sutter and Lagally (1998) and Kummer *et al* (2000). Figure 26(a) displays a Ge uncapped dome. The apex and the foot are (105) facets. This is clearly visible in the high resolution TEM micrograph displayed in figure 27(a) and in the line profile in figure 26(d) (whereas figures 27(b) and (c) show the same system at a higher temperature during Si overgrowth). The body of the domes is bound by steeper facets: four (113) planes and eight (15 3 23) planes. At a Si coverage of $\sim$1 ML (figure 26(b)), these facets shrink in size at the expense of (105) planes. At different growth stages, domes transform into asymmetric *T domes*. After exposure to 2 ML of Si (figure 26(c)) most of the domes have retransformed into pyramids. In the next evolutionary step, the pyramids display a (001) top facet, as previously noted by Sutter and Lagally (1998) and Kummer *et al* (2000). This is demonstrated in figure 26(d). Now the edges between adjacent (105) facets are replaced by vicinal planes composed of steps parallel to the (110) directions (see figure 26(e)). The (105) planes eventually disappear at $\theta_{\mathrm{Si}} = 16$ ML (figure 26(f)). The initial domes have now transformed into stepped mounds without facets. Their aspect ratio is an increasing function of island size, with morphological features very similar to those reported in (Vailionis *et al* 2000) for *prepyramids*. Upon continued exposure to a Si flux, no further evolution was observed. This is caused by kinetic limitations that hinder uniform Ge–Si intermixing.

The dramatic change in aspect ratio (caused by an increase of the base area and a simultaneous reduction in height) is induced by Ge–Si intermixing (Sutter and Lagally 1998): Si adatoms penetrate the subsurface layers of an island because of Ge segregation at the surface (Nakagawa and Miyao 1990). This lowers the surface energy of the system and, as a result, the strain is relieved. Since the formation of islands occurs precisely to reduce the strain caused by the lattice mismatch, and since this is now relieved also because of alloying, the island is no longer stable. Thus Ge adatoms diffuse away from the island apex and, by alloying with Si, rearrange into new stable configurations. At the end of this process, the island is flatter and alloyed. As discussed above, to prevent this evolution Ge surface segregation and surface mobility must be kinetically hindered.

In essence, Rastelli *et al* (2001, 2002) have demonstrated that, by means of low temperature deposition, it is possible to embed Ge islands into a Si matrix without altering appreciably their shape and composition. The island evolution does not depend critically on the Si deposition rate. At the same time a flat Si surface, necessary for producing multiple layers of QD, can be easily recovered by ramping the growth temperature up to the value used for the deposition of Ge islands. The complex pathway of shape transitions of self-assembled Ge and $Si_{1-x}Ge_x$ islands can be understood qualitatively on the basis of composition-dependent critical volumes that govern the changes from one shape to another.

Several critical issues in the growth of Ge on Si remain to be addressed, both from a fundamental point of view and for industrial applications. To obtain device quality films, for example, it is desirable to control the composition of Ge/Si nanostructures. However, intermixing processes in these systems are still far from being understood. At the same time, it is essential to develop approaches that allow fabricating arrays of islands in parallel (Motta *et al* 2003).

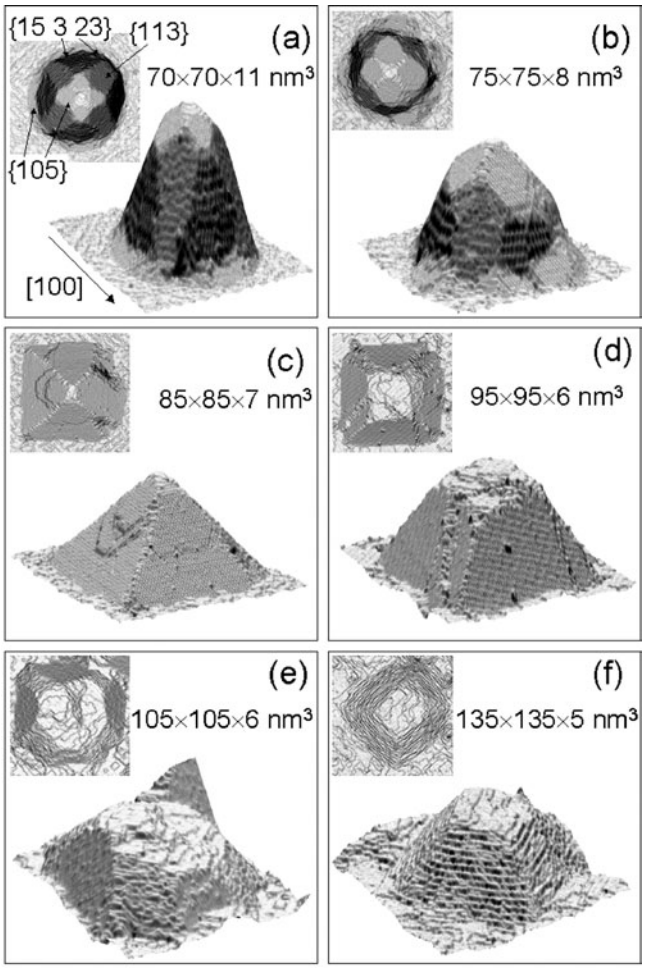

Figure 26. STM topographic images of Ge/Si(001) islands during Si capping. (a) Uncapped dome. (b)–(f) Si coverage is 1, 2, 4, 8 and 16 ML. During Si overgrowth, domes transform first into pyramids (c) and finally into stepped mounds (f), going through intermediate shapes (Rastelli *et al* 2001).

Since self-ordering does not normally occur spontaneously, several groups (Men *et al* 2002, Lin and Lagally 1997, Ogino *et al* 1999) are addressing the issue of controlling island positioning using alternative approaches. Among these, the author's group is working on several fronts in parallel, including deposition through a shadow mask (see, for example, Lüthi *et al* 1999, Brügger *et al* 2000), substrate patterning using NIL (Chou *et al* 1996) and using nanostructured surfaces as templates for growth. The substrates can be artificially patterned (e.g. using standard microfabrication techniques such as EBL, FIB and ion implantation) or self-organized reconstructions (e.g. the step-bunching process that occurs on Si(111), see Stoyanov *et al* 2000, Miki and Tokumoto 1992, Sgarlata *et al* 2003).

Finally, recent dynamic low energy electron microscopy (LEEM) studies (Ratto *et al* 2003) have confirmed that Ge/Si nanostructures are metastable upon annealing to 500 °C. Clearly, this observation is quite discouraging for possible applications in optoelectronics and warrants further investigations to circumvent this problem.

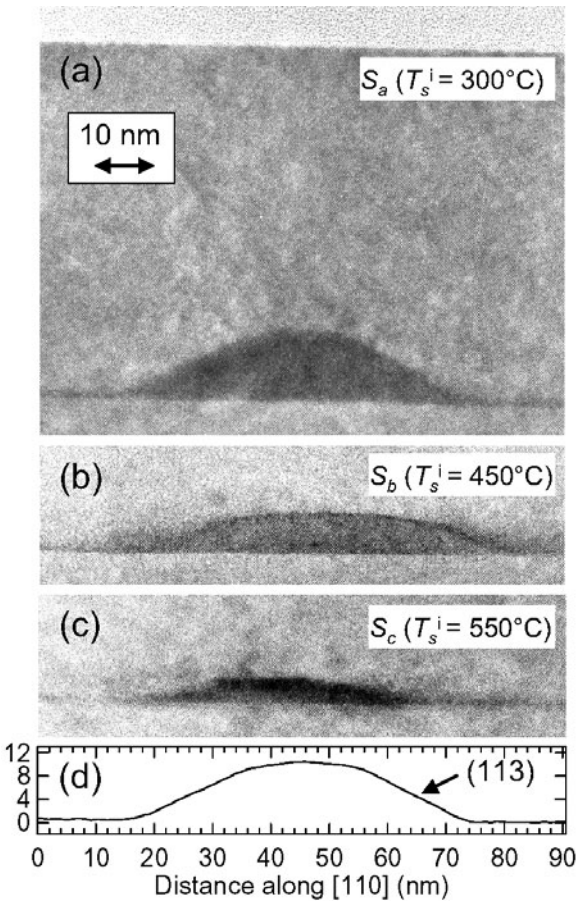

Figure 27. (a)–(c) High resolution TEM micrographs of Ge *domes* capped with 60 nm of Si. The first 30 nm were deposited at $T = 300\,^{\circ}\mathrm{C}$ (a), 450 °C (b) and 550 °C (c). The final temperature was 550 °C, allowing us to recover a flat surface (shown in (a)). (d) Height profile (measured in nm) of the uncapped dome shown in (a), cut along the broken line. A (113) facet is indicated (also visible in (a)). The scale is the same for all the images (Rastelli *et al* 2002).

7.3. Surface alloying processes

Surface alloying processes and segregation phenomena are common during heteroepitaxial crystal growth. In some cases, as I have shown for Ge/Si and InAs/GaAs, they are, to some extent, undesirable, since they severely affect film properties and morphology. In other cases, such processes can actually be exploited for specific applications. Indeed, controlling the alloy structure on the nanometre length scale should offer new routes to engineer the chemical, magnetic, optical, mechanical and ferroelectric properties of surfaces (Holmar Johannesson *et al* 2002). Alloys are widely used as technologically relevant metallic materials, as opposed to pure metals, for example. Often, the complex phase diagrams of alloys may be exploited to optimize the properties of materials (Logadottir *et al* 2001). For example, by depositing small quantities of Au on Ni substrates (Nielsen *et al* 1993, 1995, Holmblad *et al* 1996, Besenbacher *et al* 1998) the performance of Ni as a catalyst for the steam reforming reaction was greatly improved, also drastically reducing the poisoning effects that are caused by carbon incorporation and subsequent graphitization. It is therefore desirable to arrive at an atomic-

scale description of processes that are ultimately responsible for intermixing, interdiffusion and alloy formation. Images of the static structure of surface alloys have shown that the mechanisms of surface alloying can be very different and more complicated than their bulk counterparts.

Generally speaking, the homoepitaxial and heteroepitaxial growth of metals is a complex process. The occurrence of intermixing between the growing layer and the substrate is quite common (Rousset *et al* 1992, Chambliss and Chiang 1992) when the two materials involved are miscible, but has also been observed for immiscible metals (Nielsen *et al* 1993, 1995).

Another interesting example comes from the study of Sn alloying with Cu, which forms *bronze*, an alloy that has been widely used as the basis of the earliest metallurgical technologies since ancient times. Today, bronze remains relevant in many modern technologies, because of some specific surface properties. For example, it is quite resistant to corrosion. Moreover, because of its very low friction coefficient, it is often employed as a bearing material. A STM image of a Sn–Cu surface obtained after annealing to 750 °C for 2 h is displayed in figure 28 (Contini *et al* 1998). During the annealing process, tin segregates to the surface of Cu(111) and readily forms a single-layer $Sn_{0.33}Cu_{0.66}$ alloy phase with a $p(\sqrt{3} \times \sqrt{3})R30°$ reconstruction. Further annealing at higher temperature (750 °C) reduces the tin concentration to 0.20, while the $p(\sqrt{3} \times \sqrt{3})R30°$ structure is maintained. Contini *et al* (1998) were the first to report direct-space images of this system.

The seminal work by Contini *et al* (1998) was soon followed by Schmid *et al* (2000a), who studied the formation of Sn–Cu islands on Cu(111) by dynamic STM and LEEM. The segregation of Sn and Cu is quite remarkable because of the large difference in the melting point and in the atomic size of the two components. Even though the RT solubility of Sn in Cu is low, Sn atoms can incorporate quite easily into the atomic planes of Cu(111), where the size mismatch is partially relieved by out-of-plane displacements.

Following recent advances in microscopy techniques (Plass *et al* 2001, Pohl *et al* 1999) that now allow the investigation of surface structure evolution in real time, it was found that the chemical energy released during alloy formation is responsible for the surprising motion of alloyed Sn–Cu islands on Cu(111). The work by Schmid and co-workers actually opened up new perspectives on how to harness energy and power on the nanometre scale (Besenbacher and Nørskov 2000).

If self-assembly is to become a viable technology, new approaches and concepts must be developed. New ways are to be explored to control the growth of advanced functional materials. Another interesting example in this context is silicon carbide (SiC) (Derycke *et al* 2003). Since they are compatible with today's existing Si technology, carbon-enriched silicon systems are good potential materials for optoelectronic applications. Attempts to assembly these systems by direct growth are generally hampered by the extremely low solubility (a few per cent) of C in Si under thermodynamic equilibrium. This is caused by the huge mismatch in bond length and bond energy between Si and C.

To circumvent this problem, non-equilibrium methods may be employed. These allow us to increase atomic mobility and thus enhance solubility, even for immiscible systems such as Si and C. This concept has been applied to incorporate carbon in the first atomic layers of Si(001) by MBE (Butz and Lüth 1998, Leifeld *et al* 1999), exposure to fullerene (Chen *et al* 1994) and ethylene (Takaoka *et al* 1996, Miki *et al* 1997) in the 550–675 °C temperature range. The adsorption of a low amount of C leads to a $c(4 \times 4)$ reconstruction (Kelires 1995, Kelires and Kaxiras 1997, Remediakis *et al* 2001), which confirms the early theoretical predictions (Tersoff 1995).

Recently Castrucci *et al* (2003) have observed the growth of silicon carbide by exposing the (111) surface of Si to C_2H_2. This molecule is observed to dissociate at T 450 °C, while the

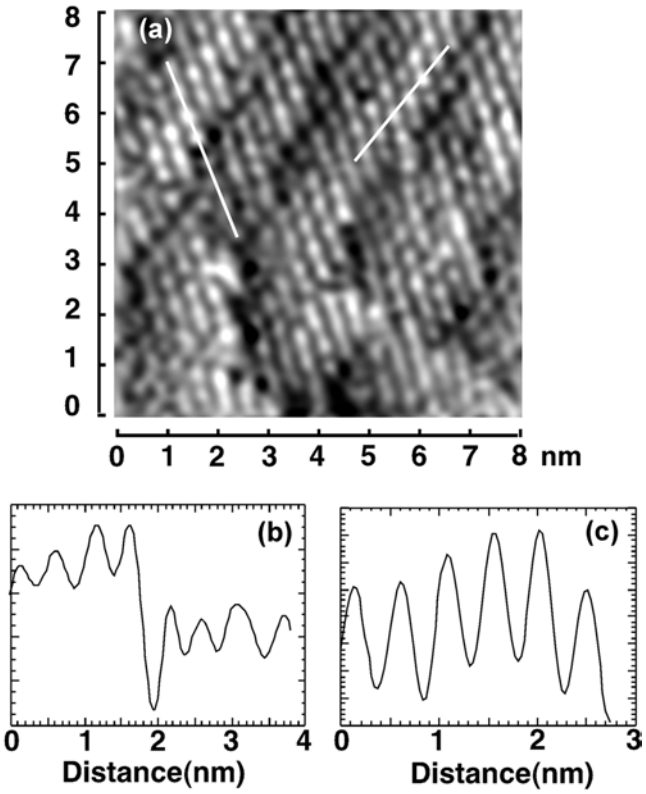

Figure 28. (a) STM image (8.0 nm × 8.0 nm; $V_t = -0.4$ V, $I_t = 2$ nA) of the Sn–Cu surface obtained after annealing the sample at 750 °C for 2 h. (b) Line profile taken from left to right across a step (white line on the left). The modulation has a period of $d = 0.51$ nm. (c) Line profile taken from left to right along the steps (white line on the right). The regular modulation ($d = 0.47$ nm) of atomic protrusions is clearly visible (Contini *et al* 1998).

onset for the formation of cubic SiC(111) begins at $T = 600\,^{\circ}$C. The reaction process leads to a drastic change of the original 7×7 reconstruction into a $(\sqrt{3} \times \sqrt{3})$R30° surface arrangement. Initially it involves the lower part and then the upper part of the step edge and it expands progressively throughout terraces as the amount of carbon increases. A similar expansion mechanism characterizes surface areas, where defects or vacancies existed prior to exposure. This particular mechanism is similar to the so-called step meandering or step flow that is typically observed in the homoepitaxy of semiconductors (Ehrlich and Hudda 1966) and copper vicinal surfaces (Schwöbel 1968). This reaction pathway increases the adatom incorporation rate into the step from the lower terrace than from the upper one, because the Ehrlich–Schwöbel barrier prevents diffusing atoms from leaving the monatomic step (Vladimirova *et al* 2001, Hamers and Demuth 1988). In the case reported by Castrucci *et al* (2003), the higher mobility of Si adatoms from the lower terrace towards the upper one supplies more silicon atoms that react with carbon, thus leading to the formation of a greater number of reacted layers above step edges. Small clusters (identified as bright features in STM images) are observed to grow in both size and height as the exposure time is increased. After dosing 360 L of C_2H_2 these clusters have a diameter in the range 1–5 nm and a height between 0.4 and 0.6 nm. These aggregates can be considered as *seeds* of cubic SiC (De Crescenzi *et al* 1999, 2001). The LEED pattern reported in figure 29(a) (diffraction pattern of the sample after exposure to

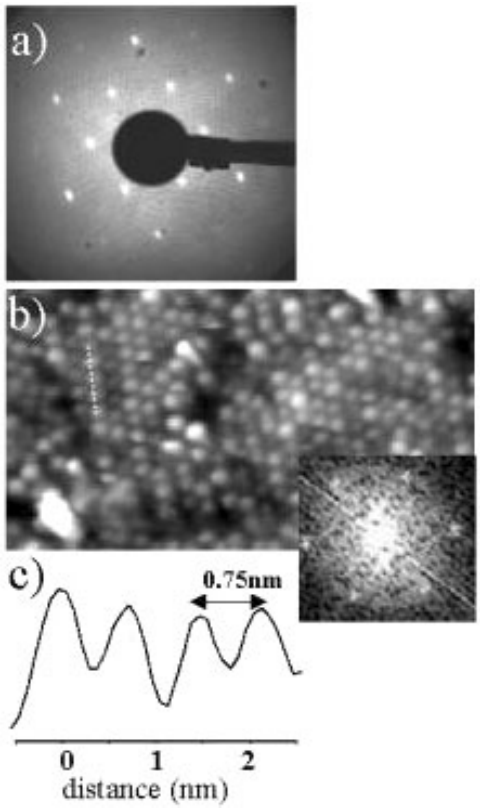

Figure 29. (a) LEED pattern showing the surface reconstruction ($\sqrt{3} \times \sqrt{3}$)R30° induced by growing acetylene on Si(111). (b) 18×10 nm^2 STM image ($V_t = -4.5$ V, $I_t = 2.5$ nA) of a silicon substrate after exposure to 360 L of C_2H_2. The inset shows the power spectrum of the same STM image. (c) Plot profile across the line indicated in (b), showing that the atomic distance is 0.75 ± 0.02 nm (the same as silicon 7×7 adatoms) (Castrucci *et al* 2003).

360 L of acetylene) shows the coexistence of two phases, relative to a bulk 1×1 unit cell and a ($\sqrt{3} \times \sqrt{3}$)R30° cell. Figure 29(b) displays a STM image of a region mainly covered by the ($\sqrt{3} \times \sqrt{3}$)R30° reconstruction. The corrugation profile in figure 29(c) represents the vertical tip displacement as a function of position along the line indicated in figure 29(b), taken along one of the main directions of the ($\sqrt{3} \times \sqrt{3}$)R30° unit cell. A statistical analysis of line profiles yields 0.75 ± 0.02 nm for the atom registry in the ($\sqrt{3} \times \sqrt{3}$)R30° domain. This value is consistent with that of the silicon adatoms in 7×7 areas. The Si-terminated hexagonal SiC(0001) surface also reconstructs with ($\sqrt{3} \times \sqrt{3}$)R30° symmetry but, in this case, the distance between adatoms is only 0.53 nm (Starke *et al* 1999). This means that, in the present case, the interatomic distance is about 50% larger than the distance that characterizes the crystalline SiC($\sqrt{3} \times \sqrt{3}$)R30° reconstructed surface. This implies that the STM and LEED results reported by Castrucci and co-workers refer to a *novel* Si(111) phase induced by carbon incorporation, and not to silicon carbide. The incorporation of C is thought to produce local modifications of the structural and electronic properties of the surface atomic layers, leading to the specific contrast observed in STM images.

In conclusion, the examples I have described seem to suggest that surface alloying is driven essentially by two factors:

(i) chemical reactions occurring at the substrate during growth (depending on reactivity);
(ii) the tendency of the system to partially relieve the strain caused by the constraint of accommodating atoms of different sizes and crystal structures with different lattice parameters.

The ability to control these factors should allow us, in principle, to grow novel functional materials with fine-tuned chemical and physical properties.

8. Conclusions and perspectives

In this paper, I have drawn from various examples in the recent literature which clearly show that nanostructured surfaces present interesting and surprising size effects that are observed when the typical dimensions of the material being investigated are below a critical length (typically ∼1–100 nm).

8.1. Advances in instrumentation

One of the problems which so far has hampered our progress in the study of surfaces and interfaces lies in the fact that experimental techniques, for the lack of spatial or time resolution (or both), typically measure an '*ensemble*' of different elementary steps and therefore the relevant parameters are averaged out over several processes (Rosei and Rosei 2002, Besenbacher 1996). An important challenge to be addressed is thus the ability to single out and characterize every step at the atomic level, separately. This will require a substantial improvement of present microscopy techniques and, most likely, the development of new ones. The effort will be extremely exciting, however, since it may also lead to the detection of new important *co-operative* many-body effects, of which we have had, so far, only occasional glimpses.

Another major obstacle is the so-called 'pressure gap'. While most model surface science studies carried out so far have used very low pressures (less than about 10^{-6} mbar), industrial processes occur at pressures many orders of magnitude higher. Higher pressures mean very high coverage of the reactants. Many experiments have shown that, as the coverage of adsorbed species increases, the lateral interactions that develop strongly influence all surface processes. In this different regime all the elementary steps and the overall reaction rate may change dramatically.

It will therefore be compulsory to improve experimental techniques to enable probing surface processes at higher environmental pressures. Special STM prototypes have already been developed, demonstrating the capability of performing *in situ* high pressure studies of the atomic structure of surfaces. These first results show that, in general, when dealing with the adsorption of a single gas (H_2 on Cu(110) (Österlund *et al* 2001, Laegsgaard *et al* 2001), CO on Pt(111), (Vestergaard *et al* 2002)), phases that form at high pressures are also accessible at typical UHV pressures, as long as the temperature is kept sufficiently low. This basically means that increasing pressure is equivalent to decreasing temperature, at least insofar as the structure at thermodynamic equilibrium remains kinetically accessible. The case of CO on Pt(110) was reported very recently (Hendriksen and Frenken 2002). Here CO adsorption effectively lifts off the (1×2) missing row reconstruction typical of this surface. Although no new phase was reported, it was shown that pressure increase is not exactly equivalent to a temperature decrease. In fact, at low temperature the rearrangement of substrate Pt atoms would not have the energy required to form the equilibrium structure.

Recent work was performed using transmission electron microscopy *in situ* on a heterogeneous catalyst (Hansen *et al* 2001) with atomic resolution, which has shown that

the surface structure of a real catalyst (barium-promoted ruthenium catalyst supported on boron nitride) changes dramatically in the presence or absence of reagents (3:1 mixture of H_2 and N_2 at a pressure of 50 bar). A surface's response to high pressure therefore appears to be highly system-specific and further developments of present experimental techniques will be necessary for a detailed understanding of real catalysts (Campbell 2001).

Finally, it will be important to bridge the gap that currently exists between physics and chemistry, on the one side, and biology on the other. To achieve this, closer collaboration and multidisciplinary research projects are necessary.

8.2. Nanoscale imaging of insulators: a new frontier

Surfaces of insulating materials are intrinsically difficult to study, particularly because most surface-sensitive probes—typically electron spectroscopies and electron microscopies—will cause them to charge during observation. This seriously hampers further analysis: as soon as the sample acquires an excess electrical charge, it becomes next to impossible to extract any useful information from it. Thus, a new frontier in nanoscience is being able to image the surface structure of insulators with atomic resolution (Giessibl 1995, 2003, Giessibl *et al* 2000, Hofer *et al* 2003). Although a number of groups have already achieved this (Pethica and Egdell 2001, Brobrov *et al* 2001, Barth and Reichling 2001: for a recent review, see Giessibl 2003), it is still far from a routine experiment.

By using the STM in an unconventional resonant electron injection mode, Brobrov *et al* (2001) were able to image insulating diamond surfaces with atomic resolution and probe their electronic properties at the atomic scale. This work revealed striking electronic features in high-purity diamond single crystals, such as the existence of one-dimensional fully delocalized electronic states and an unexpectedly long diffusion length for conduction-band electrons. The ability to image an insulator by STM is quite surprising, and perhaps even more surprising is the possibility of obtaining atomic resolution.

Barth and Reichling (2001) used a dynamic scanning force microscopy technique, which enabled them to image in real space the atomic structure of the high temperature phase of the α-$Al_2O_3(0001)$ surface, which is a technologically important oxide crystal because of its applications in catalysis and microelectronics. This particular surface of alumina exists in several ordered phases that can be transformed reversibly into each other by appropriate thermal treatment and oxygen exposure. They found evidence for a surface reconstruction that appears in the form of a protrusion network with a rhombic unit cell, with the atoms arranged in hexagonal domains with atomic order at the centre and peripheral disorder.

Several groups (Gnecco *et al* 2000, 2002, Riedo and Brune 2003) have used AFM and scanning force microscopy (SFM) to study the microscopic properties of friction and abrasive wear on insulating surfaces.

The phenomenological laws of friction were derived several centuries ago from the three following empirical macroscopic observations:

(a) friction forces are proportional to the contact area between two sliding objects;
(b) friction is proportional to the applied load;
(c) kinetic friction does not depend on the velocity (but dynamic friction does).

In their first study, Gnecco *et al* (2000) used the tip of a friction force microscope to measure its sliding friction on a NaCl(100) surface. In fact, the laws of friction stated above, which are commonly observed in everyday life on the macroscopic scale, stem from the collective behaviour of microscopic asperities that interact during sliding processes[23]. Investigations

[23] This interaction is believed to be essentially electromagnetic.

performed at low velocities showed that atomic-scale friction is an increasing logarithmic function of the sliding velocity. This dependence is ascribed to the thermal activation of irreversible jumps, which leads to the hysteretic behaviour of lateral forces.

In more recent work, Riedo and Brune (2003) studied sliding friction forces between a Si AFM tip and diamond, diamond-like carbon (DLC) and CrN thin films. All these materials are employed in industry because of their high performance as hard coatings. In particular, the variations of the friction coefficient in CrN films grown at different temperatures were fully ascribed in terms of the different Young moduli. Moreover, it was shown that these CrN thin films, together with DLC and diamond films, exhibit the same linear dependence between the nanoscopic friction coefficient and the inverse of the Young modulus (Riedo and Brune 2003). These observations show that there are materials with similar values of critical shear strength and that for such materials nanoscopic wearless friction only depends on their Young modulus.

Finally, atomic-scale wear on KBr(001) was reported by Gnecco *et al* (2002), who employed a SFM in UHV first to induce a scratching process and then to observe its effects on the surface. Using a silicon tip, it was shown that the debris extracted from this surface by a scratching process reorganizes itself on the nanoscale. It was possible to use the same tip for scratching and observing the surface, without changes in resolution even after repeating scratches thousands of times. Gnecco *et al* observed that the damaged surface is smoothly modified by tip-induced pressure. Moreover, the debris removed by the tip rearranges itself in a process similar to epitaxial growth. This leads to the formation of KBr mounds with the same structure as the underlying substrate. The observed depth of grooves and pits increases at high loads, whereas the process is not affected by the tip's velocity during scratching. Comparison with theoretical calculations suggests in this case that KBr ions are detached pair by pair and displaced by the AFM tip to form ordered structures. This local epitaxial growth of debris may be used in the fabrication of future nanoscale devices, for example to control the local growth of insulating materials.

8.3. Nanostructured biomaterials

Millions of implants made of diverse biocompatible materials are surgically placed in humans each year. These biomedical devices are extremely useful but still far from perfect. Their duration is limited, complications can arise at many points and their use is normally limited to patients in good health. At the same time, the ageing population of the industrialized nations is generating an increased demand for such implants. As a result, the creation of improved prostheses is an important priority for the health industry.

Recent advances in molecular design and synthesis, materials science and engineering, molecular biology, surface science and imaging techniques are converging, providing new opportunities to develop revolutionary biomaterials for applications in health (Stupp and Braun 1997, Murphy and Mooney 2002, Cochran and Boyan 1995). In particular, imaginative high-throughput techniques for synthesis now allow whole libraries of new compounds to be made in the time previously needed to synthesize a single compound and chemical, physical and biological properties of biomaterials can therefore be optimized rapidly. At the same time, our understanding of the structure and modification of surfaces at the atomic and molecular level has improved significantly. Atoms and molecules are now being used as functional building blocks for fabricating totally new nanostructured materials, including those with a variety of tailor-made properties. Moreover, the underlying biology of processes is increasingly understood at the molecular level. These powerful new tools offer significant opportunities for applications in human health and nanotechnology is on the verge of having a revolutionary impact in biology and medicine.

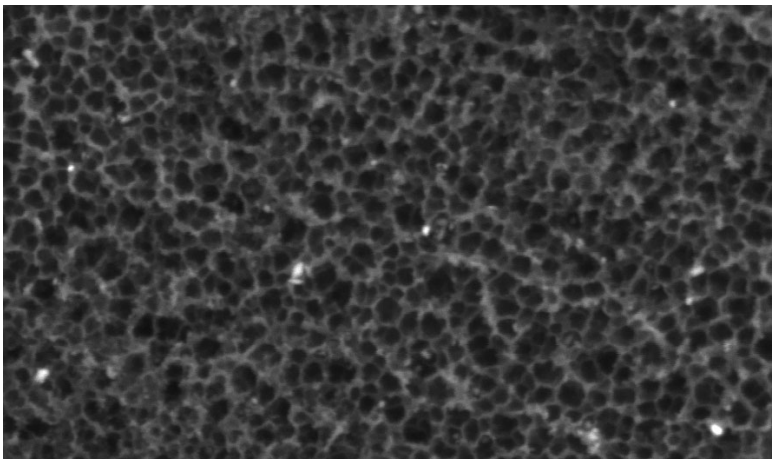

Figure 30. High resolution SEM micrograph ($300 \times 500\,nm^2$) of nanotextured Ti substrate obtained after H_2SO_4/H_2O_2 treatment (Nanci and Zalzal 2003).

In the human body, most reactions occur at surfaces and interfaces. Thus, the key to the design of improved biomaterials is properly managing interactions with the surface and at the interface between the material and the host tissue. To improve implants, it is essential to engineer materials on the nanoscale in ways that promote tissue integration and improve biological function. Regardless of the specific implantation site, the basic mechanisms of integration are likely to be similar, so that advances in making new nanostructured biomaterials can be applied to different types of implants and are likely to have a broad impact on human health.

A long-standing hypothesis asserts that four surface properties control events at tissue-implant interfaces: (i) composition, (ii) energy, (iii) roughness and (iv) topography (Brunski *et al* 2000). Various surface textures have been used to stimulate cell and tissue responses (Puleo and Nanci 1999). In bone tissues, microtextured surfaces generate an advantageous three-dimensional environment leading to improved bone formation, at least during the initial stages of *osteointegration* (Martin *et al* 1995). However, if surface features are to optimize tissue repair, their characteristics must take into consideration cellular and molecular events since cell/matrix/substrate interactions associated with cell signalling occur at the nanoscale (Tambasco de Oliveira and Nanci 2004). Such signalling regulates cell attachment, spreading, migration, differentiation and gene expression. Indeed, various cell types respond to nanotopography and increased cellular responses have been reported in cultures grown on nanophase ceramics (Webster *et al* 2001), polymers with nanotopography (Dalby *et al* 2002) and nanometric carbon fibres (Elias *et al* 2002).

Recent progress in this field has shown that *nanotextured* surfaces can be obtained by controlled chemical oxidation of Ti using H_2SO_4/H_2O_2, as shown in figure 30 (Nanci *et al* 1998), and that such substrates exhibit an increased biological activity (Tambasco de Oliveira and Nanci 2004). Further progress in this field will require a closer than ever collaboration between biologists, chemists and physicists.

Acknowledgments

This paper is dedicated to the memory of my uncle, the late Professor Fabrizio Galluzzi (1945–1999), who acted as an exceptional source of inspiration and guidance throughout my studies and at the earliest stages of my scientific career. In particular, I am grateful for his timely

suggestion to study quantum dots (which I only followed much later). His lively spirit, kindness and memory live on.

I would like to thank R Rosei, J C Polanyi, T W Johnston, M Chaker, P H McBreen and F Besenbacher for stimulating discussions and for continuous support. I am grateful to A Nanci and J D Wuest for helpful brainstorming sessions. I acknowledge A Pignolet for introducing me to ferroelectric materials.

I am indebted to all the scientists and friends who provided me with their original figures reproduced in this work, and in particular to C Africh, T Zambelli, A Nanci, J V Lauritsen, P Grütter, C Harnagea, R Hoffmann, R Dolbec, F Arciprete, A Rastelli, A Sgarlata and M De Crescenzi.

Finally, I acknowledge financial support from the Fond Quebecois de Recherche en Nature et Technologies (FQRNT) under the program 'subvention stratégique nouveaux chercheurs', from the Natural Science and Engineering Research Council (NSERC) of Canada, from the Canada Research Chairs (CRC) Program and from INRS start-up funds.

References

Africh C, Esch F, Comelli G and Rosei R 2001 *J. Chem. Phys.* **115** 477
Africh C, Esch F, Comelli G and Rosei R 2002 *J. Chem. Phys.* **116** 7200
Albrecht T R, Grütter P, Horne D and Rugar D 1991 *J. Appl. Phys.* **69** 668
Alexe M, Gruverman A, Harnagea C, Zakharov N D, Pignolet A, Hesse D and Scott J F 1999a *Appl. Phys. Lett.* **75** 1158
Alexe M, Harnagea C, Erfurth W, Hesse D and Gösele U 2000 *Appl. Phys.* A **70** 247
Alexe M, Harnagea C, Hesse D and Gösele U 1999b *Appl. Phys. Lett.* **75** 1793
Alfè D, de Gironcoli S and Baroni S 1998 *Surf. Sci.* **410** 151
Andres R P, Bein T, Dorogi M, Feng S, Henderson J I, Kubiak C P, Mahoney W, Osifchin R G and Reifenberger R 1996 *Science* **272** 1323
Ashcroft N W and Mermin N D 1976 *Solid State Physics* (Philadelphia, PA: Saunders)
Aviram A and Ratner M 1974 *Chem. Phys. Lett.* **29** 277
Avouris Ph 1995 *Acc. Chem. Res.* **28** 95
Bales G S and Zangwill A 1990 *Phys. Rev.* B **41** 5500
Bamwenda G R, Tsubota S, Nakamura T and Haruta M 1997 *Catal. Lett.* **44** 83
Barabasi A L 1997 *Appl. Phys. Lett.* **70** 2565
Baraldi A, Cerda J, Martin-Gago J A, Comelli G, Lizzit S, Paolucci G and Rosei R 1999 *Phys. Rev. Lett.* **82** 4874
Bartels L, Meyer G and Rieder K-H 1997 *Phys. Rev. Lett.* **79** 697
Barth C and Reichling M 2001 *Nature* **414** 54
Barth J V 2000 *Surf. Sci. Rep.* **40** 75
Barth J V, Weckesser J, Cai C, Gunter P, Burgi L, Jeandupeux O and Kern K 2000 *Angew. Chem. Int. Ed.* **39** 1230
Barth J V, Weckesser J, Lin N, Dmitriev A and Kern K 2003 *Appl. Phys.* A **76** 645
Becker R S, Golovchenko J A and Swartzentruber B S 1985 *Phys. Rev.* B **32** 8455
Besenbacher F 1996 *Rep. Prog. Phys.* **59** 1737
Besenbacher F and Norskov J K 1993 *Prog. Surf. Sci.* **44** 5
Besenbacher F, Chorkendorff I, Clausen B S, Hammer B, Molenbroek A M, Norskov J K and Stensgaard I 1998 *Science* **279** 1913
Besenbacher F and Nørskov J K 2000 *Science* **290** 1520
Binnig G, Quate C F and Gerber Ch 1986 *Phys. Rev. Lett.* **50** 930
Binnig G and Röhrer H 1999 *Rev. Mod. Phys.* **71** S324
Binnig G, Röhrer H, Gerber Ch and Weibel E 1982a *Phys. Rev. Lett.* **49** 57
Binnig G, Röhrer H, Gerber Ch and Weibel E 1982b *Appl. Phys. Lett.* **40** 178
Braun K F and Rieder K H 2002 *Phys. Rev. Lett.* **88** 096801
Boal A K, Ilhan F, De Rouchey J E, Thurn-Albrecht T, Russell T P and Rotello V M 2000 *Nature* **404** 746
Bochi G, Hug H J, Paul D I, Stiefel B, Moser A, Parashikov I, Güntherodt H-J and O'Handley R C 1995 *Phys. Rev. Lett.* **75** 1839
Böhringer M, Morgenstern K, Schneider W-D and Berndt R 1999 *Angew. Chem.* **38** 821

Boland J J 1990 *Phys. Rev. Lett.* **65** 3325
Boland J J 1992 *Surf. Sci.* **261** 17
Boscherini F 1992 *Mater. Res. Symp. Proc.* **258** 217
Boscherini F, Capellini G, Di Gaspare L, Rosei F, Motta N and Mobilio S 2000a *Appl. Phys. Lett.* **76** 682
Boscherini F, Capellini G, Di Gaspare L, De Seta M, Rosei F, Motta N, Sgarlata A and Mobilio S 2000b *Thin Solid Films* **380** 173
Bottomley D J 1998 *Appl. Phys. Lett.* **72** 783
Brobrov K, Mayne A and Dujardin G 2001 *Nature* **413** 616
Brügger J, Berenschot J W, Kuiper S, Nijdam W, Otter B and Elwenspoek M 2000 *Microelectron. Eng.* **53** 403
Brune H 1998 *Surf. Sci. Rep.* **31** 121
Brunner K 2002 *Rep. Prog. Phys.* **65** 27
Brunski J B, Puleo D A and Nanci A 2000 *Int. J. Oral Maxillofac Implants* **15** 15
Brust M, Bethell D, Schiffrin D J and Kiely C J 1995 *Adv. Mater.* **7** 795
Brust M, Walker M, Bethell D, Schiffrin D J and Whyman R 1994 *J. Chem. Soc. Chem. Commun.* 801
Burton W K, Cabrera N and Frank F C 1951 *Phil. Trans. R. Soc.* A **243** 299
Butz R and Lüth H 1998 *Surf. Sci.* **411** 61
Campbell C T 2001 *Science* **294** 1471
Casalis L, Danisman M F, Nickel B, Bracco G, Toccoli T, Iannotta S and Scoles G 2003 *Phys. Rev. Lett.* **90** 206101
Castellarin-Cudia C, Hla S W, Comelli G, Sljivan!canin Ž, Hammer B, Baraldi A, Prince K C and Rosei R 2001 *Phys. Rev. Lett.* **87** 196104
Castrucci P, Gunnella R, Pinto N and De Crescenzi M 2002 *J. Phys.: Condens. Matter* **14** 8333
Castrucci P, Sgarlata A, Scarselli M and De Crescenzi M 2003 *Surf. Sci.* **531** L329
Chambliss D D and Chiang S 1992 *Surf. Sci.* **264** L187
Chen D, Gallagher M J and Sarid D 1994 *J. Vac. Sci. Technol.* B **12** 1947
Chen K M, Jesson D E, Pennycook S J, Thundat T and Warmack R J 1997 *Phys. Rev.* B **56** R1700
Chou S Y, Krauss P R and Renstrom P J 1996 *Science* **272** 85
Cochran D L and Boyan B D 1995 *J. Biomed. Mater. Res.* **29** 389
Comelli G, Dhanak V R, Kiskinova M, Prince K C and Rosei R 1998 *Surf. Sci. Rep.* **32** 165
Contini G, Di Castro V, Motta N and Sgarlata A 1998 *Surf. Sci.* **405** L509
Coulman D J, Wintterlin J, Behm R J and Ertl G 1990 *Phys. Rev. Lett.* **64** 1761
Cowburn R P, Koltsov D K, Adeye A O and Welland M E 1999 *Phys. Rev. Lett.* **83** 1042
Cowburn R P and Welland M E 2000 *Nature* **287** 1466
Cvetko D, Floreano L, Morgante A, Peloi M, Tommasini F, Prince K C, Vendruscolo M and Tosatti E 1994 *Surf. Sci.* **318** L1193
Dalby M J, Riehle M O, Johnstone H, Affrossman S and Curtis A S G 2002 *Biomaterials* **23** 2945
Damjanovic D 1998 *Rep. Prog. Phys.* **61** 1267
Daruka I, Tersoff J and Barabási A L 1999 *Phys. Rev. Lett.* **82** 2753
De Crescenzi M, Bernardini R, Pollano S, Gunnella R, Castrucci P, Dufour G and Rochet F 2001 *Surf. Sci.* **489** 185
De Crescenzi M, Gunnella R, Bernardini R, De Marco M and Davoli I 1995 *Phys. Rev.* B **52** 1806
De Crescenzi M, Marucci M, Gunnella R, Castrucci P, Casalboni M, Dufour G and Rochet F 1999 *Surf. Sci.* **426** 277
De Gironcoli S, Giannozzi P and Baroni S 1991 *Phys. Rev. Lett.* **66** 2116
Derycke V, Soukiassian P G, Amy F, Chabal Y J, D'Angelo M D, Enriquez H B and Silly M G 2003 *Nature Mater.* **2** 253
Dolbec R, El Khakani M A, Serventi A M, Trudeau M and Saint-Jacques R G 2002 *Thin Solid Films* **419** 230
Eaglesham D J and Cerullo M 1990 *Phys. Rev. Lett.* **64** 1943
Ehrlich G and Hudda F G 1966 *J. Chem. Phys.* **44** 1039
Eigler D M, Lutz C P and Rudge W E 1991 *Nature* **352** 600
Eigler D M and Schweizer E K 1990 *Nature* **344** 524
Elder K R, Katakowski M, Haataja M and Grant M 2002 *Phys. Rev. Lett.* **88** 245701
Elias K L, Price R L and Webster T J 2002 *Biomaterials* **23** 3279
El Khakani M A, Dolbec R, Serventi A C, Horrillo M C, Trudeau M, Saint-Jacques R G, Rickerby D G and Sayago I 2001 *Sensors Actuators* B **77** 383
Ertl G 1967 *Surf. Sci* **6** 208
Feynman R P 1960 *Caltech Eng. Sci. J.* (1959 http://www.zyvex.com/nanotech/feynman.html)
Finnie P and Homma Y 2002 *Surf. Sci.* **500** 437
Fishlock T W, Oral A, Egdell R G and Pethica J B 2000 *Nature* **404** 743
Floro J A, Chason E, Freund L B, Twesten R D, Hwang R Q and Lucadamo G A 1999 *Phys. Rev.* B **59** 1990
Forrest S R 1997 *Chem. Rev.* **97** 1793

Fukuda T 1996 *Surf. Sci.* **351** 103
Gambardella P, Rusponi S, Veronese M, Dhesi S S, Grazioli C, Dallmeyer A, Cabria I, Zeller R, Dederichs P H, Kern K, Carbone C and Brune H 2003 *Science* **300** 1130
Gehanno V, Marty A, Gilles B and Samson Y 1997 *Phys. Rev.* B **55** 12552
Giessibl F J 1995 *Science* **267** 68
Giessibl F J 2003 *Rev. Mod. Phys.* **75** 949
Giessibl F J, Hembacher S, Bielefeldt H and Mannhart J 2000 *Science* **289** 422
Gimzewski J K, Modesti S and Schlittler R R 1994 *Phys. Rev. Lett.* **72** 1036
Gnecco E, Bennewitz R, Gyalog T, Loppacher C, Bammerlin M, Meyer E and Guntherodt H J 2000 *Phys. Rev. Lett.* **84** 1172
Gnecco E, Bennewitz R and Meyer E 2002 *Phys. Rev. Lett.* **88** 215501
Gopel W and Schierbaum K D 1995 *Sensors Actuators* B **26** 1
Gray J L, Hull R and Floro J A 2002 *Appl. Phys. Lett.* **81** 2445
Gross L, Moresco F, Alemani M, Tang H, Gourdon A, Joachim C and Rieder K-H 2003 *Chem. Phys. Lett.* **351** 750
Grütter P, Mamin H J and Rugar D 1992 *Scanning Tunnelling Microscopy* vol 2 (Berlin: Springer) pp 151–207
Hahn J R and Ho W 2001 *Phys. Rev. Lett.* **87** 166102
Hamers R J 2001 *Nature* **412** 489
Hamers R J and Demuth J E 1988 *Phys. Rev. Lett.* **60** 2527
Hammer B 1999 *Phys. Rev. Lett.* **83** 3681
Hammer B and Norskov J K 1995 *Nature* **376** 238
Hansen T W, Wagner J B, Hansen P L, Dahl S, Topsoe H and Jacobsen C J H 2001 *Science* **294** 1508
Harnagea C 2001 *PhD Thesis in Physics* Max Planck Institute for Microstructural Physics, Halle (Germany) unpublished results
Harnagea C, Alexe M, Hesse D and Pignolet A 2003 *Appl. Phys. Lett.* **83** 338
Harnagea C, Pignolet A, Alexe M, Hesse D and Gösele U 2000 *Appl. Phys.* A **70** 261
Haruta M 1997 *Catal. Today* **36** 153
Hehn M, Padovani S, Ounadjela K and Bucher J P 1996 *Phys. Rev.* B **54** 3428
Heinrich A J, Lutz C P, Gupta J A and Eigler D M 2002 *Science* **298** 1381
Helveg S, Lauritsen J V, Lægsgaard E, Stensgaard I, Nørskov J K, Clausen B S, Topsøe H and Besenbacher F 2000 *Phys. Rev. Lett.* **84** 951
Hembacher S, Giessibl F J, Mannhart J and Quate C F 2003 *Proc. Natl Acad. Sci. USA* **100** 12539
Hendriksen B L M and Frenken J W M 2002 *Phys. Rev. Lett.* **89** 046101
Hersam M C and Chung Y-W 2003 *Proc. Natl Acad. Sci. USA* **100** 12531
Hla S W, Bartels L, Meyer G and Rieder K H 2000 *Phys. Rev. Lett.* **85** 2777
Hla S-W and Rieder K-H 2003 *Annu. Rev. Phys. Chem.* **54** 307
Ho W 1998 *Acc. Chem. Res.* **31** 567
Hofer W and Fischer A J 2003 *Phys. Rev. Lett.* **91** 036803
Hofer W, Foster A S and Shluger A L 2003 *Rev. Mod. Phys.* **75** 1287
Hofer W A and Fisher A J 2002 *Surf. Sci.* **498** L65
Hofer W A, Fisher A J, Wolkow R A and Grutter P 2001 *Phys. Rev. Lett.* **87** 236104
Hoffmann R, Bürgler D E, van Schendel P J A, Hug H J, Martin S and Güntherodt H-J 2002 *J. Magn. Magn. Mater.* **250** 32
Hoffmann R, Samson Y, Marty A, Gehanno V, Gilles B and Mazille J E 1999 *J. Magn. Magn. Mater.* **192** 409
Holmar Johannesson G, Bligaard T, Ruban A V, Skriver H L, Jacobsen K W and Nørskov J K 2002 *Phys. Rev. Lett.* **88** 255506
Holmblad P M, Larsen J H, Chorkendorff I, Nielsen L P, Besenbacher F, Stensgaard I, Laegsgaard E, Kratzer P, Hammer B and Norskov J K 1996 *Catal. Lett.* **40** 131
Horn-von Hoegen M 2003 *Surf. Sci.* **537** 1
Isichenko M B 1992 *Rev. Mod. Phys.* **64** 961
Jensen F, Besenbacher F, Laesgaard E and Stensgaard I 1990 *Phys. Rev.* B **41** 10233
Jesson D E, Kastner M and Voigtlander B 2000 *Phys. Rev. Lett.* **84** 330
Jiang G, Polanyi J C and Rogers D 2003 *Surf. Sci.* **544** 147
Joachim C, Gimzewski J K and Aviram A 2000 *Nature* **408** 41
Joyce P B, Krzyzewski T J, Bell G R, Joyce B A and Jones T S 1998 *Phys. Rev.* B **58** R15981
Jung T A, Schlittler R R, Gimzewski J K, Tang H and Joachim C 1996 *Science* **271** 181
Kajiyama H, Muramatsu S, Shimada T and Nishino Y 1992 *Phys. Rev.* B **45** 14005
Kandel D and Weeks J D 1994 *Phys. Rev.* B **49** 5554
Kane B 1998 *Nature* **393** 11

Kawamura M, Paul N, Cherepanov V and Voigtländer B 2003 *Phys. Rev. Lett.* **91** 096102
Kelires P C 1995 *Phys. Rev. Lett.* **75** 1114
Kelires P C and Kaxiras E 1997 *Phys. Rev. Lett.* **78** 3479
Kellogg G L 1994 *Surf. Sci. Rep.* **21** 1
Kern K, Niehus H, Schatz A, Zeppenfeld P, George J and Comsa G 1991 *Phys. Rev. Lett.* **67** 855
Kiely C J, Fink J, Brust M, Bethell D and Schiffrin D J 1998 *Nature* **396** 444
Kleiber M, Kümmerlen F, Löhndorf M, Wadas A, Weiss D and Wiesendanger R 1998 *Phys. Rev.* B **58** 5563
Koch R, Sturmat M and Schulz J J 2000 *Surf. Sci.* **454–456** 543
Kruse P, Johnson E R, DiLabio G A and Wolkow R A 2002 *Nano Lett.* **2** 807
Kühnle A, Linderoth T R, Hammer B and Besenbacher F 2002 *Nature* **415** 891
Kummer M, Vögeli B and von Känel H 2000 *Mater. Sci. Eng.* B **69** 247
Kuntze J, Berndt R, Jiang P, Tang H, Gourdon A and Joachim C 2002 *Phys. Rev.* B **65** 233405
Kürpick U and Rahman T S 1999 *Phys. Rev. Lett.* **83** 2765
Laegsgaard E, Osterlund L, Thostrup P, Rasmussen P B, Stensgaard I and Besenbacher F 2001 *Rev. Sci. Instrum.* **72** 3537
Lauhon L J and Ho W 2000 *Phys. Rev. Lett.* **84** 1527
Lauritsen J V, Helveg S, Lægsgaard E, Stensgaard I, Clausen B S, Topsøe H and Besenbacher F 2001 *J. Catal.* **197** 1
Lauritsen J V, Nyberg M, Vang R T, Bollinger M V, Clausen B S, Topsøe H, Jacobsen K W, Lægsgaard E, Nørskov J K and Besenbacher F 2003 *Nanotechnology* **14** 385
Lee H J and Ho W 1999 *Science* **286** 1719
Leifeld O, Grützmacher D, Müller B, Kern K, Kaxiras E and Kelires P C 1999 *Phys. Rev. Lett.* **82** 972
Lin F and Lagally M G 1997 *Surf. Sci.* **386** 169
Linderoth T R 1998 *PhD Thesis in Physics* University of Aarhus
Linderoth T R, Horch S, Lægsgaard E, Stensgaard I and Besenbacher F 1997 *Phys. Rev. Lett.* **78** 4978
Linderoth T R, Horch S, Petersen L, Helveg S, Lægsgaard E, Stensgaard I and Besenbacher F 1999 *Phys. Rev. Lett.* **82** 1494
Lippel P H, Wilson R J, Miller M D, Wöll Ch and Chiang S 1989 *Phys. Rev. Lett.* **62** 171
Liu C-P, Gibson J M, Cahill D G, Kamins T I, Basile D P and Williams R S 2000 *Phys. Rev. Lett.* **84** 1958
Logadottir A, Rod T H, Nørskov J K, Hammer B, Dahl S and Jacobsen C J H 2001 *J. Catal.* **197** 129
Lopinski G P, Moffatt D J, Wayner D D M and Wolkow R A 1998 *Nature* **392** 909
Lopinski G P, Moffatt D J, Wayner D D M and Wolkow R A 2000a *J. Am. Chem. Soc.* **122** 3548
Lopinski G P and Rosei F 2004 in preparation
Lopinski G P, Wayner D D M and Wolkow R A 2000b *Nature* **406** 48
Lu P H, Polanyi J C and Rogers D 1999 *J. Chem. Phys.* **111** 9905
Lu P H, Polanyi J C and Rogers D 2000 *J. Chem. Phys.* **112** 11005
Lüth H 1997 *Surfaces and Interfaces of Solid Materials* (Berlin: Springer)
Lüthi R, Schlittler R R, Brügger J, Vettiger P, Welland M E and Gimzewski J K 1999 *Appl. Phys. Lett.* **75** 1314
Madou M J and Morrison S R 1989 *Chemical Sensing with Solid State Devices* (New York: Academic)
Maltezopoulos T, Bolz A, Meyer C, Heyn C, Hansen W, Morgenstern M and Wiesendanger R 2003 *Phys. Rev. Lett.* **91** 196804
Manoharan H C, Lutz C P and Eigler D M 2000 *Nature* **403** 512
Martin J Y, Schwartz Z, Hummert T W, Schraub D M, Simpson J, Lankford J Jr, Dean D D, Cochran D L and Boyan B D 1995 *J. Biomed. Mater. Res.* **29** 389
Marchenko O and Cousty J 2000 *Phys. Rev. Lett.* **84** 5363
Masuda K and Shigeta Y 2001 *Appl. Surf. Sci.* **175** 77
Medeiros-Ribeiro G, Bratkovski A M, Kamins T I, Ohlberg D A A and Williams R S 1998 *Science* **279** 353
Medeiros-Ribeiro G, Kamins T I, Ohlberg D A A and Williams R S 1999 *Mater. Sci. Eng.* B **67** 31
Men F K, Liu F, Wang P J, Chen C H, Cheng D L, Lin J L and Himpsel F J 2002 *Phys. Rev. Lett.* **88** 096105
Meyer zu Heringdorf F J, Reuter M C and Tromp R M 2001 *Nature* **412** 517
Miki K, Sakamoto K and Sakamoto T 1997 *Appl. Phys. Lett.* **71** 3266
Miki K and Tokumoto H 1992 *Nanotechnology* **3** 142
Mo Y-W, Savage D E, Swartzentruber R S and Lagally M G 1990 *Phys. Rev. Lett.* **65** 1020
Moison J M, Houzay F, Barthe F, Leprince L, Andre E and Vatel O 1994 *Appl. Phys. Lett.* **64** 196
Moresco F, Gross L, Alemani M, Rieder K H, Tang H, Gourdon A and Joachim C 2003a *Phys. Rev. Lett.* **91** 036601
Moresco F, Meyer G, Rieder K H, Jiang P, Tang H and Joachim C 2002 *Surf. Sci.* **499** 94
Moresco F, Meyer G, Rieder K H, Tang H, Gourdon A and Joachim C 2001a *Appl. Phys. Lett.* **78** 306
Moresco F, Meyer G, Rieder K H, Tang H, Gourdon A and Joachim C 2001b *Phys. Rev. Lett.* **86** 672
Moresco F, Meyer G, Tang H, Joachim C and Rieder K H 2003b *J. Electron. Spectrosc. Relat. Phenom.* **129** 149

Motta N 2002 *J. Phys.: Condens. Matter* **14** 8353
Motta N, Rosei F, Sgarlata A, Capellini G, Mobilio S and Boscherini F 2002a *Mater. Sci. Eng.* B **88** 264
Motta N, Sgarlata A, Balzarotti A and Rosei F 2002b *Mater. Res. Soc. Symp. Proc.* **696** N2.2
Motta N, Sgarlata A, Calarco R, Nguyen Q, Patella F, Castro Cal J, Balzarotti A and De Crescenzi M 1998 *Surf. Sci.* **406** 254
Motta N, Sgarlata A, De Crescenzi M and Derrien J 1996 *Appl. Surf. Sci.* **102** 57
Motta N, Sgarlata A, Rosei F, Szkutznik P D, Nufris S, Scarselli M and Balzarotti A 2003 *Mater. Sci. Eng.* B **101** 77
Moriarty P 2001 *Rep. Prog. Phys.* **57** 362
Murphy W L and Mooney D J 2002 *Nature Biotech.* **20** 30
Murray P W, Brookes I M, Haycock S A and Thornton G 1998 *Phys. Rev. Lett.* **80** 988
Murray P W, Pederson M Ø, Læsgaard E, Stensgaard I and Besenbacher F 1997 *Phys. Rev.* B **55** 9360
Murray P W, Thornton G, Bowker M, Dhanak Vr, Baraldi A, Rosei R and Kiskinova M 1993 *Phys. Rev.* B **47** 12976
Nakagawa K and Miyao M 1990 *J. Appl. Phys.* **69** 3058
Nanci A, Wuest J D, Peru L, Brunet P, Sharma V, Zalzal S and McKee M D 1998 *J. Biomed. Mater. Res.* **40** 324
Nanci A and Zalzal F S 2003 unpublished results
Naumkin F Y, Polanyi J C and Rogers D 2003a *Surf. Sci.* **547** 335
Naumkin F Y, Polanyi J C, Rogers D, Hofer W and Fisher A 2003b *Surf. Sci.* **547** 324
Neddermeyer H 1996 *Rep. Prog. Phys.* **59** 701
Nielsen L P, Besenbacher F, Stensgaard I and Laegsgaard E 1995 *Phys. Rev. Lett.* **74** 1159
Nielsen L P, Besenbacher F, Stensgaard I, Laegsgaard E, Engdahl C, Stoltze P, Jacobsen K W and Norskov J K 1993 *Phys. Rev. Lett.* **71** 754
Nilius N, Wallis T M and Ho W 2002 *Science* **297** 1853
Oberbeck L, Curson N J, Simmons M Y, Brenner R, Hamilton A R, Schofield S R and Clark R G 2002 *Appl. Phys. Lett.* **81** 3197
Ogino T, Hibino H, Homma Y, Kobayashi Y, Prabhakaran K, Sumitomo K and Omi H 1999 *Acc. Chem. Res.* **32** 447
Oh S-M, Koh S J, Kyuno K and Ehrlich G 2002 *Phys. Rev. Lett.* **88** 236102
Okawa Y and Aono M 2001 *Nature* **409** 683
Österlund L *et al* 2001 *Phys. Rev. Lett.* **86** 460
Otero R, Rosei F, Naitoh Y, Jiang P, Thostrup P, Gourdon A, Laegsgaard E, Stensgaard I, Joachim C and Besenbacher F 2003 *Nanoletters* **3** at press
Paparazzo E 2003 *Nature Mater.* **2** 351
Patella F, Arciprete F, Placidi E, Nufris S, Fanfoni M, Sgarlata A, Schiumarini D and Balzarotti A 2002 *Appl. Phys. Lett.* **81** 2270
Patella F, Fanfoni M, Arciprete F, Nufris S, Placidi E and Balzarotti A 2001 *Appl. Phys. Lett.* **78** 320
Pedersen M Ø, Österlund L, Mortensen J J, Mavrikakis M, Hansen L B, Lægsgaard E, Stensgaard I, Nørskov J K and Besenbacher F 2000 *Phys. Rev. Lett.* **84** 4898
Pethica J B and Egdell R 2001 *Nature* **414** 27
Petsalakis I D, Polanyi J C and Theodorakopoulos G 2003 *Surf. Sci.* **544** 162
Pignolet A, Schäfer C, Satyalakhshmi K M, Harnagea C, Hesse D and Gösele U 2000 *Appl. Phys.* A **70** 283
Plass R, Last J A, Bartelt N C and Kellogg G L 2001 *Nature* **412** 875
Pohl K, Bartelt M C, de la Figuera J, Bartelt N C, Hrbek J and Hwang R Q 1999 *Nature* **397** 238
Puleo D A and Nanci A 1999 *Biomaterials* **20** 2311
Qin X R, Swartzentruber B S and Lagally M G 2000 *Phys. Rev. Lett.* **84** 4645
Qiu X H, Nazin G V and Ho W 2003 *Science* **299** 542
Raiteri P, Migas D B, Miglio L, Rastelli A and von Känel H 2003 *Phys. Rev. Lett.* **88** 256103
Rastelli A, Kummer M and von Känel H 2001 *Phys. Rev. Lett.* **87** 256101
Rastelli A, Muller E and von Känel H 2002 *Appl. Phys. Lett.* **80** 1438
Rastelli A and von Känel H 2002 *Surf. Sci.* **515** L493
Rastelli A and von Känel H 2003 *Surf. Sci.* **532–535** 769
Rastelli A, von Känel H, Spencer B J and Tersoff J 2003 *Phys. Rev.* B **68** 115301
Ratto F and Rosei F 2003 *Surf. Sci.* **530** 221
Ratto F, Rosei F, Heun S, Cherifi S, Locatelli A, Fontana F, Szkutnik P D, Sgarlata A, Motta N and De Crescenzi M 2003 in preparation
Reed M A and Tour J M 2000 *Sci. Am.* **6** 86
Remediakis I N, Kaxiras E and Kelires P C 2001 *Phys. Rev. Lett.* **86** 4556
Renish S, Schuster R, Wintterlin J and Ertl G 1999 *Phys. Rev. Lett.* **82** 3839
Riedo E and Brune H 2003 *Appl. Phys. Lett.* **83** 2986
Röhrer H 1994 *Surf. Sci.* **299/300** 956

Rosei F 2001 *PhD Thesis in Physics* University of Rome 'La Sapienza'
Rosei F 2003 *Science Technology and Education of Microscopy: An Overview* vol 1 pp 84–92
Rosei F and Fontana S 2001 *Appl. Surf. Sci.* **183** 278
Rosei F, Motta N, Sgarlata A and Balzarotti A 2002a *Lecture Notes Phys.* **588** 252
Rosei F, Motta N, Sgarlata A and Balzarotti A 2002b *Mater. Res. Soc. Symp. Proc.* **696** N5.9
Rosei F, Motta N, Sgarlata A, Capellini G and Boscherini F 2000 *Thin Solid Films* **369** 29
Rosei F and Raiteri P 2002 *Appl. Surf. Sci.* **195** 16
Rosei F and Rosei R 2002 *Surf. Sci.* **500** 395
Rosei F and Rosei R 2003 *Science Technology and Education of Microscopy: An Overview* vol 1 pp 24–33
Rosei F, Schunack M, Jiang P, Gourdon A, Laegsgaard E, Stensgaard I, Joachim C and Besenbacher F 2002c *Science* **296** 328
Rosei F, Schunack M, Naitoh Y, Jiang P, Gourdon A, Laegsgaard E, Stensgaard I, Joachim C and Besenbacher F 2003 *Prog. Surf. Sci.* **71** 95
Ross F M, Tersoff J and Tromp R M 1998 *Phys. Rev. Lett.* **80** 984
Ross F M, Tromp R M and Reuter M C 1999 *Science* **286** 1931
Rousset S, Chiang S, Fowler D E and Chambliss D D 1992 *Phys. Rev. Lett.* **69** 3200
Ruiz R, Nickel B, Koch N, Feldman L C, Haglund R F, Kahn A and Scoles G 2003 *Phys. Rev.* B **67** 125406
Rusponi S, Cren T, Weiss N, Epple M, Buluschek P, Claude L and Brune H 2003 *Nature Mater.* **2** 546
Satyalakshmi K M, Alexe M, Pignolet A, Zakharov N D, Harnagea C, Senz S and Hesse D 1999 *Appl. Phys. Lett.* **74** 603
Sautet P 1997 *Chem. Rev.* **97** 1097
Sautet P and Joachim C 1991 *Chem. Phys. Lett.* **185** 23
Sautet P and Joachim C 1992 *Surf. Sci.* **271** 387
Schaub R, Wahlström E, Rønnau A, Lægsgaard E, Stensgaard I and Besenbacher F 2003 *Science* **299** 377
Schmid A K, Bartelt N C and Hwang R Q 2000a *Science* **290** 1561
Schmid A K, Bartelt N C and Hwang R Q 2000b *Surf. Rev. Lett.* **7** 515
Schmidt O G, Denker U, Eberl K, Kienzle O and Ernst F 2000 *Appl. Phys. Lett.* **77** 2509
Schmidt O G and Eberl K 2001 *IEEE Trans. Electron Devices* **48** 1175
Schneider M, Hoffman H and Zweck J 2000 *Appl. Phys. Lett.* **77** 2909
Schofield S R, Curson N J, Simmons M Y, Rueß F J, Hallam T, Oberbeck L and Clark R G 2003 *Phys. Rev. Lett.* **91** 136104
Schukin V A and Bimberg D 1999 *Rev. Mod. Phys.* **71** 1125
Schukin V A, Ledentsov N N, Kop'ev P S and Bimberg D 1995 *Phys. Rev. Lett.* **75** 2968
Schulz M 1999 *Nature* **399** 729
Schunack M 2002 *PhD Thesis* University of Aarhus
Schunack M, Linderoth T R, Rosei F, Laegsgaard E, Stensgaard I and Besenbacher F 2002a *Phys. Rev. Lett.* **88** 156102
Schunack M, Petersen L, Kühnle A, Lægsgaard E, Stensgaard I, Johannsen I and Besenbacher F 2001 *Phys. Rev. Lett.* **86** 456
Schunack M, Rosei F and Besenbacher F 2003 *Science Technology and Education of Microscopy: An Overview* vol 1 pp 43–51
Schunack M, Rosei F, Naitoh Y, Jiang P, Gourdon A, Laegsgaard E, Stensgaard I, Joachim C and Besenbacher F 2002b *J. Chem. Phys.* **117** 6259
Schwöbel R L 1968 *J. Appl. Phys.* **40** 614
Schwöbel R L and Shipsey E J 1966 *J. Appl. Phys.* **37** 3682
Sgarlata A, Szkutnik P D, Balzarotti A, Motta N and Rosei F 2003 *Appl. Phys. Lett.* **83** 4002
Shen J, Klaua M, Ohresser P, Jenniches H, Barthel J, Mohan Ch V and Kirschner J 1997 *Phys. Rev.* B **56** 11134
Shinjo T, Okuno T, Hassdorf R, Shigeto K and Ono T 2000 *Science* **289** 930
Siegert M and Plischke M 1994 *Phys. Rev. Lett.* **73** 1517
Sørensen M R, Jacobsen K W and Jonsson H 1996 *Phys. Rev. Lett.* **77** 5067
Starke U, Scardt J, Bernhardt J, Franke M and Heinz K 1999 *Phys. Rev. Lett.* **82** 2107
Stoyanov S, Métois J J and Tonchev V 2000 *Surf. Sci.* **465** 227
Stroscio J A and Eigler D M 1991 *Science* **254** 1319
Stupp S I and Braun P V 1997 *Science* **277** 242
Sutter P and Lagally M G 1998 *Phys. Rev. Lett.* **81** 3471
Sutter P and Lagally M G 2000 *Phys. Rev. Lett.* **84** 4637
Swartzentruber B S 1996 *Phys. Rev. Lett.* **76** 459
Takaoka T, Takagali T, Igari Y and Kusunoki I 1996 *Surf. Sci.* **347** 105
Takayanagi K, Tanishiro Y, Takahashi S and Takahashi M 1985 *Surf. Sci.* **164** 367

Tambasco de Oliveira P and Nanci A 2004 *Biomaterials* **25** 403
Tersoff J 1995 *Phys. Rev. Lett.* **74** 5080
Tersoff J, Spencer B J, Rastelli A and von Känel H 2003 *Phys. Rev. Lett.* **89** 196104
Theobald J A, Oxtoby N S, Phillips M A, Champness N R and Beton P H 2003 *Nature* **424** 1029
Thurmer K, Koch R, Weber M and Rieder K H 1995 *Phys. Rev. Lett.* **75** 1767
Trost J, Zambelli T, Wintterlin J and Ertl G 1996 *Phys. Rev.* B **54** 17850
Tsu R, Esaki L and Ludeke R 1969 *Phys. Rev. Lett.* **23** 977
Vailionis A, Cho B, Glass G, Desjardins P, Cahill D G and Greene J E 2000 *Phys. Rev. Lett.* **85** 3672
Valden M, Lai X and Goodman D W 1998 *Science* **281** 1647
Venables J A, Spiller G D T and Hanbücken M 1984 *Rep. Prog. Phys.* **47** 399
Vescan L, Grimm K, Goryll M and Hollander B 2000 *Mater. Sci. Eng.* B **69** 324
Vesselli E, Africh C, Baraldi A, Comelli G, Esch F and Rosei R 2001 *J. Chem. Phys.* **114** 4221
Vestergaard E K, Thostrup P, An T, Laegsgaard E, Stensgaard I, Hammer B and Besenbacher F 2002 *Phys. Rev. Lett.* **88** 259601
Vladimirova M, DeVita A and Pimpinelli A 2001 *Phys. Rev.* B **64** 245420
Voigtländer B 2001 *Surf. Sci. Rep.* **43** 127
Voigtländer B and Zinner A 1993 *Appl. Phys. Lett.* **63** 3055
Wahlström E, Lopez N, Schaub R, Thostrup P, Rønnau A, Africh C, Lægsgaard E, Nørskov J K and Besenbacher F 2003 *Phys. Rev. Lett.* **90** 026101
Weaver J H and Poirier D M 1994 *Solid State Physics* vol 48 (New York: Academic) p 1
Webster T J, Schadler L S, Siegel R W and Bizios R 2001 *Tissue Eng.* **7** 291
Weckesser J, Barth J V and Kern K 1999 *J. Chem. Phys.* **110** 5351
Weckesser J, Barth J V and Kern K 2001a *Phys. Rev.* B **64** 161403
Weckesser J, Cepek C, Fasel R, Barth J V, Baumberger F, Greber T and Kern K 2001b *J. Chem. Phys.* **115** 9001
Weisbuch C and Vinter B 1991 *Quantum Semiconductor Structures: Fundamentals and Applications* (London: Academic)
Weiss P S 2001 *Nature* **413** 585
Wiesendanger R 1994 *Scanning Probe Microscopy and Spectroscopy: Methods and Applications* (Cambridge: Cambridge University Press)
Wintterlin J, Schuster R and Ertl G 1996 *Phys. Rev. Lett.* **77** 123
Wintterlin J, Völkening S, Janssens T V W, Zambelli T and Ertl G 1997 *Science* **278** 1931
Woodruff D P 2002 *Surf. Sci.* **500** 147
Woodruff D P and Delchar T A 1986 *Modern Techniques of Surface Science* vol 3 (Cambridge: Cambridge University Press)
Yokoyama T, Yokoyama S, Kamikado T, Okuno Y and Mashiko S 2001 *Nature* **413** 619
Zambelli T, Jiang P, Lagoute J, Grillo S E, Gauthier S, Gourdon A and Joachim C 2002 *Phys. Rev.* B **66** 075410
Zambelli T, Tang H, Lagoute J, Gauthier S, Gourdon A and Joachim C 2001 *Chem. Phys. Lett.* **348** 1
Zambelli T, Trost J, Wintterlin J G and Ertl G 1996a *Phys. Rev. Lett.* **76** 795
Zambelli T, Wintterlin J, Trost J and Ertl G 1996b *Science* **273** 1688
Zhong Z, Stangl J, Schäffler F and Bauer G 2003 *Appl. Phys. Lett.* **83** 3695
Zhu X, Grütter P, Metlushko V and Ilic B 2002a *Appl. Phys. Lett.* **80** 4789
Zhu X, Grütter P, Metlushko V and Ilic B 2002b *J. Appl. Phys.* **91** 7340
Zhu X, Grütter P, Metlushko V and Ilic B 2002c *Phys. Rev.* B **66** 024423
Zhu X B, Grütter P, Hao Y, Castano F J, Haratani S, Ross C A, Vogeli B and Smith H I 2003a *J. Appl. Phys.* **93** 1132
Zhu X B, Grütter P, Metlushko V and Ilic B 2003b *J. Appl. Phys.* **93** 7059
Zinke-Allmang M 1999 *Thin Solid Films* **346** 1
Zinke-Allmang M, Feldman L C and Grabow M H 1992 *Surf. Sci. Rep.* **16** 377